Design of nanowire-based hybrid structures for wastewater treatment

Ph.D. Dissertation

Mohammed Ahmed Shehab

Supervisor

Dr. Zoltán Németh

Head of the Doctoral School

Prof. Dr. Valéria Mertinger

Antal Kerpely Doctoral School of Materials Science and Technology

Faculty of Materials and Chemical Engineering

University of Miskolc

Miskolc 2024

"In loving memory of my brother, Samer (1984 - 2015). His aspiration to achieve a Ph.D. was a beacon of inspiration. Tragically, his life and dreams were cut short by an act of terror. Yet his spirit endures. This thesis not only honours his memory but also fulfils the dream he once held. Samer, your legacy is immortalized in these pages. Your absence is deeply felt, but your dream has been realized. Rest in peace, dear brother."

Mohammed

2024

Table of Contents

List of Figures

List of Tables

Abbreviations

E. coli	Escherichia coli
MS2	Emesvirus zinderi (Bacteriophage MS2)
NWs	Nanowires
SEM	Scanning electron microscopy
HRTEM	High resolution transmission electron microscopy
EDS	Energy-dispersive X-ray spectroscopy
XRD	X-ray powder diffraction
µCT	Microcomputed tomography equipment
DLS	Dynamic light scattering
ICP-OES	Inductively coupled plasma optical emission spectroscopy
FTIR	Fourier-transform infrared spectroscopy
MB	Methylene Blue
UV	Ultraviolet
UN ORG.	United nation organization
CNT	Carbon nanotube
1D	One dimension
VB	Valence band
CB	Conduction band
COD	Engine oil–seawater
EtOH	Ethanol
PVDF	Polyvinylidene
PS	Polystyrene
JCPDS	Joint Committee on Powder Diffraction Standards
RhB	Rhodamine B.
WHO	World Health Organization
LRV	Log reduction value
IEP	Isoelectric point
Gr	Graphene
MO	Methyl orange
g-C_3N_4	Graphitic carbon nitride
rGO	Reduced graphene oxide
PVA	Polyvinyl alcohol

IUPAC	International Union of Pure and Applied Chemistry
UNICEF	United Nations Children's Fund
CQDs	Carbon quantum dots
DIPA	DIPA Inc.

1. Introduction

Water is one of the world's most vital natural resources, essential for all living organisms' existence and humanity's growth [1]. About 2.5-3% of the Earth's water is freshwater; of this 3%, around 70% resides as ice, while the remaining 30% is groundwater, which can be difficult to access. By 2050, the global population is expected to exceed 9 billion; and by 2075, 75% of the world's population will have inadequate access to freshwater [2], due to growing populations, industrialization, and urbanization have all been related to extensive use of a wide range of pollutants. Additionally, product manufacturing industries are releasing numerous wastes that lead to contaminants accumulation in various ecosystems and environments [3]. These days, among the most hazardous contaminants in natural water sources are dyes and microorganism such as viruses and bacteria [4]. Dyes act as toxic pollutants responsible for a range of serious adverse effects, including drinking water poisoning and killing aquatic life. They are highly soluble in water, making them difficult to remove using conventional methods [5,6]. Meanwhile, waterborne contaminants (bacteria and viruses) cause various illnesses (e.g., diarrhea, gastrointestinal disease, etc.), ranging from mild, self-limiting illnesses to severe, fatal illnesses. According to the World Health Organization (WHO), every year, 2.9 million people, primarily children, die from water-related diseases [7], and every day, 4,000 children die as a result of contaminated water, according to an assessment by the United Nations Children's Fund (UNICEF) [8]. For that, various remediation techniques have been developed to remove these pollutants, including precipitation [9], flocculation [10], coagulation [11], ion exchange [12], and reverse osmosis [13]. Nevertheless, current water treatment methods are not effective enough to entirely remove all pollutants and still adhere to stringent quality requirements for the water supply [14]. In addition, these methods have several limitations, including high energy requirements, expensive, incomplete removal of pollutants, and generation of harmful sludge [15,16]. To solve this problem, nanotechnology offers a potential solution to purify water with a low cost and high efficiency [17]. The growth of nanotechnology and nanoscience has created new opportunities for water pollution cleanup. Due to their smaller size, high surface area to volume ratio, extremely reactive, high solution mobility, excellent mechanical properties, porosity, hydrophilicity, dispersibility, hydrophobicity, and outstanding chemical characteristics, nanotechnological routes are more efficient than traditional ones [11,18]. Several different treatment techniques have recently been developed to enhance the quality of treated wastewater. These include membrane separation, photocatalytic methods, and

adsorption using cheap materials [19]. Membrane technology is one of the wastewater treatment technologies that has expanded dramatically over the past two decades due to its advantages in water and wastewater treatment. Membrane technology offers various advantages for wastewater treatment, including significantly reducing equipment size, energy requirements, and capital costs [20]. Membrane-using adsorption techniques are considered the most promising method for removing pollutant ions from effluents. Many materials, including activated carbons [21], clay minerals [22], chelating materials [23], and chitosan/natural zeolites [24], have been studied for their ability to adsorb metal ions from aqueous solutions. However, low sorption capacities and efficiencies severely limit their applicability [25].

Recently, cellulose-based nanomaterials have been investigated as promising materials that can be used partly or totally as membranes or support for other materials during water treatment to remove pollutant ions [26,27]. Furthermore, cellulose has outstanding properties such as non-toxic, renewability, biodegradability, hydrophilicity, simple processing, and inexpensive, in contrast to other supports, improving nanoparticle's stability, reactivity, and reusability, then inhibiting their agglomeration [28,29]. Attributed to its chemical structure and characteristics, porosity, and hydrophilicity, it can store a lot of water and transfer oxygen and nutrients efficiently. Hence, cellulose offers the optimal environment for bacterial development. Using antibacterial materials to modify cellulose is extensively investigated to solve this issue [30,31,32,33]. Most metal and metal oxide nanoparticles, such as gold (Au), silver (Ag), copper (Cu), tungsten oxide (WO_3), titania (TiO_2), and zinc oxide (ZnO) have gained more attention due to optical, electrical, conductivity, catalytic, and antimicrobial properties suitable for different applications [34,35,36,37,38,39]. They are also often used as photocatalysts to decompose organic compounds [40]. Several semiconductors have been developed as photocatalysts in the past few decades, among them titanium dioxide (TiO_2) and tungsten trioxide (WO_3) [41,42]. TiO_2 and WO_3 are often used and widely studied photocatalytic materials due to their inexpensive, availability, good chemical stability, photocatalytic activity, and low toxicity [43, 44].

This dissertation focuses on the synthesis of novel nanowire-based hybrid membranes using cellulose as a reinforcement material for different applications in the removal of bacteria (such as *E. coli*), the removal of viruses (such as MS2), and organic dyes (such as methylene blue). The main objectives of this dissertation are as follows:

a) Preparation of TiO_2 NWs and WO_3 NWs by the hydrothermal method and using Fe_2O_3 and CuO as additives to fabricate different types of composites (Fe_2O_3/TiO_2 NW, CuO/TiO_2 NW, Fe_2O_3/WO_3 NW, and CuO/WO_3 NW) to improve the photocatalytic, antibacterial, and antiviral properties of the nanowires. Nanowires and composites were widely investigated using different modern characterization techniques.
b) Synthesis of TiO_2 NWs and WO_3 NWs-based hybrid membranes using cellulose as matrix reinforcement material. Four types of hybrid membranes were produced by vacuum filtration. The as-prepared membranes were characterized using scanning electron microscopy (SEM), energy-dispersive X-ray spectroscopy (EDS), Raman spectroscopy, X-ray powder diffraction (XRD), microcomputed tomography equipment (μCT), dynamic light scattering (DLS), Inductively coupled optical emission spectrometry (ICP-OES), specific surface area and toxicology measurements.
c) The performance of the hybrid membranes in the decolorization of methylene blue (MB) under UV irradiation, the removal of MS2, and the removal of Escherichia coli (*E. coli*) were studied and presented.

2. Literature review and knowledge gap

The world faces many problems and one of them to need for more clean and fresh water. The World Economic Forum 2019 identified freshwater scarcity as one of the biggest global threats with prospective effects over the next ten years [45]. Consequently, according to UN Water ORG, 1.8 billion people live without enough water for everyone, and two-thirds of the world's population will live in places with water scarcity by 2025. Due to having little or no hygienic water, millions die yearly from diseases that spread through unsafe water [46,47]. As a result, the world's water scarcity problem necessitates highly efficient, highly sustainable water treatment techniques [48]. Many strategies and alternative water treatment techniques have been developed in the pursuit of sustainability; nevertheless, research has demonstrated the ineffectiveness of these water treatment techniques [49]. Nanomaterials such as (TiO_2, ZnO, Ag, WO_3, and carbon nanotube (CNT)) have gained remarkable attention in water and wastewater treatment applications due to their unique properties, for instance, their ability to adsorb a wide variety of pollutants efficiently [50]. However, using some nanomaterials in water treatment has limitations, such as agglomeration tendency, difficulty in isolation and

recovery from aqueous solutions for reuse, and toxicity [51]. To address this problem, nanomaterials can be improved using other materials [52,53].

2.1 TiO_2 NWs-based composites and membranes in water treatment

Titanium dioxide (TiO_2) has attracted much attention and study as a material in the last three decades, due to its chemical and photostability, availability, biocompatibility, nontoxic, cheap, physical, optical, and electrical qualities [54,55]. It generally exists in three forms, namely anatase, rutile, and brookite as shown in Figure 1 [56]. The rutile phase of TiO_2 is stable at high temperatures, whereas the anatase phase is stable at low temperatures. The brookite phase is uncommon and unstable [57]. The crystal structure of TiO_2 influences its photocatalytic activity. The anatase phase possesses the highest photocatalytic activity of all TiO_2 semiconductor phases [57]. Furthermore, anatase has a higher adsorptive affinity for organic substances and lower rates of recombination than rutile due to its 10-fold higher rate of hole trapping [58]. Besides, rutile has a lower band gap of 3.0 eV than anatase, which means each TiO_2 form has limitations. A commercial phase of TiO_2 named P25 has been used in many applications containing anatase and rutile combinations [59]. Hu et al. have comparatively studied the adsorption and photocatalytic degradation of TiO_2 anatase, rutile nanowires, and P25 against 15 pharmaceuticals in water, and the results show anatase nanowires have higher adsorption activity toward some pharmaceuticals. In comparison, rutile nanowires have higher adsorption activity toward another, and both nanowire phases have higher adsorption activity than P25 [60]. The effect of calcination on photocatalytic performance of TiO_2 NWs has been investigated by Wu et al.; the result shows the photocatalytic degradation of calcinated TiO_2 NWs against RhB higher than TiO_2 NWs without calcination [61].

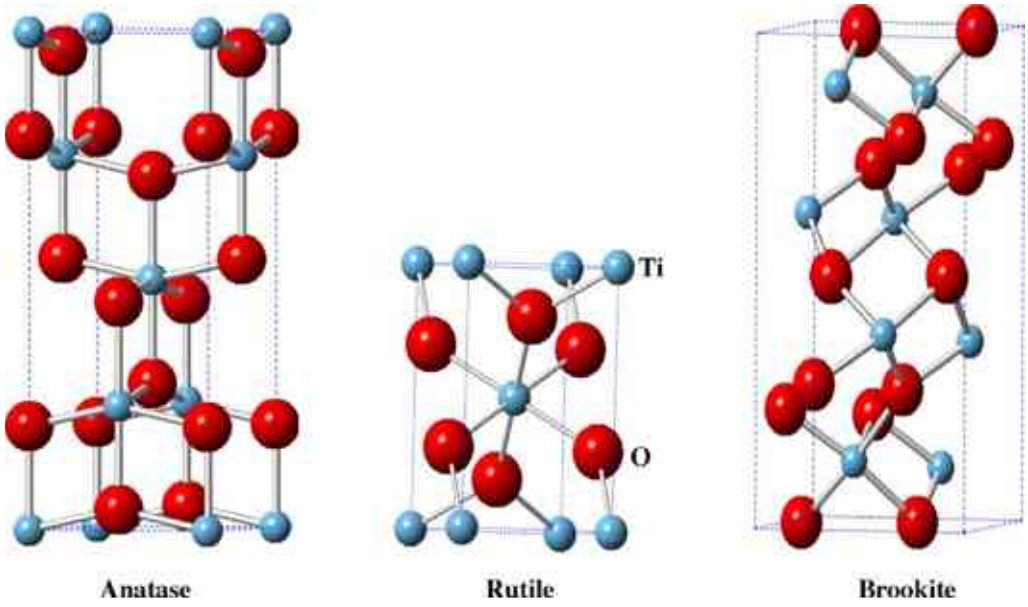

Figure 1. Crystal structure of TiO_2, adopted from [57]

TiO_2 is one of the most effective photocatalysts, exhibiting photoinduced bacterial and viral disinfection, organic pollutant photodegradation, and self-cleaning characteristics [62]. However, some drawbacks limit to use in water and wastewater treatment, such as rapid recombination of photogenerated electron-hole pairs due to its wide band gap, and difficult separation from water [63]. Nataraj et al. have investigated the antimicrobial activity of different TiO_2 morphologies, including wires and particles, against the gram-positive bacterium Staphylococcus aureus. The results demonstrated that nanowires were more active than nanoparticles under UV light [64]. Another study investigated the photocatalytic activity of TiO_2 P25 and nanowires toward organic dyes (methylene blue and methyl orange), and they found that nanowires have higher photocatalytic performance than P25 [65]. In this regard, 1D TiO_2 nanowires have been identified as a suitable photocatalyst to boost photocatalytic performance and expand application fields because of their unique 1D morphology, high specific surface area, and outstanding physical and chemical properties that enhance the separation of electron-hole pairs and electron transport [66]. Different methods have been developed to prepare TiO_2 nanowires, such as hydrothermal [67,68], chemical vapor deposition [69], electrospinning [70], and solvothermal [71]. Among them, the hydrothermal technique is one of the most effective due to its low energy requirements, low cost, ecological footprint, and easy adaption to mass production [72].

Preparation of TiO_2 NWs using the hydrothermal method depends on many factors, among them alkaline type and concentration, reaction time and temperature and annealing temperature as reported in previous studies such as Le et al. synthesized TiO_2 NWs using 10 M KOH for 24 h reaction time at 190 °C and annealed the final product at 400 °C for 30 min, the diameter and length ranges were 10-20 nm and 700-800 nm respectively [73]. Turki et al. prepared titanite nanowires using 12.5 M KOH under 155 °C for 24 h and investigated photodegradation performance towards formic acid using different annealed temperatures (400, 500, 600 and 700 °C) for 2 h in air; they found the nanowires with an annealed temperature 400 °C showed higher photodegradation activity than other samples [74]. Półrolniczak and Walkowiak synthesized TiO_2 NWs using NaOH and studied the effect of reaction temperature (110, 130, 150, 170 and 200 °C), calcination temperature (400, 600 °C), hydrothermal reaction time (24, 48, 72 and 96 h) and NaOH concentration (5, 10 and 15 M) on the NW structure. They demonstrated that the reaction temperature below 130 °C did not change the morphology; the TiO_2 NW morphology started to change at 150 °C from nanoparticle to nanowire, and with increasing temperature, the morphology didn't change, just the aspect ratio increased; the diameter and length were 60-180 nm, 2-4 μm at 150 °C became thinner 40-100 nm and longer 2-6 μm at 200 °C. The calcination temperature has an impact on TiO_2 NW; it can be observed that the NW morphology turns to irregular aggregation when the calcination temperature increases from 400 °C to 600 °C. While the reaction time doesn't change the NW morphology in the range of 24-72 h and above 72 h, the NW morphology appeared as some nanoparticles attached to the NW surface. Finally, the NaOH concentrations have a strong effect on NW morphology, at 5M, the NW shows irregular particles; increasing to 10 M the NW appears with a diameter range of 40-120 nm and 2 μm length; when the NaOH concentration increases to 15 M, the NW elongates to 6 μm. They conclude that the optimum operating conditions for TiO_2 NW preparation are a reaction temperature 150-200 °C, calcination temperature 400 °C, reaction time 24-72 h, and a NaOH concentration 10 M [75]. In another study, Hamisu et al. prepared TiO_2 NW using 10 M of different alkaline solvents (KOH, NaOH and NH_4OH) with a reaction temperature of 180 °C for 24 h. They investigated their degradation efficiency against MB under UV light. The results show that TiO_2 NW prepared using KOH has a higher photodegradation activity than others [76].

With outstanding properties, TiO_2 NWs are used in many applications, especially water treatment. For instance, Youssef and Malhat prepared TiO_2 NWs using the hydrothermal method as an adsorbent material to remove different types of heavy metals Pb^{2+}, Cu^{2+}, Fe^{3+}, Cd^{2+}, and Zn^{2+}) from contaminated water; they found that the adsorption efficiency was (97.06, 75.24, 79.77, 64.89, and 35.18%, respectively [77]. In another study, Saleh et al. prepared and investigated the adsorption ability of TiO_2 NWs toward Pb^{2+} and antimicrobial activity in a dark environment. The results demonstrated that the prepared nanowires performed adequately against gram-negative and gram-positive bacteria. Additionally, it was observed that the nanowires are significantly more active against gram-negative than gram-positive bacteria [78].

Photocatalysis is an advanced oxidation process involving light absorption by semiconductors (e.g., TiO_2) to generate highly reactive hydroxyl radicals ($OH^{\cdot}$). A semiconductor contains a valence band (VB) and a conduction band (CB). The band gap is the energy difference between these two levels, with an energy less than 3.5 V. Without excitation, electrons and holes are in the valence band. When a semiconductor surface is exposed to light ($h\nu$), electrons (e^-) are transported from the valence band to the conduction band, leaving behind holes (h^+) in the valence band and forming electron-hole pairs as shown in eq. (1):

$$\boldsymbol{TiO_2 + h\nu(UV) \longrightarrow TiO_2\left(e^-(CB) + h^+(VB)\right)} \qquad (\mathbf{1})$$

The photogenerated valence band holes (h^+) react with water to form the ($OH^{\cdot}$**)** radical eq. (2). The ($OH^{\cdot}$**)** radical is a highly strong oxidizing agent.

$$\mathbf{H_2O(ads) + h^+(VB) \longrightarrow OH^{\cdot}(ads) + H^+(ads)} \qquad (\mathbf{2})$$

At the same time, the conduction band electrons (e^-) may contribute to the reduction of O_2 molecules in the air absorbed by the TiO_2 surface, leading to the formation of peroxyl radicals ($O_2^{-\cdot}$) eq. (3). In turn, these photogenerated ($OH^{\cdot}$) ($O_2^{-\cdot}$) radicals degrade and oxidize adsorbed organic/inorganic compounds, microorganisms, and those close to the catalyst surface. The photocatalytic mechanism of TiO_2 is illustrated in Figure 2 [79,80].

$$\mathbf{O_2 + e^-(CB) \longrightarrow O_2^{-\cdot}(ads)} \qquad (\mathbf{3})$$

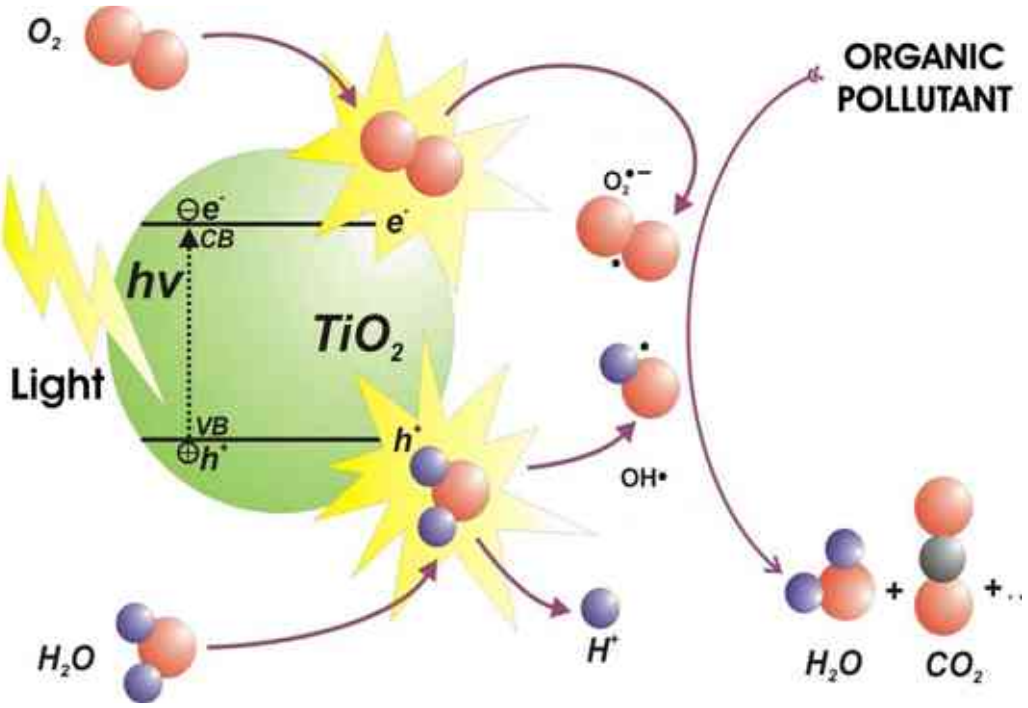

Figure 2. Schematic diagram of photocatalysis mechanism, adopted from [81]

Because of the broad band gap of TiO_2 anatase (3.2 eV), it can only absorb (3-5%) of ultraviolet light. Decorating titania with a narrow band gap semiconductor is a potentially effective method to avoid this issue, such as WO_3 [82], MoS_2 [83], and Fe_2O_3 [84, 85, 86]. Some studies used TiO_2 NWs as follows: Youssef et al. prepared a TiO_2 NWs/PS nanocomposite to remove different types of pesticides from contaminated water and demonstrated that the nanocomposite has a higher removal performance than pristine TiO_2 and PS. [87]. Xie et al. made TiO_2 NWs/Ag_2S nanocomposite and investigated photodegradation activity toward MO, and the result prove nanocomposite has higher catalytic efficiency than P25 under visible light [88]. Safajou et al. prepared nanocomposite by loading Gr/Pd on TiO_2 (nanowire and nanoparticle) and then investigated the photocatalytic degradation of these nanocomposites against RhB; the result shows the nanowire decorated on Gr/Pd nanocomposite higher degradation performance than a nanoparticle [89]. However, the recovery and reuse of materials from aqueous solution is still a problem. To solve this issue is to use a substrate or membrane technique. Membrane filtration is a common approach for eliminating water contaminants from the environment since it is a low-energy method, even at low water pollution levels. Hu et al. synthesized TiO_2 NWs

on the Ti substrate membrane and investigated the effect of UV light on degradation activity; they found that the degradation efficiency of the membrane with light was higher than in the dark environment [90]. In a recent study, Giuffrida et al. investigated enhanced photocatalytic properties of doped and undoped TiO_2 NWs synthesized on Ti substrate in the visible light range. They found that the photoactivity of doped and undoped TiO_2 NWs shows enhancement toward MB dye degradation under visible light [91]. The drawback of membrane filtering is that it produces sludge, which is difficult and expensive to dispose of. One possible solution to this undesirable phenomenon is to combine the photocatalytic with the membrane filtering process. Therefore, in the presence of UV light, photocatalytic membrane processes can degrade pollutants in feed solutions by creating reactive oxygen species, preventing the formation of a cake layer from contaminant molecules on the membrane surface by destroying traces of contaminants adhering to the surface [42,92]. Liang et al. evaluated the adsorption and photocatalytic degradation ability of TiO_2 NWs filtration membrane against Congo red dye pollutant; the results confirmed that membrane filtration degradation activity under UV light was higher than in the dark [93]. Rao et al. prepared and evaluated the antimicrobial activity of TiO_2 NWs and TiO_2 NWs/Cu membranes against *E. coli* and bacteriophages MS2 using dark and UV light; the result demonstrated that TiO_2 NWs/Cu membrane has higher antimicrobial efficiency under UV light than dark mode [94]. Unfortunately, most bacterial and viral illnesses occur indoors, making photocatalytic membranes inactive [95]. Due to the development of nanotechnology, several nanoparticles are considered promising for use as antimicrobial or antibacterial agents, such as copper oxide (CuO) and iron oxide (Fe_2O_3) [96]. Copper (II) oxide (CuO), one of the most common and cheap transition metal oxides, has been used in numerous aspects because of its narrow band gap, such as to remove organic pollutants using photocatalysis, an excellent antibacterial agent and as a catalytic material [97]. Sreeju et al. investigated the catalytic degradation of CuO NPs toward different organic dyes and antibacterial activity; the results reveal that CuO has remarkable catalytic degradation and superior bactericidal activity [97]. Hajipour et al. prepared a nanocomposite containing TiO_2/CuO and evaluated antibacterial and photocatalytic degradation under visible light; the findings show that the amount of CuO loading greatly enhances the antibacterial and photodegradation performance, which means an increase in CuO loading leads to an increase in the antibacterial and photodegradation activities [96]. In the same context, iron (III) oxide (Fe_2O_3) nanoparticles have attracted increasing interest in photocatalytic decontamination owing to their low cost, stability, nontoxicity, large specific surface area, and especially strong absorption in the visible light spectrum [98]. Liu et al. studied the photocatalytic degradation

of dibutyl phthalate (DBP) using Fe_2O_3 nanoparticles under different operating conditions; the results reveal that Fe_2O_3 nanoparticles show high photodegradation activity in the presence of H_2O_2 under 120 min of visible light [99]. Additionally, Fe_2O_3 has a significant ability to create heterojunction areas when mixed with TiO_2. In this combination, additional shallow trap sites between the conduction and valance bands appear, reducing the band gap energy of TiO_2 [100]. Cao et al. investigated the effect of Fe_2O_3 on the photocatalytic performance of TiO_2 and found that the photodegradation activity of TiO_2/Fe_2O_3 nanocomposite against MO was higher than pristine TiO_2 [101]. Furthermore, this oxide is noteworthy because it possesses nanoscale magnetic characteristics that can enhance the recyclability of photocatalysts and avoid particle clumping [42,102]. Other studies use Fe_2O_3/TiO_2 and CuO/TiO_2 to enhance photocatalytic performance against organic dyes, especially MB. For instance, Simamora et al. prepared CuO/TiO_2 NPs and investigated the photocatalytic activity towards MB; the results show 86% of MB degraded under 5h of UV irradiation light [103]. Li et al. evaluated the photodegradation of MB using Fe_2O_3/TiO_2 ceramic nanopowder under UV light, and they found the photodegradation rate was 83% in 5h [104]. Recently, Ma et al. loaded CuO NPs on TiO_2 nanomeshes and investigated the photodegradation activity against MB under 120 min of visible light; the result shows the photodegradation efficiency was 35% [105]. Another study investigated the photodegradation performance of the green synthesis of CuO/TiO_2 nanocomposite and found the green synthesis nanocomposite was more efficient than that prepared chemically under visible light [106]. A'srai et al. used CuO/TiO_2 nanocomposite as a photocatalyst for degraded MB under 180 min UV light and found the photodegradation rate was 95.47% [107]. Many studies have reported that modification of TiO_2 NWs with different metal and metal oxides enhances their ability to remove various pollutants, as summarized in Table 1.

Table 1. Removal ability of TiO_2 NWs based composite materials and membranes.

No.	Composite	Light source	Pollutant	Results	Ref.	Note
1	TiO_2 NWs (powder)	UV (50 min)	Rhodamine B (RhB)	90 %	[61]	
2	TiO_2 NWs (powder)	Dark	Pb^{2+} Cu^{2+} Fe^{3+} Cd^{2+} Zn^{2+}	97.06 % 75.24 % 79.77 % 64.89 % 35.18 %	[77]	
3	TiO_2 NWs/PS (composite)	Dark	Organochlorine pesticide (OCPs)	98.64%	[87]	
4	TiO_2 NWs/Cu (membrane)	UV (30 min)	*E. coli* MS2	99.99 % 99.99 %	[94]	Filtration
5	TiO_2 NWs/Cu (membrane)	Dark	*E. coli* MS2	~ 40 % ~ 25 %	[94]	Filtration
6	TiO_2 NWs/rGO (composite)	UV (5 h)	COD	98.6%	[66]	
7	TiO_2 NWs/MnO_2 (composite)	UV Visible light Infrared	Rhodamine B (RhB)	83 % 73 % 90.5 %	[108]	180 min
8	TiO_2 NWs (powder)	UV (6 h)	Azo dye AR 30	78.1%	[109]	
9	TiO_2 NWs/Ag (composite)	UV (80 min)	Methylene Blue (MB)	99 %	[110]	
10	TiO_2 NWs (powder)	UV (120 min)	Degradation of naphthalene	98.2 %	[111]	
11	TiO_2 NWs/CNT (membrane)	Sunlight (80-150 min)	Pathogens Organic compounds	75%	[112]	
12	TiO_2 NWs deposited on Ti plate. (membrane)	UV (4 h)	Methyl Orange (MO)	84 %	[113]	
13	TiO_2 NWs on Ti foil coated Au (membrane)	UV (3 h)	Methylene Blue (MB)	70 %	[114]	
14	TiO_2 NWs (powder)	Solar light (60 min)	Methylene Blue (MB)	89 %	[115]	
15	TiO_2 NWs (membrane)	UV (60 min)	Methylene Blue (MB) *E. coli*	~ 99 % 99.9 %	[116]	

16	TiO_2 NWs (membrane)	UV (90 min)	Humic acid	99.5 %	[117]	
17	TiO_2 NWs/rGo/cellulose acetate (membrane)	Visible light (120 min)	Methylene Blue (MB)	98 %	[118]	
18	TiO_2 NWs on Ti foil (membrane)	UV (60 min)	Trimethoprim	85 %	[90]	
19	g-C_3-N_4@TiO_2 NWs/GO (membrane)	Solar light (240 min)	Rhodamine 6G (R6G)	91 %	[119]	
20	TiO_2 NWs/synthetic zeolite (composite)	UV (180 min)	Methylene Blue (MB)	90 %	[120]	

2.2. WO_3 NWs-based composites and membranes in water treatment

WO_3 is one of the promising semiconductors with outstanding properties, such as low toxicity, inexpensive, high stability, a narrow band gap (2.4-2.8 eV) [121], high photocorrosion stability, reliable recyclability performance and physicochemical characteristics [122]; due to remarkable features, it has been investigated in many fields such as photocatalysis [123,124] water splitting [125] and gas sensor applications [126]. Among them, the photocatalytic decomposition of organic pollutants is one of the most important applications due to its high activity, better visible light absorption and being environmentally friendly [127]. Abbaspoor et al. evaluated the photocatalytic activity of WO_3 NPs against MB, and the result showed the degradation activity was 57.3 % underexposed light for 150 min [128]. Fularz et al. investigated the catalytic performance of WO_3 NWs/Ag nanocomposite compared with TiO_2/Ag nanocomposite in the visible light range. They found that WO_3 NWs/Ag is more efficient due to a lower band gap [129]. In another study, Arshad et al. studied the photocatalytic performance of Zn-doped WO_3 for MB removal using UV and visible light; the result shows the dye degradation was 78 % and 92 % under 120 min of visible light and UV, respectively [130]. However, WO_3 photocatalyst has particular limitations, such as the rapid recombination rate of photogenerated electron-hole pairs; compared to the O_2/O_2^- reduction potential, it has a more positive conduction band level, which results in a reduction of fewer O_2 molecules into superoxide anion free radicals ($O_2^{\bullet-}$) during the photocatalytic process and low specific surface

area [131,132] Many methods for overcoming these limitations have been revealed, including manipulation with metal or metal oxide, Matalkeh et al. prepared WO_3/Ag nanocomposite and investigated the degradation activity against MB as an organic dye model and antibacterial performance under light and dark conditions. The results show the WO_3/Ag nanocomposite has higher MB degradation and antibacterial activity on gram-negative bacteria (*E. coli*) than gram-positive bacteria (*S. aureus*) in the presence of visible light [133]. Sun et al. prepared ternary WO_3/TiO_2/CQDs nanocomposites and evaluated the photocatalytic degradation activity on an antibiotic (cephalexin) under solar light for 4 h, and they found that the ternary nanocomposites had higher activity than TiO_2 and WO_3 [134], and/or fabricating 1D WO_3 nanostructured to enhance the specific surface area and promote charge transfer, such as nanowires [135]. Different methods have been used to prepare WO_3 NW, such as hydrothermal [136], solvothermal [137], water bath [138], microwave assisted hydrothermal [139], bubble-electrospinning [140], and vapor-phase growth [141]. Hydrothermal and solvothermal methods are frequently used in the preparation of 1D nanostructures because the generated temperature and pressure inside the autoclave above the solvent's critical point make the materials more soluble [142], in addition to low processing cost and simplicity [143]. Nagy et al. conducted a comparative study for photocatalytic performance between WO_3 NWs and NPs to remove MO; the results demonstrated that WO_3 NWs have a significantly higher MO photodegradation than WO_3 NPs [144]. Different operating conditions can influence WO_3 NW preparation, such as reaction temperature, time of reaction, and type of salts used, as presented in earlier studies. Song et al. prepared WO_3 NW using sodium tungstate Na_2WO_4 as a precursor with reaction temperature 180 °C for 12 h in the presence of K_2SO_4; the results show that nanowires can't be obtained without K_2SO_4. In addition, they investigated the effect of reaction temperature on NW synthesis and found that at 160 °C no nanowire appeared, just nanorods, and concluded that nanowires were observed in the reaction temperature range 180-200 °C. In the same study, they investigated the effect of different inorganic salts, such as $NaNO_3$, KNO_3 and Na_2SO_4, on NW synthesis. The results demonstrate that nanowires can't be observed using these salts [145]. Tehrani et al. investigated the effect of different reaction times (6, 12, 24 and 36 h) on WO_3 nanostructures; they used sodium tungstate, sodium sulfate as starting materials, citric acid and hydrochloric acid. The results show that an irregular shape was observed with a (6 h) reaction time; with further reaction time (12 h), a few nanorods appeared, and then the nanorod became clearly observed with a (24 h). After that, the WO_3 nanostructures change to a 2D sheet with reaction time (36 h) [136]. In another study, Jamali and Tehrani investigated the effect of reaction temperature on WO_3 nanostructures; they found that increasing temperature from 90

to 180 °C for 48 h, the WO_3 nanostructures were observed as nanorods and only changed in length from 50 nm to 272 nm and diameter from 15 nm to 46 nm [146].

As mentioned earlier, WO_3 NW cannot be used alone because of the narrow band gap; consequently, it is limited to use as a photocatalyst. In order to improve photocatalytic performance and manipulate the band gap structure, the WO_3 NWs is often combined with other metals and metal oxide. Mao et al. synthesized and evaluated the photocatalytic performance of WO_3 NWs, g-C_3N_4, and rGO and their composites to remove refractory natural pollutants. The results demonstrated that WO_3 NWs/g-C_3N_4/rGO has higher degradation removal after 120 min [147]. Zhou et al. studied the photocatalytic oxygen (O_2) evolution properties of WO_3 NWs/Gr and pure WO_3 NWs by measuring the amount of evolved oxygen produced by splitting water. After 8 hours, the amount of evolved O_2 for WO_3 NWs/Gr was 1.9 times higher than for pure WO_3 NWs [148]. In an oil/water emulsion separation application, Zhou et al. studied the filtration efficiency of the WO_3 NWs/Al_2O_3 membrane. They found that the membrane has a higher separation efficiency of up to 92.35 %, and the separation efficiency after 10 cycles is maintained at 88 % when immersing the membrane in strong alkaline, acidic, and saline solutions for 24 hours [149]. Among metal oxides, copper and iron oxides are widely employed due to their photodegradation and antimicrobial activities and to enhance photocatalytic performance by expanding the photoabsorption range, improving the separation of electron-hole pairs with photoinduced activity, and enhancing the visible-light range activity [68]. Dulta et al. investigated the photodegradation and antibacterial performances of CuO NPs against MB and methyl red under sunlight, and the results show CuO has high photodegradation and antibacterial activity [150]. To investigate effect of CuO on the adsorption and photocatalysis of WO_3 performance, Dursun et al. conducted a comparative study between WO_3/CuO nanocomposite and pure WO_3 to evaluate adsorption and photocatalysis against MB; the results confirmed that nanocomposite could absorb 38.4% more methylene blue dye and degrade 25.7% faster than pure WO_3 [151]. Senthil et al. studied the photodegradation of WO_3 nanorods decorated with Fe_2O_3 NPs against MB under visible light; the results demonstrated that the degradation activity of WO_3/Fe_2O_3 nanocomposite under 60 min of visible light was 79.5 % while it was 17.2 % and 46.2 % for Fe_2O_3 and WO_3, respectively [152]. Based on the studies shown above, WO_3 NWs have been found to have a substantially higher photocatalytic performance than WO_3 NPs due to a large aspect ratio. [153]; for this, it is used in some studies as a photocatalyst for water treatment, as summarized in Table 2.

Table 2. Removal ability of WO_3 NWs based composite materials and membranes.

No.	Composite	Light source	Pollutant	Results	Ref.	Note
1	S-doped WO_3 NWs (composite)	Visible light (180 min)	Methyl Orange (MO)	97 %	[154]	
2	Mo-doped WO_3 NWs (composite)	Dark	Methylene Blue (MB)	95 %	[155]	Adsorption (10 min)
3	WO_3 NWs/rGO/g-C_3N_4 (composite)	Visible light (120 min)	Aflatoxins B1 (AFB_1)	92 %	[149]	
4	WO_3 NWs/Al_2O_3 (membrane)	Dark	Oil/water emulsions	92 %	[151]	Filtration
5	WO_3 NWs@C/g-C_3N_4 (composite)	Visible light (160 min)	Methylene Blue (MB) Crystal violet dye Benzoic acid	91 % 94 % 62 %	[156]	
6	WO_3 NWs/TiO_2 (composite)	Visible light (230 min)	Methyl Orange (MO)	65 %	[146]	
7	WO_3 NWs (powder)	Visible light (230 min)	Methyl Orange (MO)	12 %	[146]	

2.3. Cellulose as membrane reinforcement in water treatment

Over the past few decades, researchers and companies have shown a rising interest in exploring the potential of polymeric and composite materials derived from sustainable resources [157,158,159,160]. Cellulose is a sustainable supply of the polymer basic cellulose found in the highest concentrations in green plants. Natural cellulose-based materials, including wood and natural fibers, have been utilized as engineering materials for thousands of years, and this use continues to this day [161]. Cellulose is cheap, accessible, biodegradable and the most common abundant organic biopolymer found natural on Earth [162]. It has been proposed to be an excellent supporting material due to its good mechanical properties, and practically limitless supply of raw materials to meet the growing demand for biocompatible,

biodegradable, cost-effective, and ecological products [163]. It possesses a complex carbohydrate (molecular formula $(C_6H_{10}O_5)_n$) composed of carbon, hydrogen, and oxygen, as shown in Figure 3.

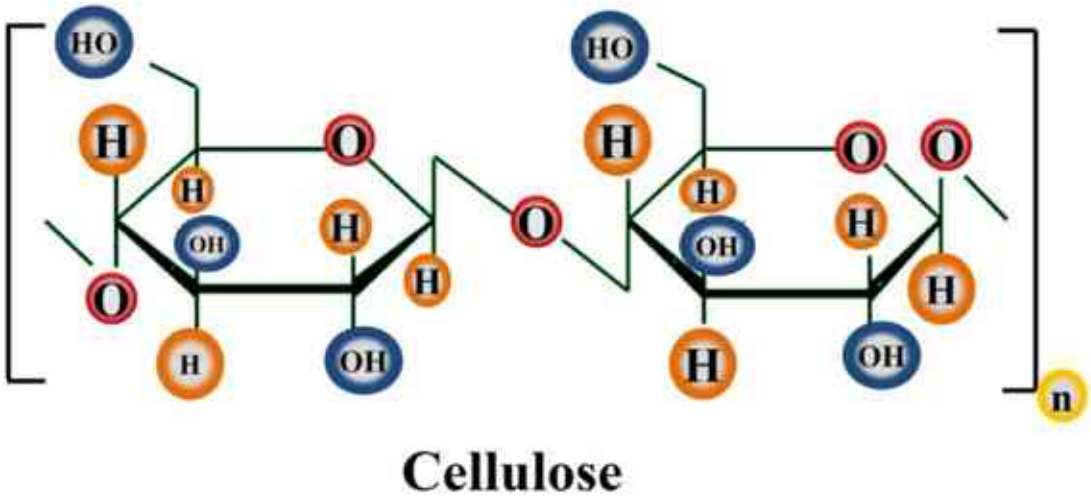

Figure 3. Structural formula of cellulose [174]

Xu et al. investigated the photodegradation of RhB using cellulose waste and cellulose modified by acid under visible light; they found cellulose waste has poor photodegradation activity and can be enhanced when treated with acid [164]. Due to the abundance of electron-rich hydroxyl groups, cellulose is highly hydrophilic and contributes to the interaction with photocatalysts *via* hydrogen bonding and electrostatic interactions. Moreover, strong interactions between electron-rich oxygen atoms of hydroxyl groups in cellulose and transition metal cations as contaminants can aid in removing these cations from wastewater, making it a promising candidate for supporting the nanomaterials with the photocatalysis process [165]. Bai et al. fabricated cellulose using g-C_3N_4 and investigated the adsorption and photodegradation performance toward MB through visible light; they found cellulose/g-C_3N_4 exhibited excellent adsorption and photocatalytic activity (99.8%) much higher than pristine g-C_3N_4 (54.2%) [166]. Numerous studies reported that using inorganic nanomaterials has some limitations as a photocatalyst, such as higher recombination rate, agglomeration, difficult separation and leaching when metal ions dissolve in the liquid [167,168,169]. Cellulose-immobilized photocatalysts improve the separation of electron-hole pairs to limit secondary pollutants and reduce the band gap by hindering the recombination rate of photogenerated charge carriers, leading to increased transmission of photoexcited charge carriers and improved

photoefficiency. Also, cellulose binds with catalysts, metal ions, and toxins in the solution, reducing the catalysts' loss, leaching, and toxic effects [170]. Morshed et al. prepared and dispersed titania on cellulose and investigated the degradation activity toward MB under UV light; the result shows that the cellulose/TiO_2 photodegradation was 98.5% in 40 min [171]. Qi et al. formed 2D-WO_3 with cellulose acetate and investigated the degradation performance against MB under sunlight; the results exhibit excellent degradation activity of 2D-WO_3/cellulose acetate with an 85% removal rate [172]. The optical dispersion property of cellulose-based membrane facilitates electron distribution and transfer to metal oxide surface and the interaction covalent bond chain of metal oxide nanoparticles with cellulose. Moreover, acts as a capping agent, avoiding nanoparticle aggregation and enhancing photocatalyst performance [170]. Table 3 summarizes the usage of cellulose in water treatment application.

Table 3. Cellulose-based composite materials and membranes for contaminants removal

No.	Composite	Light source	Pollutant	Results	Ref.	Note
1	Cellulose modified with acid	Visible light	RhB	90 %	[166]	120 min
2	Cellulose/TiO_2	UV	Methylene blue (MB)	98 %	[172]	40 min
3	Cellulose/PVA/TiO_2	Sunlight	Methylene blue (MB)	98 %	[173]	120 min
4	Al-doped ZnO/Cellulose	Visible light	Methyl orange (MO)	90 %	[174]	6 h
5	g-C_3N_4/Cellulose	Visible light	Methylene blue (MB)	99 %	[168]	80 min
6	Cellulose/MoS_2	Visible light	Rhodamine B (RhB)	96 %	[175]	60 min
7	Cellulose/Ag_3PO_4	Visible light	Rhodamine B (RhB)	96 %	[176]	60 min
8	Cellulose/TiO_2	Weak UV	Phenol	90 %	[177]	120 h
9	FeOOH-Cellulose-TiO_2	Adsorption	Pb (II)	98 %	[178]	30 min

2.4. Knowledge gap

- As can be seen and concluded from the literature review, numerous studies and journal papers have studied the fabrication and application of TiO_2 NWs using different metal and metal oxide composites such as (MnO_2, rGO, Ag, and Cu) for different photocatalytic applications. However, a limited number of studies have reported the fabrication and investigation of TiO_2 NWs utilizing cellulose as a reinforcement material. Hence, it is worth exploring the synthesis and characterization of TiO_2 NWs decorated with inorganic nanoparticles (Fe_2O_3, CuO) using cellulose as a support material and investigating their photodecolorization performance against MB.

- Furthermore, there is limited research on the antibacterial and antiviral applicability of TiO_2 NWs-based hybrid membranes as filters using light sources (UV, visible light, and infrared). However, the antibacterial and antiviral activity of TiO_2 NWs-based hybrid membrane in the dark environment, the effect of inorganic nanoparticles attached to TiO_2 NWs surface, and the surface charge of membrane surface on the performance have yet to be reported.

- On the other hand, a few studies have investigated the photocatalytic performance of WO_3 NWs-based composites. In contrast, there has been no study on fabricating WO_3 NWs with inorganic nanoparticles (Fe_2O_3, CuO) and cellulose as reinforcement support material and using it as a filter. Furthermore, the antibacterial and antiviral activity of these filters has not been reported yet.

3. Objectives

The main goal of the current work is to develop low-cost, effective membrane materials for water treatment methods derived from abundant, sustainable, and renewable resources that can be easily prepared. Therefore, stable and self-supported (Fe_2O_3/TiO_2 NWs/cellulose, CuO/TiO_2 NWs/cellulose, Fe_2O_3/WO_3 NWs/cellulose and CuO/WO_3 NWs/cellulose) membranes constituted of TiO_2 NWs and WO_3 NWs as a material with high adsorption capacity, Fe_2O_3 and CuO as a photocatalyst, and cellulose as a support material with good mechanical strength

and high hydrophilic properties was produced. We investigated the antiviral, antibacterial, and photodecolorization properties of as-prepared hybrid membranes.

During the research work, we wanted to answer the following questions:

1- Is it possible to synthesis a self-supported membrane using nanowires and cellulose as support materials?
2- What could be the effect of applying the inorganic nanoparticles (Fe_2O_3, CuO) on the performance of nanowires-based membrane?
3- What is the chemical interaction between membrane components?
4- Does the inorganic nanoparticles effect on the surface charge of as-prepared membrane?
5- Does the leaching affect the performance of the membrane? What are the amounts of metal ions dissolved through the filtration process? The concentrations of these metal ions are under the WHO's limitations?
6- Do the membranes have a toxic release?

The current thesis consists of three main parts:

1- **The first part is the preparation:** the preparation consisted of the three parts listed below:
   a- The first part is the synthesis of the TiO_2 NWs and WO_3 NWs, which was achieved by the hydrothermal method.
   b- The second part is the synthesis of the Fe_2O_3/TiO_2 NWs, CuO/TiO_2 NWs, Fe_2O_3/WO_3 NWs and CuO/WO_3 NWs composites, which was achieved by hydrothermal/solvothermal preparation methods.
   c- In the third part, the Fe_2O_3/TiO_2 NWs/cellulose, CuO/TiO_2 NWs/cellulose, Fe_2O_3/WO_3 NWs/cellulose and CuO/WO_3 NWs/cellulose hybrid membranes were produced using a vacuum technique that involves passing the prepared suspension through microfiltration under vacuum.

2- **The second part is the characterization of** the as-prepared nanowires, nanowires-based composites, and nanowires-based hybrid membranes were completely characterized using

various characterization techniques, including XRD, N_2 adsorption, SEM, HRTEM, Raman spectroscopy, contact angle measurements, zeta potential measurements, etc.

3- **The third part is the application**. The photocatalytic activity of the as-prepared hybrid membranes was applied as adsorbent materials and photodecolorization of methylene blue; furthermore, the antibacterial and antiviral activities were studied towards the *E. coli* and MS2 removal.

4. Materials and methods

4.1. Materials

For the synthesis of TiO_2 NWs:

Titanium dioxide (TiO_2) (P25) (Sigma Aldrich; Hungary)

Potassium hydroxide (KOH) (VWR International Ltd., Hungary)

Hydrochloric acid (HCl, 37%) (VWR International Ltd., Hungary)

Deionized water (H_2O)

For the synthesis of Fe_2O_3/TiO_2 NWs nanocomposite:

Iron chloride hexahydrate ($FeCl_3 \cdot 6H_2O$) (ES Lab Kft.; Hungary)

TiO_2 NWs (prepared by us)

Sodium hydroxide (NaOH) (Sigma Aldrich; Hungary)

Deionized water (H_2O)

For the synthesis of Fe_2O_3/TiO_2 NWs/cellulose hybrid membrane:

As-prepared Fe_2O_3/TiO_2 NWs nanocomposite

Absolute Ethanol (EtOH) (VWR International Ltd., Hungary)

Cellulose (DIPA Ltd.; Hungary)

Polyvinylidene (PVDF) filter (0.1 μm pore size and 47 mm diameter) (Durapore-VVLP04700); (Sigma Aldrich; Hungary)

For the synthesis of CuO/TiO_2 NWs nanocomposite:

TiO_2 NWs (prepared by us)

Copper (II) acetate monohydrate ($Cu(OOCCH_3)_2 \cdot H_2O$) (VWR International Ltd., Hungary)

Absolute Ethanol (EtOH) (VWR International Ltd., Hungary)

For the synthesis of CuO/TiO_2 NWs/cellulose hybrid membrane:

As-prepared CuO/TiO_2 NWs nanocomposite

Absolute Ethanol (EtOH) (VWR International Ltd., Hungary)

Cellulose (DIPA Ltd.; Hungary)

Polyvinylidene (PVDF) filter (0.1 μm pore size and 47 mm diameter) (Durapore-VVLP04700); (Sigma Aldrich; Hungary)

For the synthesis of WO_3 NWs:

Sodium tungstate dihydrate ($Na_2WO_4 \cdot H_2O$) (Sigma Aldrich; Hungary)

Sodium sulfate (Na_2SO_4) (VWR International Ltd., Hungary)

Hydrochloric acid (HCl, 37 %) (VWR International Ltd., Hungary)

Deionized water (H_2O)

For the synthesis of Fe_2O_3/WO_3 NWs nanocomposite:

WO_3 NWs (prepared by us)

Iron chloride hexahydrate ($FeCl_3 \cdot 6H_2O$) (ES Lab Kft.; Hungary)

Sodium hydroxide (NaOH) (Sigma Aldrich; Hungary)

For the synthesis of Fe_2O_3/WO_3 NWs/cellulose hybrid membrane:

As-prepared Fe_2O_3/WO_3 NWs nanocomposite

Cellulose (DIPA Ltd.; Hungary) Absolute Ethanol (EtOH) (VWR International Ltd.,

Hungary)

Polyvinylidene (PVDF) filter (0.1 μm pore size and 47 mm diameter) (Durapore-VVLP04700); (Sigma Aldrich; Hungary)

For the synthesis of CuO/WO_3 NWs nanocomposite:

WO_3 NWs (prepared by us)

Absolute Ethanol (EtOH) (VWR International Ltd., Hungary)

Copper (II) acetate monohydrate ($Cu(OOCCH_3)_2 \cdot H_2O$) (VWR International Ltd., Hungary)

For the synthesis of CuO/WO_3 NWs/cellulose hybrid membrane:

As-prepared CuO/WO_3 NWs nanocomposite

Cellulose (DIPA Ltd.; Hungary)

Absolute Ethanol (EtOH) (VWR International Ltd., Hungary)

Polyvinylidene (PVDF) filter (0.1 μm pore size and 47 mm diameter) (Durapore-VVLP04700); (Sigma Aldrich; Hungary)

For the filtration experiments:

Bacteriological agar, D-glucose, and sodium dihydrogen phosphate dihydrate ($NaH_2PO_4 \cdot 2H_2O$) (Simga-Aldrich; Switzerland)

Calcium chloride dihydrate ($CaCl_2 \cdot 2H_2O$), microbiology yeast extract and glycerol (Merck Eurolab; Switzerland)

Streptomycin (AppliChem PanReac; Germany)

Tryptone (Difco 0123) (Becton Dickinson)

Sodium chloride (NaCl) (VWR International; Switzerland)

Sodium hydroxide (NaOH) (Sigma Aldrich; Hungary)

Escherichia coli DH5α (SZMC 21399) Gram negative strain was used for filtration test as a model organism (this bacterial strain was provided from the Department of Microbiology, Faculty of Science and Informatics, University of Szeged).

Escherichia coli (Migula 1895) Castellani and Chalmers 1919 (DSM No.: 5695) colonies were used as host cells for MS2 bacteriophage multiplication (DSM No.: 13767).

Dry *E. coli* pellets and the MS2 phage suspension (DSMZ Braunschweig; Germany)

4.2. Syntheses

4.2.1. Preparation of nanowires

For the preparation of TiO_2 NWs, 3.0 g of TiO_2 nanoparticles (precursor) were added to 100 mL of a 10 M KOH aqueous solution and mixed for 30 minutes until a homogeneous suspension was formed. The suspension was transferred to a Teflon®-lined autoclave (125 mL capacity) with up to 80% of the total volume. The autoclave was maintained at 160°C for 24 h, then cooled to ambient temperature. The resulting product was collected by vacuum filtration, then repeatedly washed with a 0.1 M HCl aqueous solution and deionized water until the pH reached 7. The products were dried overnight in a furnace, and white TiO_2 NWs powder was eventually formed. The TiO_2 NWs powder was then calcined at 400°C for 1 h. In the same manner, WO_3 NWs were produced *via* a hydrothermal method, in detail. 2.5 g of sodium tungstate and 3 g of sodium sulfate (precursors) were dissolved in 80 mL of distilled water. Drop-by-drop, 3 M HCl was added to the solution while stirring continuously, and the pH was adjusted to 1.5. And after 10 minutes of stirring, the solution was poured into an autoclave for

48 h at 180 °C. The product was collected by vacuum filtration, rinsed many times with deionized water to neutralize the pH, and then dried at 100°C. Consequently, the powder was calcinated at 400 ° C for 1 h. The synthesis procedure is illustrated in Figure 4.

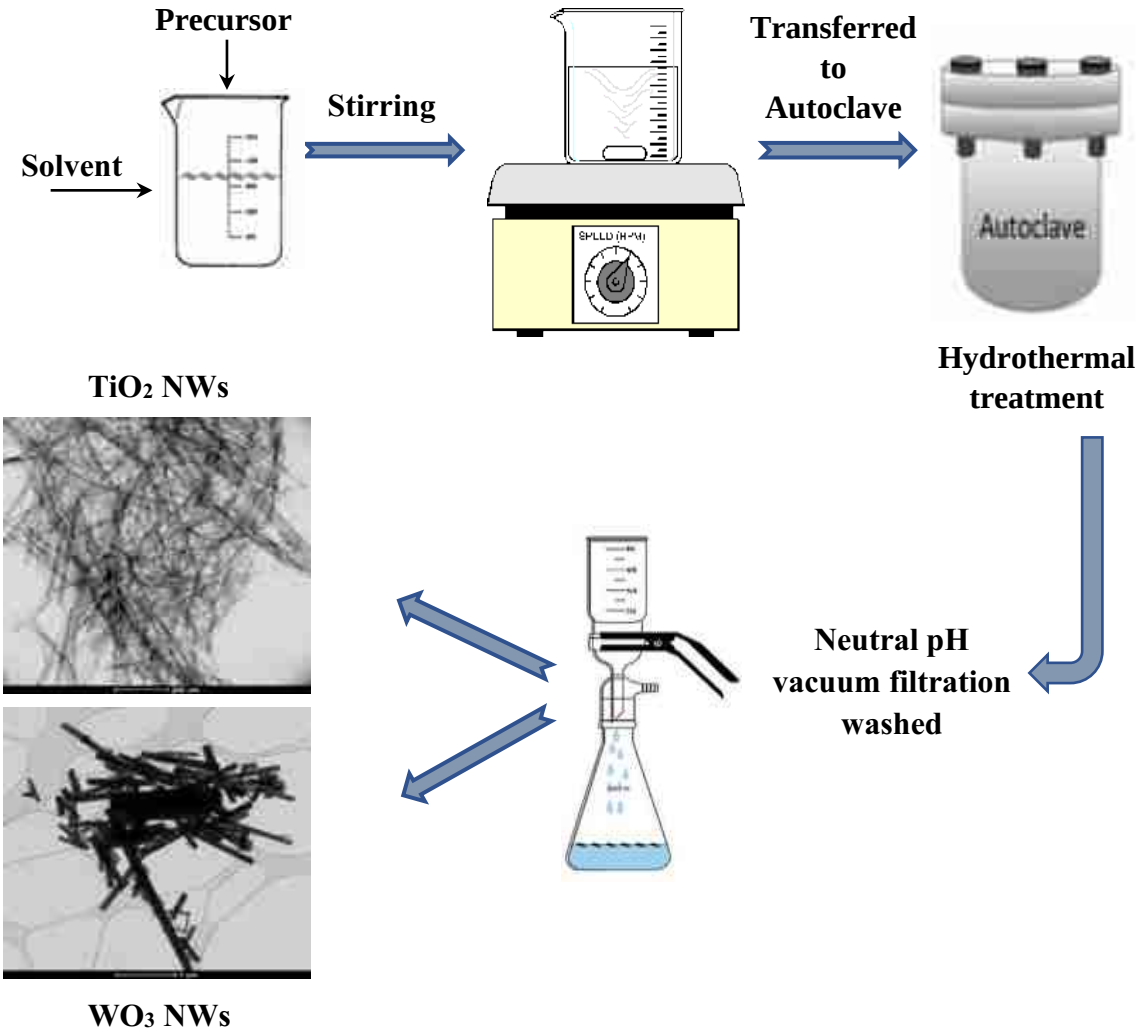

Figure 4. Schematic diagram for synthesis steps of different nanowires

4.2.2. Preparation of nanowires based Fe_2O_3 composite

Fe_2O_3/TiO_2 NW and Fe_2O_3/WO_3 NW nanocomposite were prepared by dissolving the $FeCl_3 \cdot 6H_2O$ precursor in 100 mL of deionized water to form a homogenous solution. After that, 0.95 g of previously prepared nanowires were added to the solution and stirred for 1 h, followed by adding NaOH drop by drop until the solution became base, and transferred to an autoclave at 90° C for 9 h. The resulting product was washed with 0.1 M to neutral the pH to 7, dried at 50 ˚ C for 12 h, and then calcinated at 500 ° C for 2 h using a static furnace. The nanoparticle load in the final mixture was 5% by weight. The preparation steps can be seen in Figure 5.

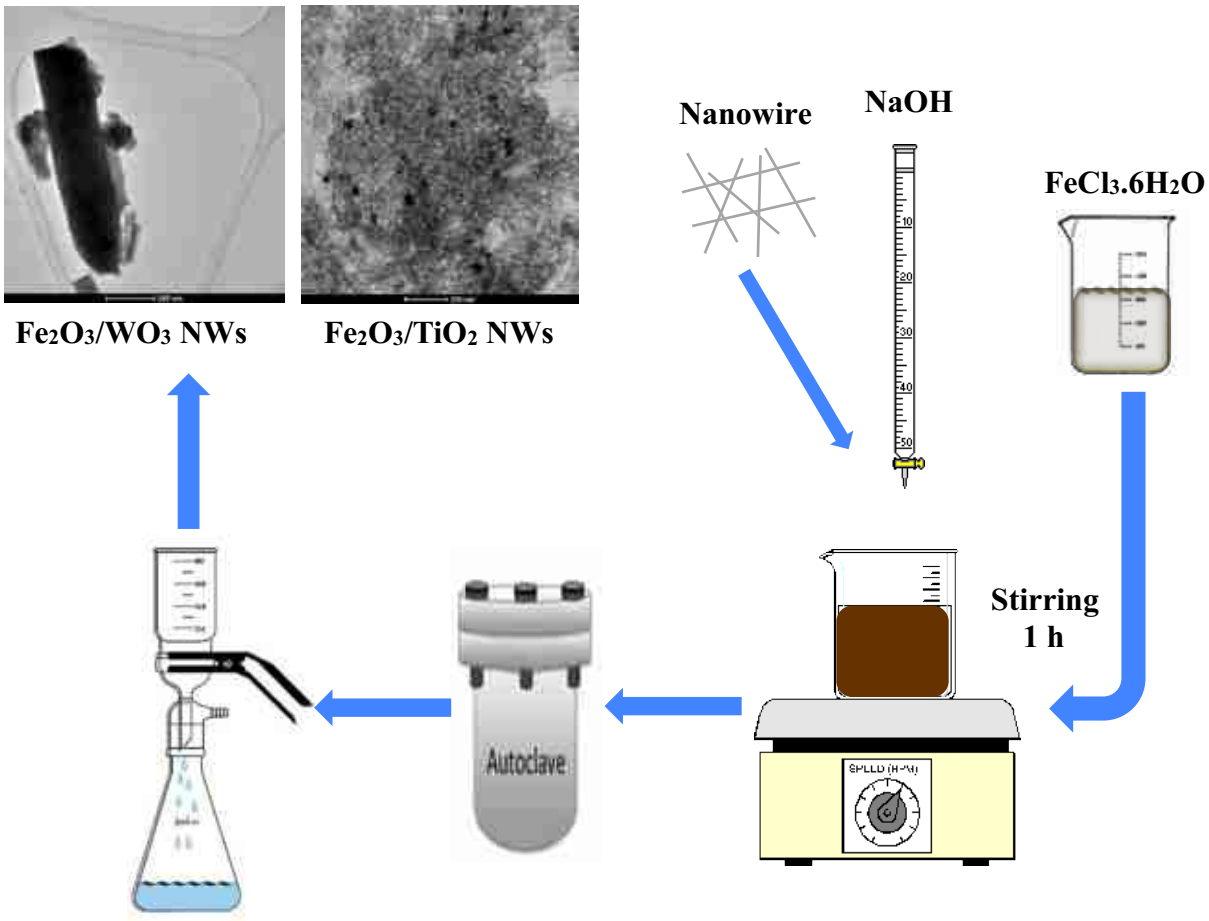

Figure 5. Schematic diagram of synthesis steps for nanowires based Fe_2O_3 composite

4.2.3. Preparation of nanowires based CuO composite

The ($Cu(CH_3COO)_2 \cdot H_2O$) precursor was dissolved in 100 mL of EtOH and vigorously stirred for 30 minutes to obtain complete dissolution. Afterward, 0.95 g of nanowires was added to the solution under stirred vigorously for 1 h. The mixture was poured into an autoclave and heated for 12 h at 150 ° C in a static furnace. The final product was collected using vacuum filtration, rinsed and then calcinated at 500 ° C for 2 h. CuO nanoparticles comprised 5 wt% of the final composition. These steps are shown in Figure 6.

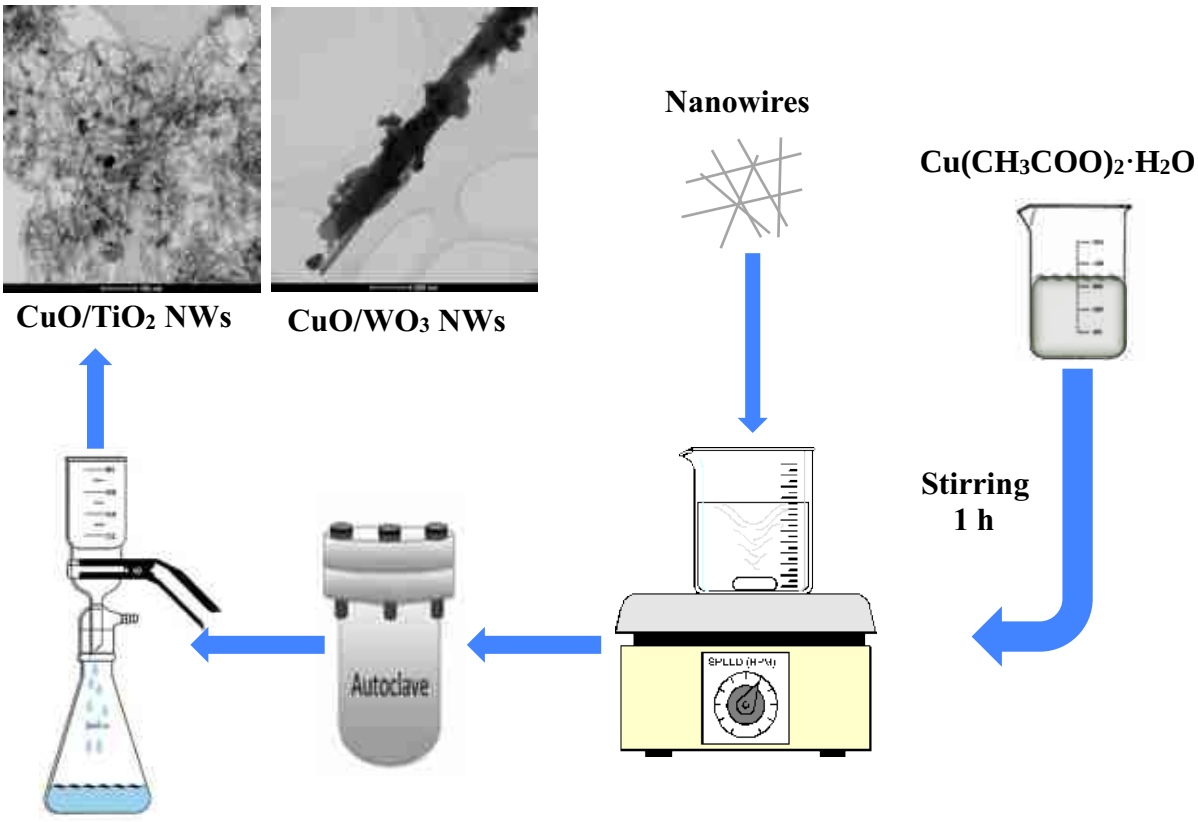

Figure 6. Schematic diagram of synthesis steps for nanowires based CuO composite

4.2.4. Preparation of nanowires-based hybrid membranes

0.2 g of the as-prepared nanowires-based nanocomposite powder was mixed in 100 mL of EtOH for 1 h; after that, 5 g of a cellulose solution (1 w/w%) was added and mixed for another 1 h. The solution was then filtrated with a vacuum using a PVDF membrane to obtain

cellulose-based hybrid membranes (total mass of 250 mg/membrane) and then dried in an oven for 30 minutes at 40 ° C. The preparation steps are shown in Figure 7.

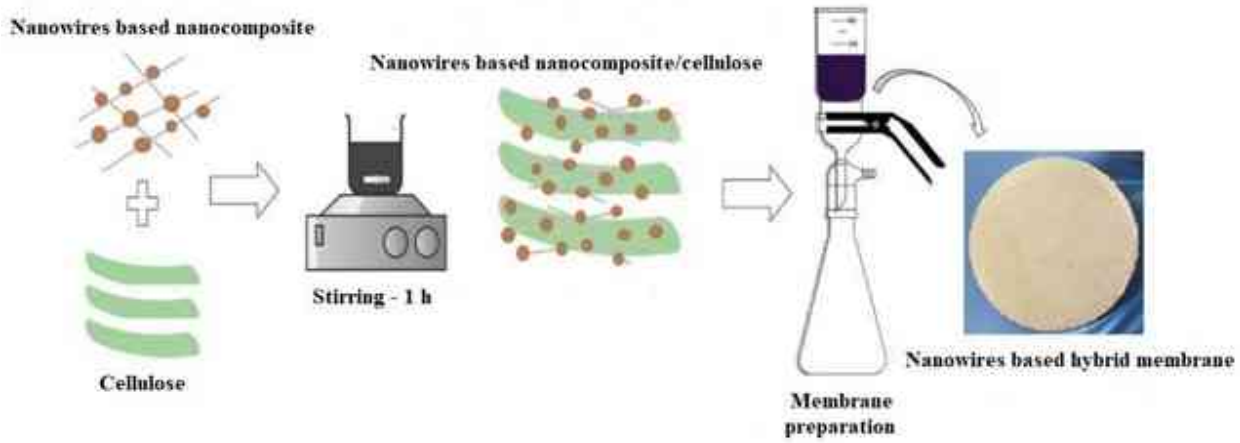

Figure 7. Schematic diagram of the hybrid membrane preparation procedure

4.3. Characterization of composite materials and hybrid membranes

4.3.1. Transmission Electron Microscopy (TEM)

High-resolution transmission electron microscopy (FEI Technai G^2 F20 HRTEM, Hillsboro, OR, USA) has been performed to confirm the formation of (Fe_2O_3 and CuO) NPs on the TiO_2 NWs and WO_3 NWs surface. Powder samples were suspended in ethanol and sonicated for 5 minutes to prepare TEM grids. A droplet of suspension was deposited on a Cu TEM grid (300 mesh copper grids, lacey carbon, Ted Pella Inc.).

4.3.2. Scanning Electron Microscopy (SEM)

We utilized scanning electron microscopy to investigate surface morphology. SEM and EDS analyses were conducted on hybrid membranes using a Hitachi S-4700 Type II FE-SEM (Tokyo, Japan) with a 0-30 KeV range. At the same time, the pristine nanowires were examined with a Thermo Helios G4 PFIB CXe instrument (Thermo Fisher, Eindhoven, Netherlands) equipped with an EDS system for elemental analysis (EDAX Inc., Mahwah, NJ, USA). The EDS system was equipped with an Octane Elect Plus X-ray detector. Standard EDS maps and

spectra were obtained with Acceleration Voltage ranging from 10 kV to 25 kV, a take-off angle of 35 degrees, and a dwell duration of 200 milliseconds. Powder was placed on adhesive carbon tape for SEM examination. Every sample, including powders and membranes, was viewed directly without any conductive covering. The standard SEM working distance was 5 mm with an acceleration voltage between 2 kV and 25 kV, based on image quality and charging conditions.

4.3.3. Energy-dispersive X-ray spectroscopy (EDS)

Energy-dispersive X-ray spectroscopy (EDS) from AMETEK Inc. was utilized in conjunction with the HRTEM equipment to analyze the elemental compositions of the nanocomposites. The EDS system had an active area of 30 mm^2.

4.3.4. X-ray micro-computed tomography equipment (µCT)

The YXLON FF35 dual-beam X-ray micro-computed tomography equipment assessed hybrid membranes' surface morphology and three-dimensional structure. The equipment features a microfocus X-ray tube, transmission beam, and acceleration voltage of 50 kV.

4.3.5. X-ray powder diffraction (XRD)

The X-ray powder diffraction (XRD) technique was employed to identify the crystal structure of the nanocomposites and membranes using a Bruker D8 Advance diffractometer (Billerica, MA, USA). While WO_3-based hybrid membranes using a Rigaku Miniflex diffractometer in parallel beam geometry with a position-sensitive detector (Vantec1) at 40 kV and 40 mA utilizing CuKα radiation (0.15418 nm) and a Göbel mirror, with a 1° opening. Measurements were conducted on specimens put on top in Si sample containers with zero background. The measurements were taken in the 5–70° (2 Theta) range at a goniometer speed of 0.007° (2 Theta) per 14 seconds. The International Centre for Diffraction Data (ICDD®) is a nonprofit scientific institution dedicated to obtaining, examining, releasing, and distributing powder diffraction data for material identification. The previous name was JCPDS. Each substance is

assigned a specific card number; for example, TiO_2 anatase is identified by the card numbers 21-1272. To calculate the interplanar spacing (d-spacing), we used the formula below (Bragg's law).

$$d = \frac{n\lambda}{2 \sin\theta}$$

Where d is the interplanar spacing in Å

n is the diffraction order, for first order n=1

λ is the x-ray wavelength, CuKα=1.5418 Å

θ is the Bragg's angle in degree

4.3.6. Specific surface area measurement

N_2 adsorption experiments were conducted at 77 K using an ASAP 2020 instrument (Micromeritics Instrument Corp. Norcross, GA, USA) to measure the specific surface area of the nanowires, nanowires-based nanocomposites, and nanowires-based hybrid membranes.

4.3.7. Dynamic light scattering (DLS)

An electrophoretic measurement was conducted using dynamic light scattering (DLS) equipment called ZetaSizer NS-Malvern from the UK. The measurement relies on Malvern's M3-PALS technology, which combines laser Doppler velocimetry and phase analysis of light scattering.

4.3.8. Raman spectroscopy

Raman spectroscopy was conducted with a high-resolution Raman spectrometer (Nicolet Almega XR, Thermo Electron Corporation, Waltham, MA, USA) that had a 532 nm Nd: YAG laser with a power output of 50 mW.

4.3.9. Contact angle measurement

The contact angle of the hybrid membranes was evaluated using the sessile drop method using an SP 12 melt microscope from Sunplant Ltd, Hungary, capturing a silhouette shot. The KSV software from KSV Instrument Ltd in Finland assessed the recording and calculated the angular values.

4.3.10. Fourier-transform infrared spectroscopy (FTIR)

FTIR spectra were obtained using a Bio-Rad Digilab Division FTS65A/896 FT-IR spectrometer with a DTGS detector and a Ge/KBr beamsplitter. The spectra were recorded between 4000 and 400 cm^{-1} with an optical resolution of 4 cm^{-1}. The experiment utilized a Harrick's Meridian SplitPea Single Reflection Diamond ATR attachment without sample preparation. The spectrometer was operated using Win IR Pro v. 3.3 software from Bio-Rad Digilab Division, and the spectra were examined with GRAMS/AI v. 7.0 software from Thermo Galactic.

4.3.11. Inductively coupled optical emission spectrometry (ICP-OES)

ICP-OES measurements were conducted using a Varian 720 ES ICP-OES system to quantify the dissolved Cu and Fe in the filtration tests.

4.4. Photocatalytic Experiments

The adsorption and photocatalytic performance of as-prepared hybrid materials were examined in the decolorization of methylene blue (MB). Initially, each membrane (250 mg) was immersed in a solution of MB (100 mL of 0.03 mM) and left in the dark for 2 hours to achieve adsorption-desorption equilibrium. Subsequently, the solution was subjected to UV-A lamps (300–500 W, Cosmedico N 400 R7S; Cosmedico, Stuttgart, Germany) for 60 minutes. The specimens were collected at consistent time intervals and then subjected to centrifugation and filtration. The reduction in MB concentration was assessed using a UV-vis spectrophotometer (BEL UV-M51; Bel Engineering, Monza, Italy). The membranes' removal effectiveness was

determined by measuring the absorbance at 664 nm. The decolorization efficiency, expressed as a percentage (% dec.), was computed using the following formula:

$$\% \, \boldsymbol{dec.} = \frac{\mathbf{C_0 - C}}{\mathbf{C_0}} \times \mathbf{100} \, \%$$

Where C_0 & C are initial and final concentrations of MB and % deg. is the photodecolorization efficiency of the materials for MB removal.

4.5. Filtration Experiments

4.5.1. Bacterial filtration tests

The bacterial filtration efficiency testing was conducted as follows: A ten-fold serial dilution was prepared using a 30 mL Lysogeny Broth (LB) medium from the first starter culture. The concentration of colony-forming units (cfu) in the sixth ten-fold dilution was determined to be $1.21 \pm 0.24 \times 10^3$ cfu/mL using the colony counting method. The suspension was utilized in the filtering experiment to provide a quantifiable quantity of colonies on the agar plate. Prior to each filtration, a 3×100 μL sample was uniformly distributed on the surface of an LB agar plate to assess the initial concentration of colony-forming units (CFU_0). The filtering was conducted using a glass vacuum filtration apparatus (Sartorius Stedim Biotech 16306–25 mm) without the use of a vacuum pump, employing gravity-driven filtration. After filtration, a sample of 3×100 μL was collected from the filtered suspension to quantify the number of colony-forming units in the filtrate (CFU_f). This data was then used to calculate the BFE% values using the following formula:

$$\boldsymbol{BFE\%} = \frac{\boldsymbol{CFU_0 - CFU_f}}{\boldsymbol{CFU_0}} \, \mathbf{X \, 100} \, \%$$

Where BFE% is the bacterial filtration efficiency percentage, CFU_0 & CFU_f are the initial and final concentration of colony forming units.

4.5.2 Virus filtration tests

The necessary culture media for the growth and filtration of bacteria and MS2, including antibiotic solution, broth, viral dilution buffer, and hard and soft agar, were prepared according

to the methods described by B.M. Pecson et al. [179]. The replication of MS2 was carried out using its host Escherichia coli strain, followed by purification and concentration through a series of procedures as described in the DSMZ protocol. Periodically, it was necessary to ascertain the quantity of plaque-forming units (PFUs) present in a suspension of MS2 bacteriophages due to their sensitive nature. The original stock of purified MS2 had a concentration of 7.6×10^7 plaque-forming units per milliliter (PFU/mL). To facilitate future utilization, the original sample was diluted in a viral dilution buffer (VDB). Therefore, the phage enumeration method utilized a maximum sample amount of 2 mL to determine the detection limit of approximately 4 LRV (Log Reduction Value) or 99.99%. The VDB was made by combining $NaH_2PO_4{\cdot}2H_2O$, NaCl, and water. The pH was modified to a value of 7.0 by adding drops of a 0.1M NaOH solution. The virus filtering studies were conducted at a constant room temperature of 23 °C. The concentration of the MS2 bacteriophages was assessed after the incubation period. 2 rounds were conducted for each enumeration of MS2 samples, and 3 trials were conducted for each condition.

In filtration experiments, the as-prepared hybrid membranes were placed into a 200 mL glass funnel equipped with a porous glass insert at the bottom. Gravity-driven filtration was utilized in the tests without the need for vacuum suction to increase the flow rate of the filtered liquid. In order to examine the impact of the equipment on the retention of the bacteriophages, a control experiment was conducted without a filter. 30 mL of the virus dilution buffer was contaminated with the specific volume of bacteriophage stock required to achieve an active phage concentration of 10 PFU/mL. This allowed the study of retention of up to 2 magnitudes (2 log). After each filtering, 1 mL of the filtered liquid was taken and utilized to infect *E. coli* for the virus enumeration. The pH levels of the experiment filtrations were conducted at 7.0 to simulate real-life conditions.

4.6. Toxicology Experiments

The toxicology test was conducted in Kisanalitika Ltd. in Sajóbábony, Hungary. Fish tests can evaluate surface water's environmental danger or examine pollution's harmful consequences. Acute toxicity is the noticeable harmful impact on an organism shortly after exposure to a toxin, typically within days. This study measures acute toxicity using the lethal concentration 50 (LC50), which is the concentration of a toxic substance in water that results in the death of 50% of the test fish group within a specific time frame. A static test was conducted, meaning the test solution did not flow and remained constant during the experiments. Zebrafish (Danio

rerio) were utilized to conduct the studies. The fish must be in optimal health without apparent physical abnormalities. Water toxicity testing was carried out by creating a dilution series utilizing water from the fish aquarium as the dilution water, which also worked as the water for the control test group. The aquarium's dilution water was aerated, and its oxygen and pH levels were monitored consistently. The test groups were immersed in 500 mL of hybrid membrane soaking water for 24 hours or in water filtered through the hybrid membranes being tested. Each test group consisted of 5 fish. Fish were exposed to the test water at varying concentrations for 48 hours. Fish mortality was monitored at specific time points: 2 hours, 24 hours, and 48 hours.

5. Results and discussion

5.1. Investigation of as-prepared materials

5.1.1. Surface morphology of pristine nanowires, nanowire-based nanocomposites and hybrid membranes

After the synthesis of TiO_2 and WO_3 nanowires, TiO_2 and WO_3 nanowire-based composites and hybrid membranes, SEM investigations were carried out to gain information about their surface morphology. As can be seen in Figure 8 a–d, the preparation of both TiO_2 NWs and WO_3 NWs was successful. Based on SEM observations it was found that the TiO_2 NW had an average diameter of 10-15 nm, while the WO_3 NWs had an average diameter of 100-200 nm.

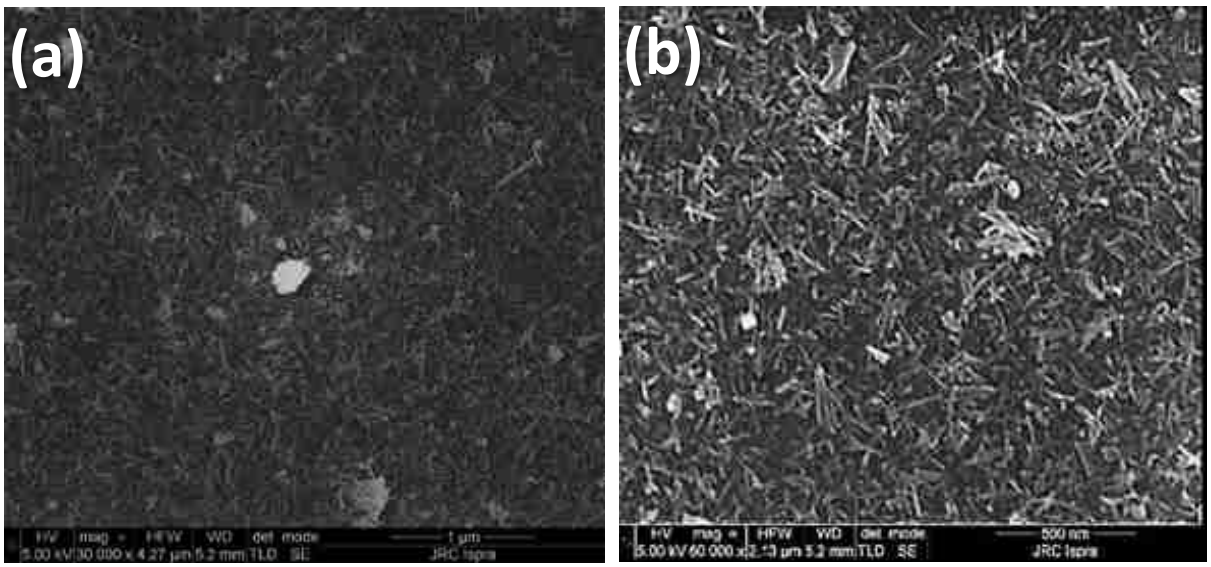

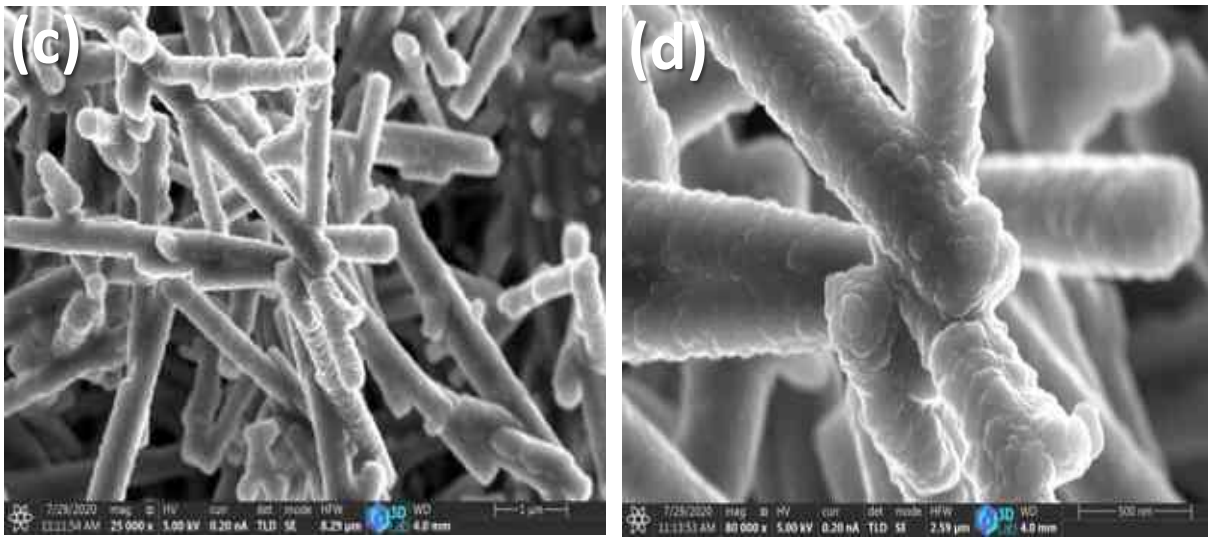

Figure 8. SEM images of **(a)** TiO_2 NWs with lower and **(b)** higher magnifications **(c)** WO_3 NWs with lower and **(d)** higher magnifications

The surface morphology of as-prepared samples is sometimes not clear enough using the SEM technique, especially when modifying the surface with additives, so we need another technique to investigate them. For that, high-resolution transmission electron microscopy (HRTEM) was performed. As illustrated in Figures 9 (a-b), and 10 (a-d), the average diameters of TiO_2 NWs and WO_3 NWs are 2-10 nm and 60-140 nm, respectively, while the average length was determined to be several microns.

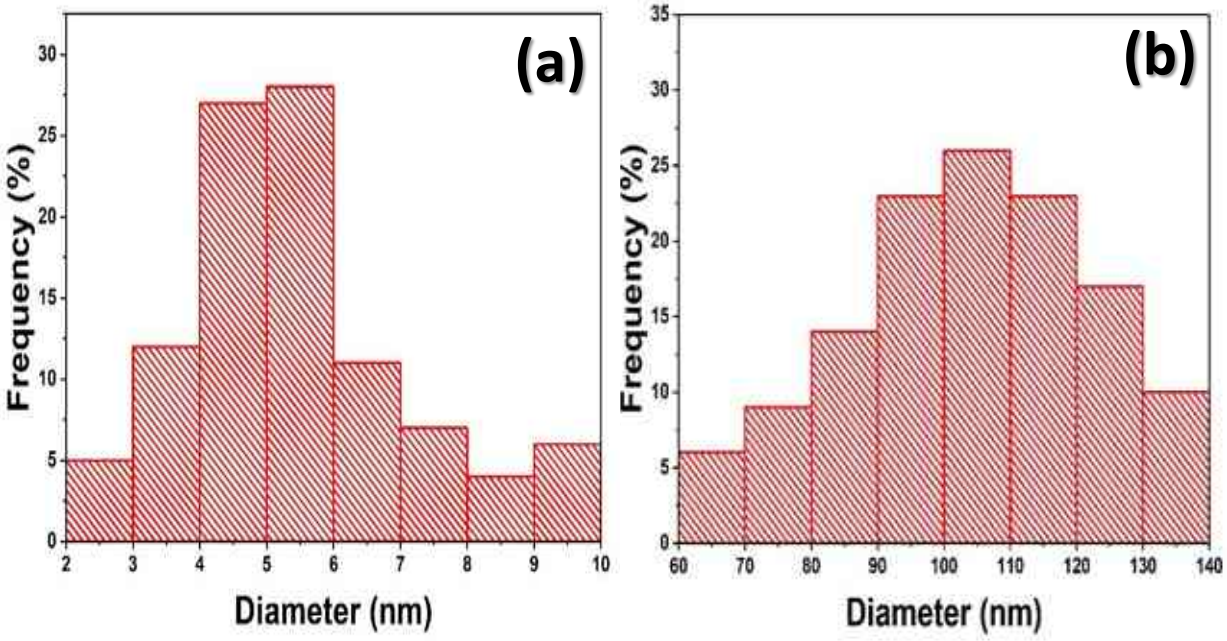

Figure 9. Diameter distribution of **(a)** TiO_2 NWs and **(b)** WO_3 NWs

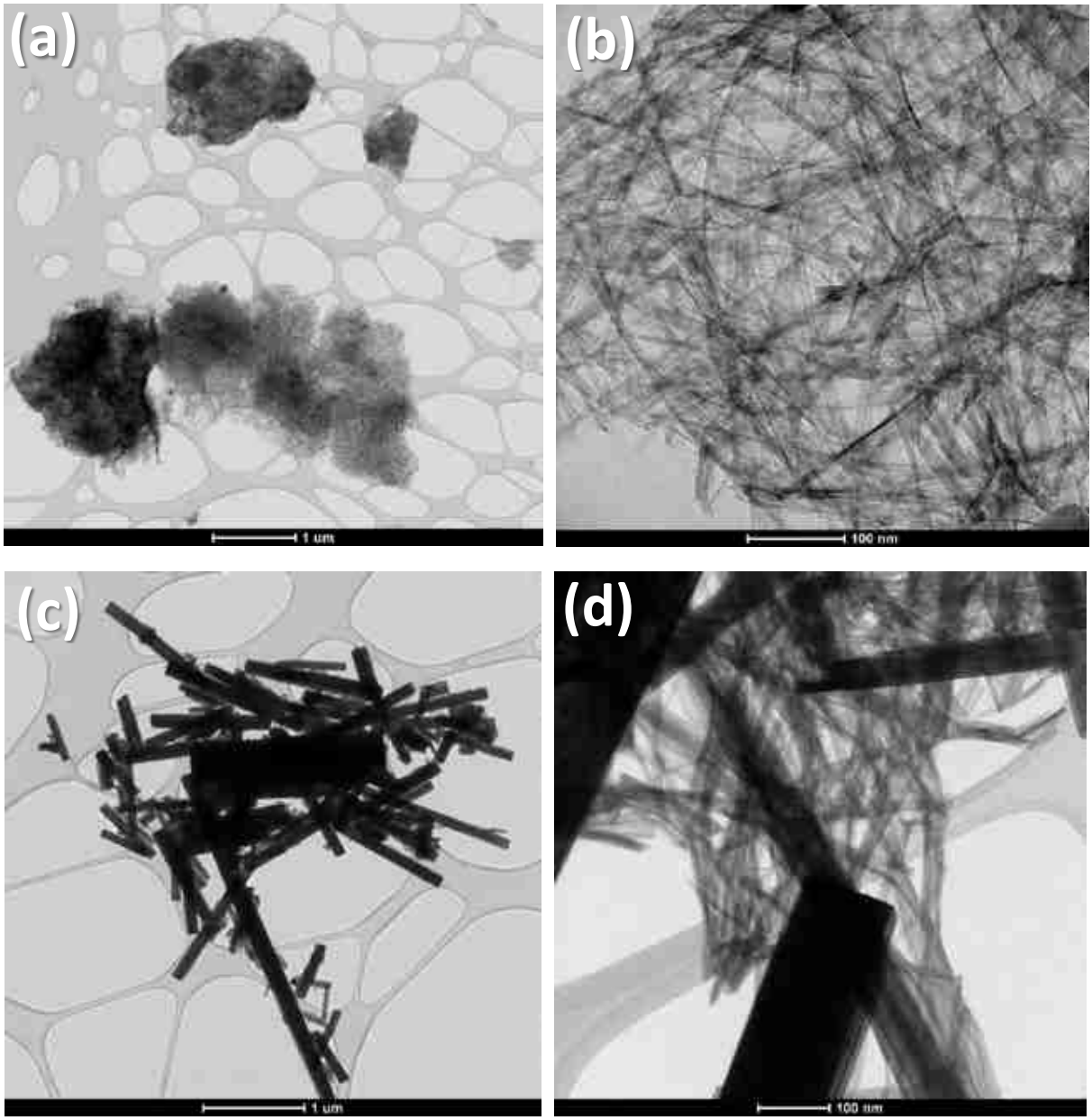

Figure 10. TEM images of **(a)** TiO_2 NWs with lower and **(b)** higher magnifications **(c)** WO_3 NWs with lower and **(d)** higher magnifications

As presented above, the nanowires were produced without any deformations. Now, we must ensure the nanoparticle additives are attached to the nanowire surface. Hence, the HRTEM technique was used. Fe_2O_3/TiO_2 NW and CuO/TiO_2 NW nanocomposites are shown in HRTEM micrographs (Figure 11). These HRTEM images showed that both nanocomposites had been successfully fabricated, although with slightly different nanocomposite structures. The HRTEM images revealed that the surface of the TiO_2 NW was covered in inorganic

nanoparticles (Fe_2O_3 and CuO), and segregated particles were not visible, as shown in Figures 11 a, b. Furthermore, the average particle sizes of Fe_2O_3 and CuO nanoparticles were also estimated from the HRTEM images using the iTEM software (Olympus Soft Imaging Solutions). 100 particles from each sample were measured to get an average particle size. Figure 11 a demonstrates that the estimated diameter of Fe_2O_3 nanoparticles is in the range of 20-30 nm, while Figure 11 b shows that the diameter of CuO nanoparticles is on average 2-3 nm.

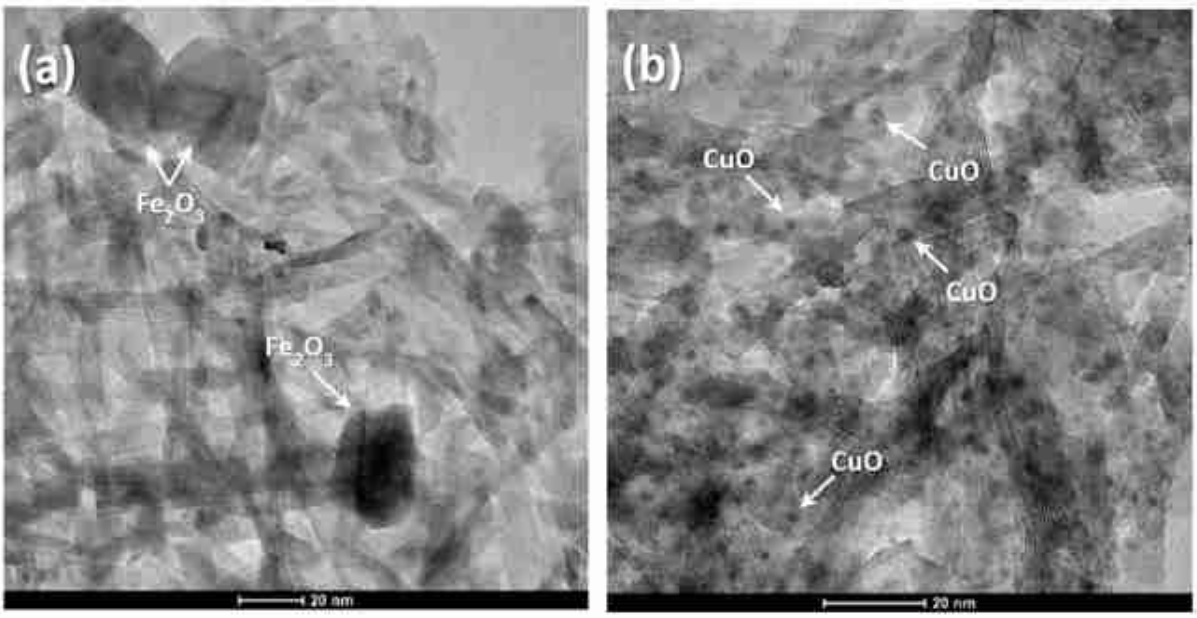

Figure 11. HRTEM images of **(a)** Fe_2O_3/TiO_2 NW and **(b)** CuO /TiO_2 NW nanocomposite

In the same manner, WO_3-based nanocomposites were investigated also by the HRTEM technique. TEM micrographs demonstrated the successful synthesis of Fe_2O_3/WO_3 NW and CuO/WO_3 NW nanocomposites. In addition, the nanoparticle structures were quite similar. However, the average particle size of the Fe_2O_3 and CuO nanoparticles attached to the surface of WO_3 NW was different, as shown in Figures 12 a and b, and segregated particles were not seen. iTEM software (Olympus Soft Imaging Solutions) was utilized to determine the average diameter of the Fe_2O_3 and CuO nanoparticle particle sizes based on the HRTEM images. 100 individual particles from each sample were measured to estimate the average particle size. According to these calculations, the average diameter of CuO nanoparticles was 20-30 nm, whereas the Fe_2O_3 nanoparticles had a diameter in the 40-50 nm range.

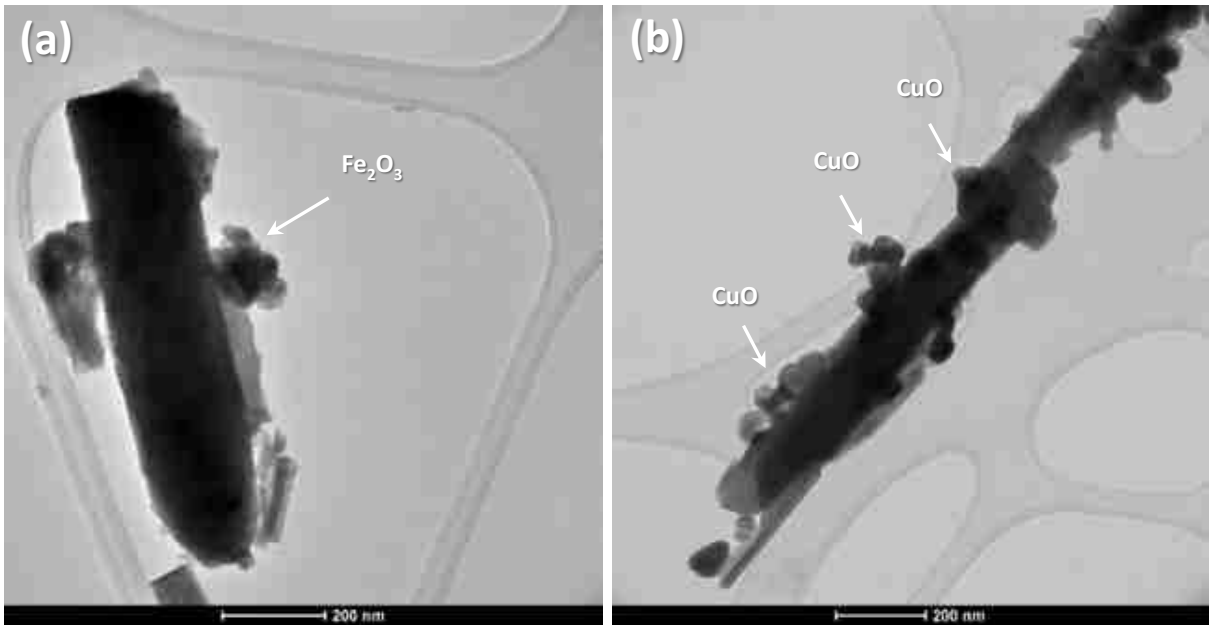

Figure 12. TEM images **(a)** Fe_2O_3/WO_3 NW and **(b)** CuO/WO_3 NW nanocomposite

SEM was also applied to characterize the hybrid membranes of the as-prepared TiO_2 NWs/cellulose (Figure 13 a, b), Fe_2O_3/TiO_2 NWs/cellulose (Figure 13 c, d) and CuO/TiO_2 NWs/cellulose (Figure 13 e, f). Self-supported hybrid membranes are shown in Figures 13 a, c, e, and the microstructure of Fe_2O_3/TiO_2 NWs/cellulose and CuO/TiO_2 NWs/cellulose is shown in Figures 13 b, d, f. The Fe_2O_3 particles clumped together in the Fe_2O_3/TiO_2 NWs/cellulose membrane, leading to larger agglomerates and pores.

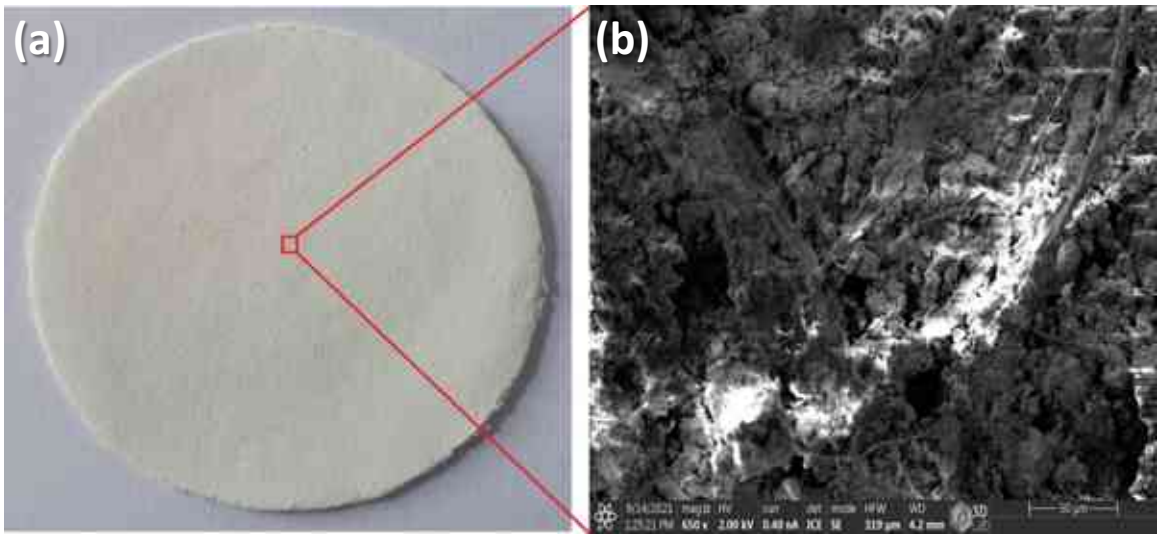

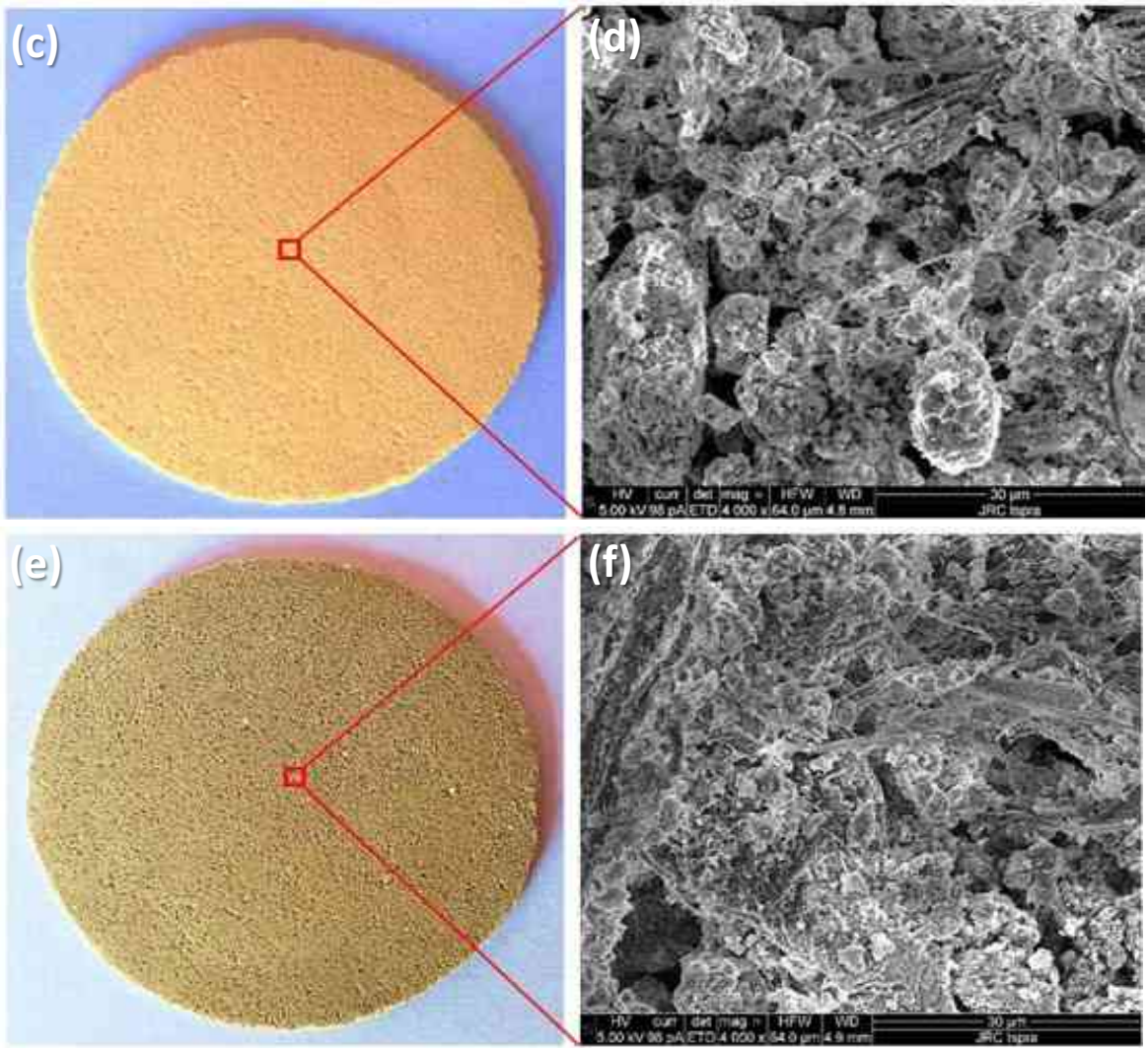

Figure 13. Photograph and SEM images of **(a, b)**; TiO_2 NW/cellulose; **(c, d)**; Fe_2O_3/TiO_2 NW/cellulose and **(e, f)**; CuO/TiO_2 NW/cellulose hybrid membranes

Figure 14 a, c, and e shows the as-prepared WO_3 NW/cellulose (Figure 14 a), Fe_2O_3/WO_3 NW/cellulose (Figure 14 c) and CuO/WO_3 NW/cellulose (Figure 14 e) hybrid membranes. In contrast, Figure 14 b, d, and f shows the microstructure of WO_3 NW/cellulose (Figure 14 b), Fe_2O_3/WO_3 NW/cellulose (Figure 14 d), and CuO/WO_3 NW/cellulose (Figure 14 f) hybrid membranes. Because of the smaller individual particle size of the CuO nanoparticles, the CuO/WO_3 NWs/cellulose membrane exhibited a larger pore size.

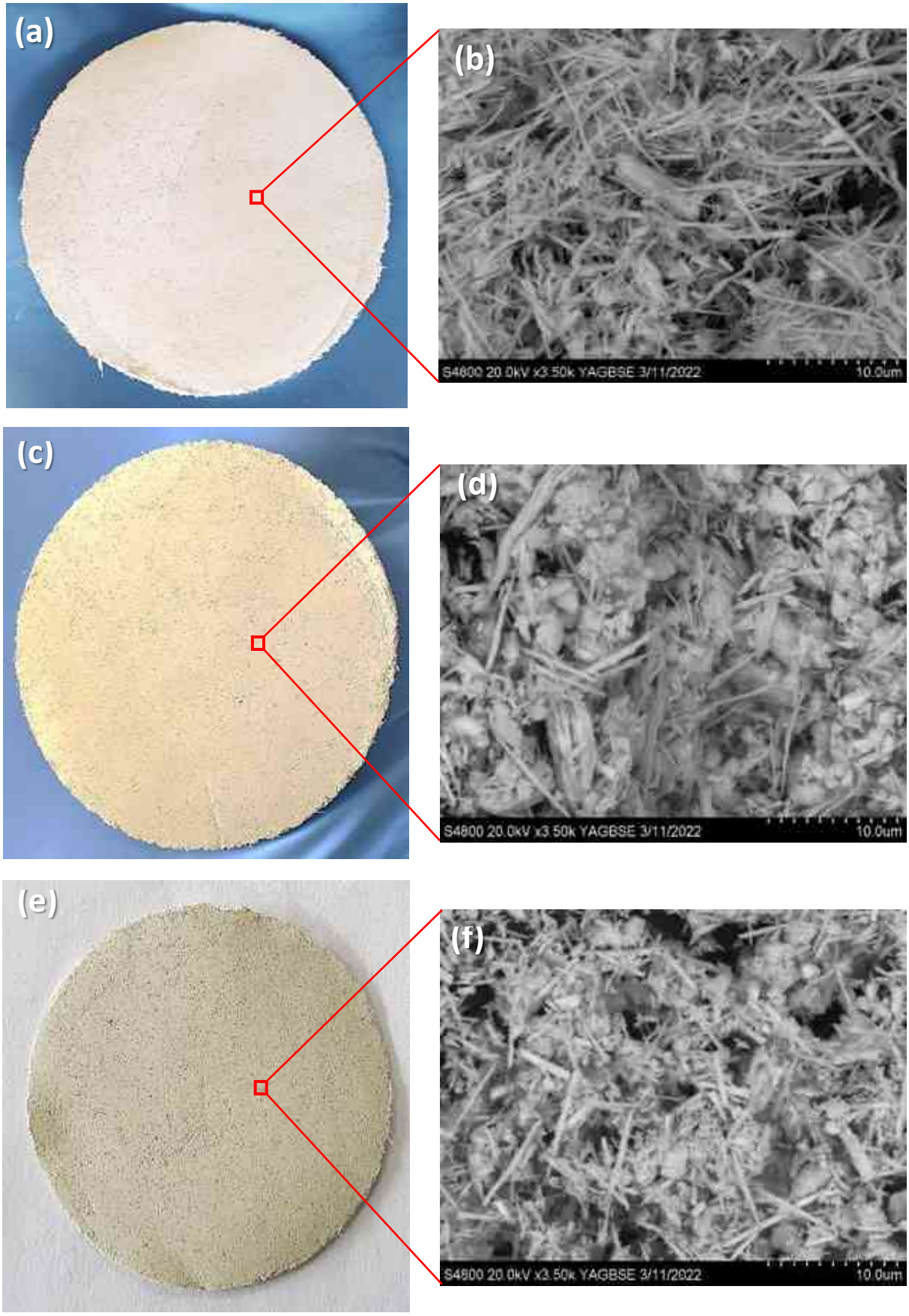

Figure 14. Photographs and SEM images of **(a, b)** WO_3 NW/cellulose **(c, d)** Fe_2O_3/WO_3 NW/cellulose and **(e, f)** CuO/WO_3 NW/cellulose hybrid membranes

Although nanowires-based nanocomposite and hybrid membranes were investigated using SEM and TEM, these measurements did not reveal the 3D structure of the hybrid membranes. The small size of the investigated area is one of the major limitations of using electron microscopy techniques in the field of membrane technology. Therefore, μCT analysis was conducted to learn more about the homogeneity and 3D morphology of the hybrid membrane structure. The 3D cross-section analysis of the nanowires-based hybrid membranes is shown in Figure 15 (a-l). The brighter forms in hybrid membranes denote cellulose's presence. At the same time, the grey fibrous material originated from the nanowires decorated with nanoparticles additives (Figure 15 a-l). The hybrid membrane structure was found to have a roughly homogenous distribution of the nanocomposite additives and cellulose.

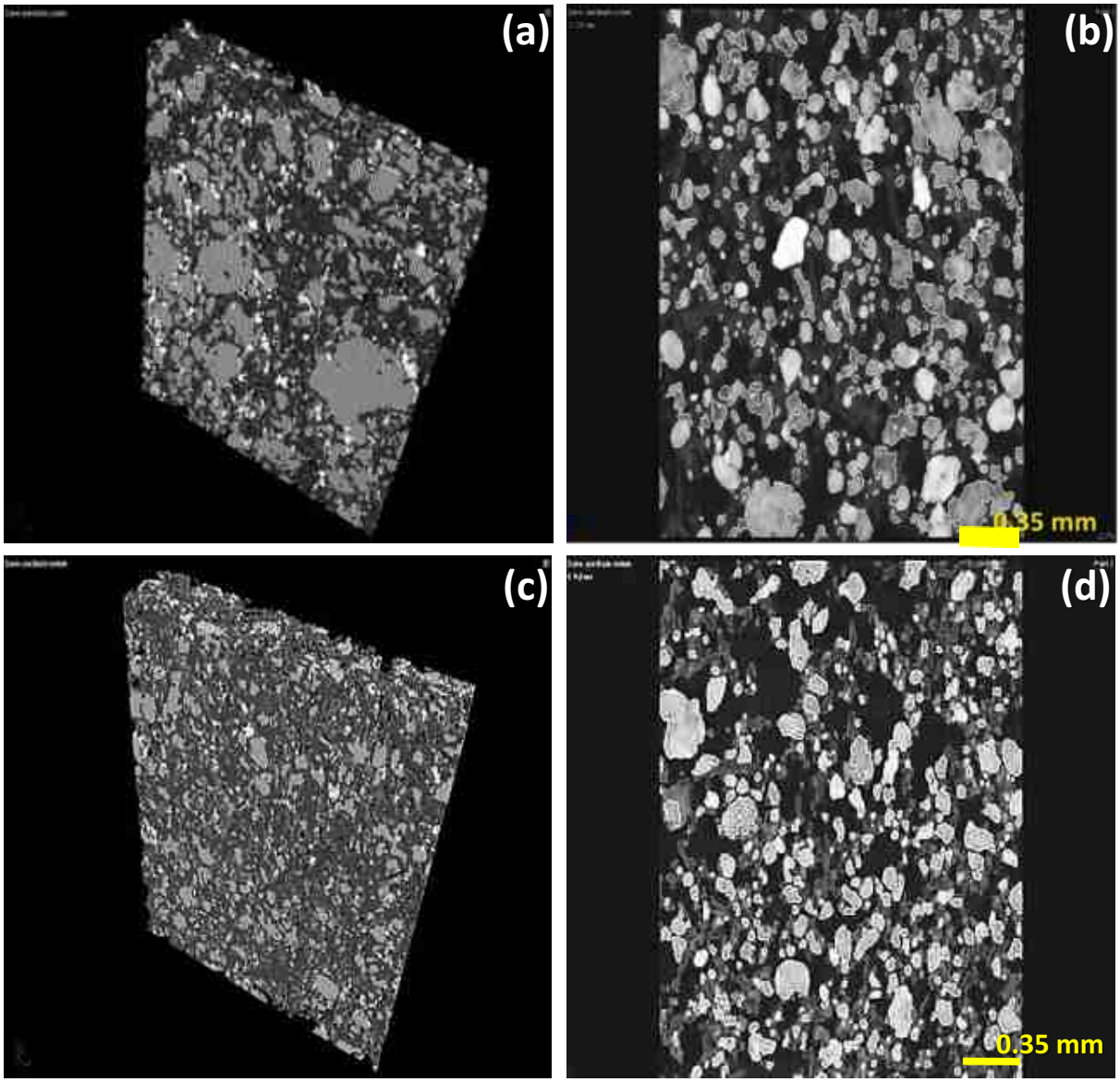

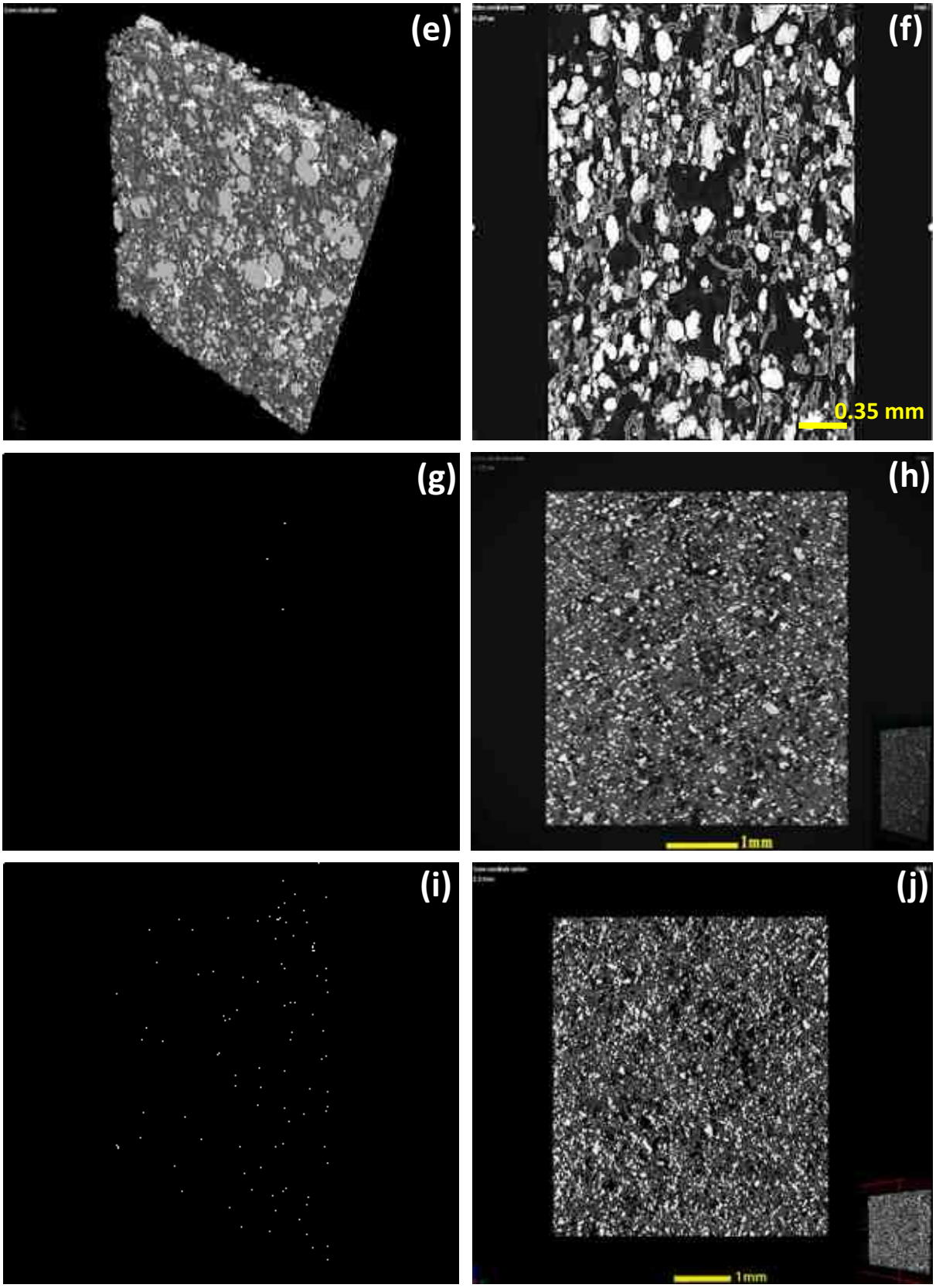
(e)
(f)
0.35 mm
(g)
(h)
1 mm
(i)
(j)
1 mm

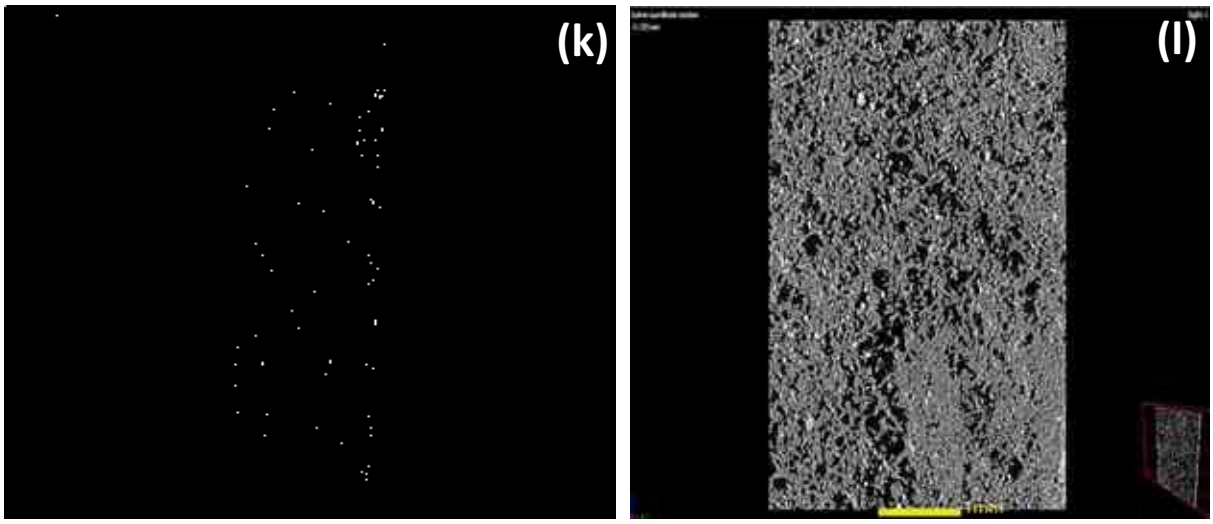

Figure 15. 3D CT cross section analysis of TiO_2 NW/cellulose **(a, b)**, Fe_2O_3/TiO_2 NW/cellulose **(c, d)**, CuO/TiO_2 NW/cellulose **(e, f)**, WO_3 NW/cellulose **(g, h)**, Fe_2O_3/WO_3 NW/cellulose **(i, j)** and CuO/WO_3 NW/cellulose hybrid membranes **(k, l)**

As shown in Table 4, the nanowires-based hybrid membranes' material volume values were also calculated in the full 3D extension. The measured volume of the materials for TiO_2 NW based hybrid membrane was the same in both instances (0.33 mm^3). The resulting volume percentages of materials were also very similar with only a 0.5% variation; according to the results obtained, the 3D structure of the membranes developed is the same. The differences seen in the *E. coli* and MS2 filtration studies are attributed to differences in the material quality of the membranes rather than morphological differences. On the other hand, a substantial difference was found when comparing the volume of material values, which were calculated in the full 3D extension of the WO_3 NWs based hybrid membranes and shown in Table 4. It was 43.8 % for the WO_3 NW/cellulose and 47.5% for the Fe_2O_3/WO_3 NWs/cellulose membrane, but only 36.7% for the CuO/WO_3 NWs/cellulose membrane. Based on the findings mentioned above, it is possible to conclude that although the 3D structure of the membranes produced is relatively similar, the morphology of the membranes, particularly the volume of material ratios is different. Besides the material quality, this may have contributed to the differences seen during the bacteria and virus filtration experiments. Based on the results obtained in μCT, as shown in Figure 15 the TiO_2 NW-based hybrid membranes have a larger pore size than that of WO_3 NW-based hybrid membranes. This result is in good agreement with the SEM and surface area measurements results.

Table 4. Material volume values of the hybrid membranes

Sample	Material volume (mm^3)	Volume percentage of material (%)
TiO_2 NWs/cellulose	0.42	48.0
Fe_2O_3/TiO_2 NWs/cellulose	0.33	45.6
CuO/TiO_2 NWs/cellulose	0.33	46.1
WO_3 NW/cellulose	2.68	43.8
Fe_2O_3/WO_3 NW/cellulose	2.42	47.5
CuO/WO_3 NW/cellulose	1.12	36.7

5.1.2. Chemical compositions of pristine nanowires, nanowire-based nanocomposites and hybrid membranes

After investigating the surface morphology of the as-prepared membrane materials by SEM, HRTEM and μCT techniques, the chemical structure and chemical bonds were also examined with different characterization methods. Firstly, EDS analysis was carried out to determine the elemental composition (Figure 16). As can be observed in the case of TiO_2 NWs (Figure 16 a) the signals are originating from oxygen (O), titanium (Ti), and potassium (K) and copper (Cu). While, in the case of WO_3 NWs (Figure 16 b) the next most important signals which are the tungsten (W) and (O) the copper (Cu) and carbon (C) was also indicated. The presence of other elements, including potassium (K), copper (Cu) and carbon (C), originated from the TiO_2 NW preparation procedure (K) and the sample holder (lacey Cu TEM grid).

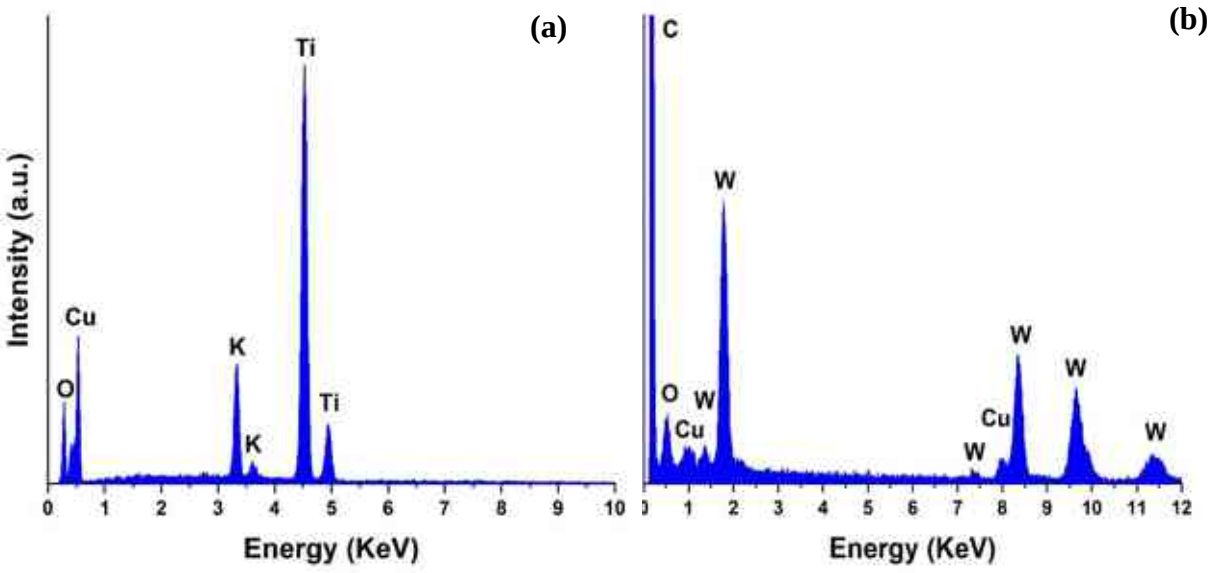

Figure 16. EDS spectra of **(a)** TiO_2 NWs and **(b)** WO_3 NWs

In order to confirm the presence of the CuO and Fe_2O_3 nanoparitlces on the surface of the as-prepared TiO_2 NW-based nanocomposite samples, EDS analysis was performed. As illustrated in Figure 17 a and b; the results revealed that the most important signals were from titanium (Ti), oxygen (O), potassium (K), iron (Fe), and copper (Cu). These signals confirmed the presence of TiO_2, Fe_2O_3, and CuO in the samples. In the case of the Fe_2O_3/TiO_2 NW nanocomposite sample, the (Cu) peak is originated from the sample holder (lacey Cu TEM grid), and the (K) peak was due to the residual KOH used in the preparation of the TiO_2 NW. It was also observed that the copper (Cu) signal is significantly stronger in the case of CuO/TiO_2 NW sample, because these signals are originating not only from the lacey Cu TEM grid, but also from the CuO decorated TiO_2 NW-based nanocomposite.

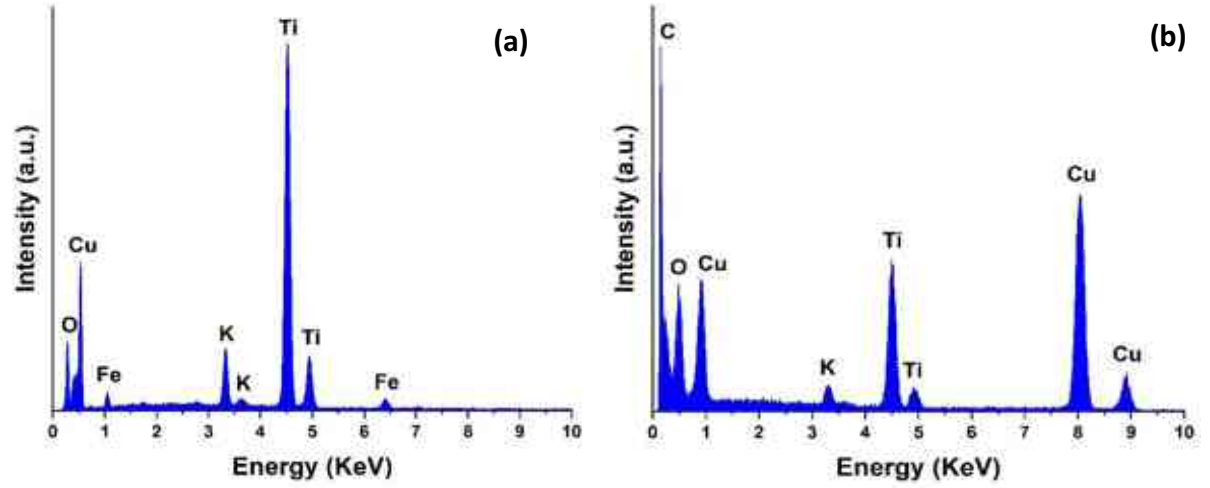

Figure 17. EDS spectra of **(a)** Fe_2O_3/TiO_2 NW and **(b)** CuO/TiO_2 NW nanocomposites

Simultaneously, Figure 18 a and b show the EDS spectra of Fe_2O_3/WO_3 NW and CuO/WO_3 NW nanocomposites. The results demonstrate that the most important signals come from copper (Cu), tungsten (W), iron (Fe), and oxygen (O). The signals of the O, W, Fe, and Cu peaks confirm the presence of WO_3, Fe_2O_3, and CuO in the nanocomposite powders. For the Fe_2O_3/WO_3NW nanocomposite sample, the Cu and C peaks can be attributed to the sample holder (lacey Cu TEM grid). Similarly, the WO_3 NW-based nanocomposite the Cu peak is stronger in the case of CuO coated WO_3 NW sample than Fe_2O_3 decorated nanocomposite powder, which confirms the presence of CuO nanopartilces in the sample next to the lacey Cu TEM grid.

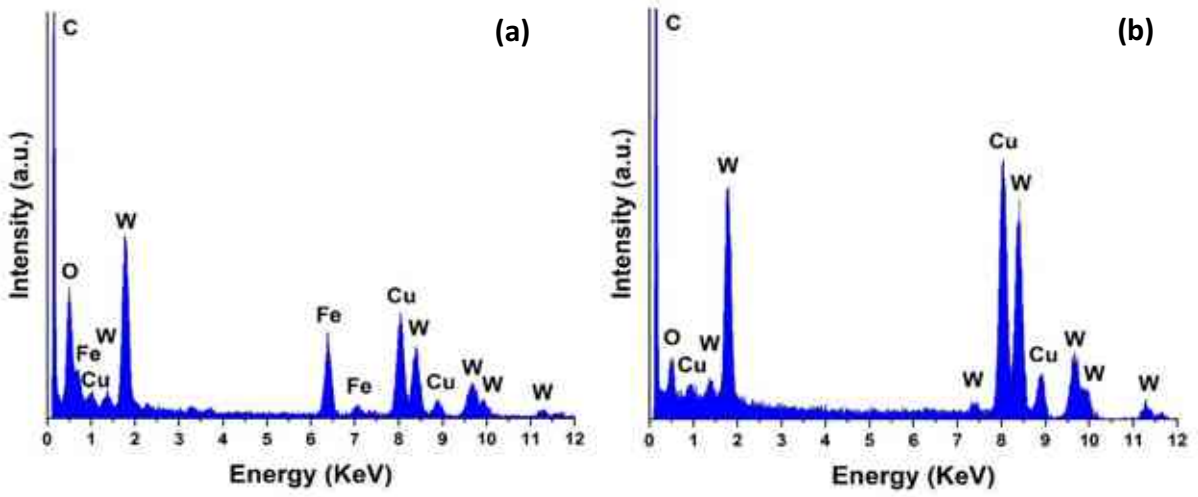

Figure 18. EDS spectra of **(a)** Fe_2O_3/WO_3 NW and **(b)** CuO/WO_3 NW nanocomposites

Additionally, EDS analysis was carried out on all the as-prepared hybrid membrane samples to identify their elemental composition and verify the existence of Fe_2O_3 and CuO nanoparticles. The EDS results shown in Table 5 reveal the atomic percentage (atomic%) of the detected element in all samples (i.e., pure, composites and membranes). Titanium (Ti), tungsten (W), oxygen (O), and carbon (C) signals indicated that cellulose, TiO_2 and WO_3 were present in the hybrid membranes. Moreover, iron (Fe) and copper (Cu) signals were detected, which were correlated to the Fe_2O_3 and CuO nanoparticles, respectively. We also found traces of other elements such as potassium (K) and sodium (Na) originate from the TiO_2 NW, WO_3 NW and Fe_2O_3 preparation process. The obtained results are in good correlation with HRTEM and SEM.

Table 5. Elemental (EDS) analysis in atomic percentage (%) of the nanowires, nanowires-based composites and nanowires-based membranes

Sample name	C	Ti	O	W	K	Na	Fe	Cu
TiO_2 NW	-	34	63	-	2	-	-	1
WO_3 NW	-	-	76	23	-	-	-	1
Cellulose	45	-	55	-	-	-	-	-
TiO_2 NW/cellulose	33	14	50	-	3	-	-	-
WO_3 NW/cellulose	36	-	48	14	-	2	-	-
Fe_2O_3/TiO_2 NW	13	28	47	-	4	-	5	3
CuO/TiO_2 NW	16	28	48	-	-	-	-	8
Fe_2O_3/WO_3 NW	7	-	24	55	-	5	6	3
CuO/WO_3 NW	9	-	20	61	-	2	-	8
Fe_2O_3/TiO_2 NW/cellulose	20	23	50	-	3	-	3	1
CuO/TiO_2 NW/cellulose	25	11	58	-	2	-	-	4
Fe_2O_3/WO_3 NW/cellulose	32	-	48	16	-	2	2	-
CuO/WO_3 NW/cellulose	31	-	49	14	-	2	-	4

5.1.3. Structural properties of pristine nanowires, nanowire-based nanocomposites and hybrid membranes

In the previous chapters, we have presented the surface morphology and chemical compositions of nanowires, nanowires-based nanocomposite, and nanowires-based hybrid membranes. In the next step, XRD analysis was carried out to identify and characterize the crystal structure of the as-prepared nanowires Figure 19. The diffraction peaks are located at around 25°, 33.8°, 39.2°, 48°, 54.2°, 56.5°, 66.4° and 68.8°, corresponding to (101), (211), (220), (200), (105), (213), (004) and (403) refer to tetragonal anatase phase with lattice parameters a=b= 3.784 Å, c= 9.514 (JCPDS 21-1272) (Figure 19 a). The other peaks located at 27.4°, 36.1° and 41.2° correspond to (110), (101) and (111) relate to rutile phase (JCPDS no-21-1276). Furthermore,

the diffraction peaks at 11.4°, 29.2°, 42.9°, and 59.8° correspond to the monoclinic phase of potassium hexatitanate $K_2Ti_6O_{13}$ with lattice parameters a= 15.593, b= 3.796, c= 9.108 (PDF no. 40-0403) and represent the crystallographic planes (200), (310), (602), and (610). These findings are consistent with [180]. In the same context, The diffraction peaks observed at angles of 14°, 18°, 22.7°, 24.3°, 26.8°, 28.1°, 33.6°, 36.5°, 37.6°, 42.8°, 44.3°, 46.5°, 49.8°, 52.2°, 53.5°, 55.4°, 57.5°, 58.5°, and 63.5° correspond to the crystallographic planes (100), (111), (001), (110), (101), (200), (111), (201), (210), (300), (211), (002), (220), (310), (112), (221), (202), (400), and (401), respectively. These peaks are indicative of the hexagonal structure of WO_3 NW, with lattice parameters a=b= 7.298 and c= 3.897 (PDF no. 75-2187) (Figure 18 b). All these results are in agreement with [181,182].

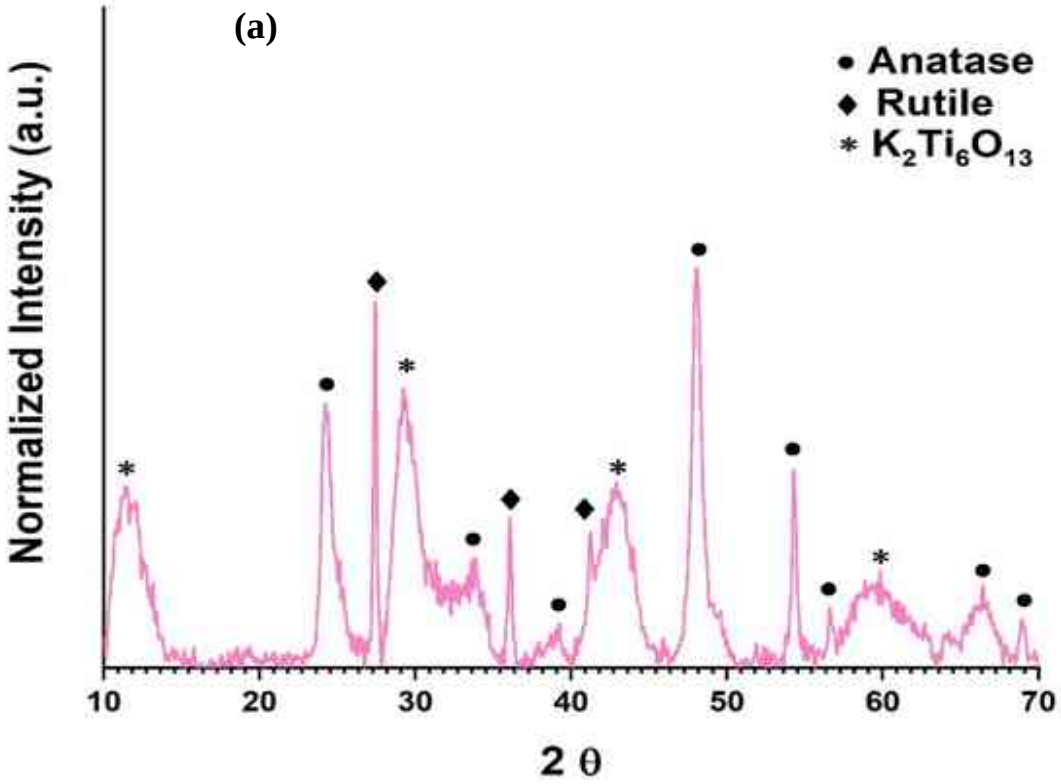

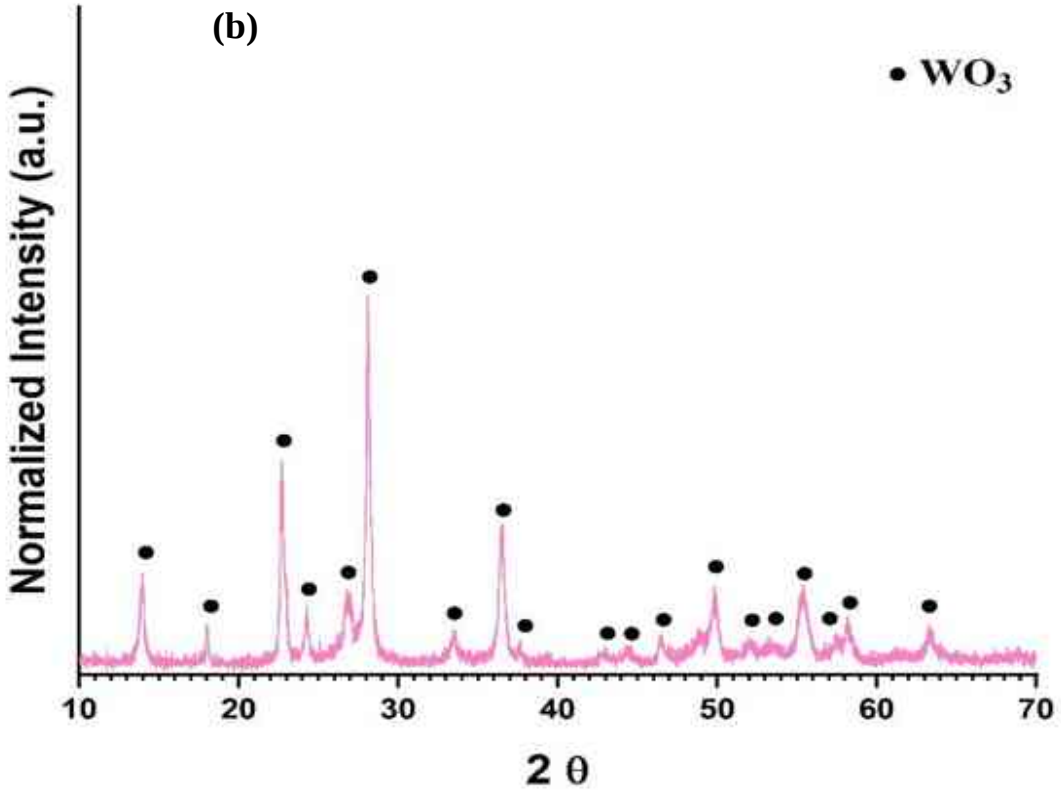

Figure 19. XRD analysis of **(a)** TiO_2 NWs and **(b)** WO_3 NWs

The crystal structure of the as-prepared nanocomposites and membranes was identified using XRD analysis. The diffraction peaks at 25.1°, 33.2°, and 39.2° in Figure 20a correspond to crystallographic planes (012), (104), and (110), respectively. The peaks come from hematite (α-Fe_2O_3) as identified by (JCPDS 33-0664). The diffraction peaks at around 25°, 36.2°, 37.5°, 38.5°, 48.0°, 54.3° and 56,6° correspond to the (101), (103), (004), (112), (200), (105) and (211) reflections, respectively, and relate to tetragonal anatase phase of the TiO_2 NW (JCPDS 21-1276). Furthermore, the diffraction peaks at 24.2°, 29.2°, 43.2°, and 60.1° correspond to the crystal phase (002), (310), (602), (610) of monoclinic potassium hexatitanate $K_2Ti_6O_{13}$ (PDF no. 40-0403). Cellulose diffraction peaks (PDF no. 03-0289) were detected at 16.3°, 22.7°, and 34.5°, corresponding to the crystal planes (110), (110), (200), and (400) reflections. All these findings are in agreement with previous reports [183, 184, 185]. Figure 20 a below clearly illustrates the unique occurrence of Fe_2O_3, without any other forms of iron oxide (namely, FeO and Fe_3O_4) being identified. Moreover, a noticeable peak shift in the characteristic peaks of TiO_2 NW after Fe_2O_3 loading is observed. For instance, the peak at 42.9° shifts to 43.2°, which can be attributed to the replacement effect. This effect occurs when Fe ions replace Ti ions at

specific locations, resulting in the incorporation of Fe ions into the TiO_2 lattice [186, 187, 188, 189] To support this statement, we calculated the interplanar spacing (d-spacing - the distance between interatomic) using Bragg's law. The result clearly shows that the d-spacing reduced from 2.106783 to 2.090479, providing strong evidence that the TiO_2 NW is subjected to compressive strain after loading additives.

To investigate the effect of additives on the lattice parameters of nanowires, firstly, the lattice constants were calculated based on the data obtained from the as-prepared materials and then compared with JCPD cards. The results show that the lattice constants of TiO_2 NW changed from a=b= 3.786 Å, c= 9.43 Å to a=b= 2.67 Å, c= 10.88 after Fe_2O_3 particles attached on TiO_2 NW surface, then a=b= 2.67 Å, c= 10.86 for the Fe_2O_3/TiO_2 NW/cellulose membrane.

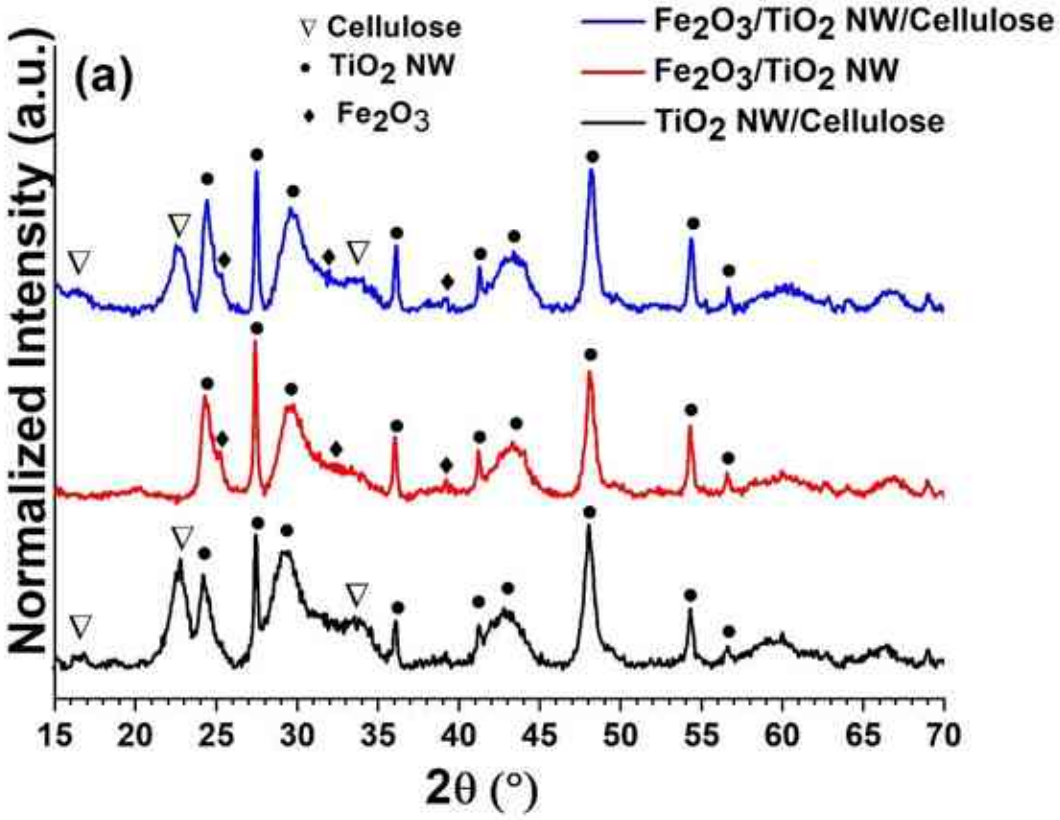

Figure 20 b shows the XRD analysis of the TiO_2 NWs-based nanocomposite and hybrid membrane. The diffraction peaks at 38.3°, 49.4°, and 55° index to (200), (202), and (020) reflections, respectively, related to the monoclinic crystal phases of copper oxide (CuO) as identified by (JCPDS 45-0937), which agreed with [190], [191]. Figure 20 b below clearly demonstrates the absence of Cu_2O or any other forms, as only characteristic CuO peaks were

detected. Furthermore, a noticeable shift in TiO_2 NW peaks can be observed after CuO loading. Specifically, the peak at 42.9 (d-spacing = 2.106783) shifted to 43.28 (d-spacing = 2.088816). This phenomenon has been previously explained [192, 193]. The lattice parameters of TiO_2 NW were confidently altered from a=b=3.783 Å, c=9.43 Å to a=b=3.789 Å, c=8.987 Å after CuO particles attached to the TiO_2 NW surface. Furthermore, the lattice parameters were changed to a=b=3.786 Å, c=8.987 Å for the CuO/TiO_2 NW/cellulose membrane.

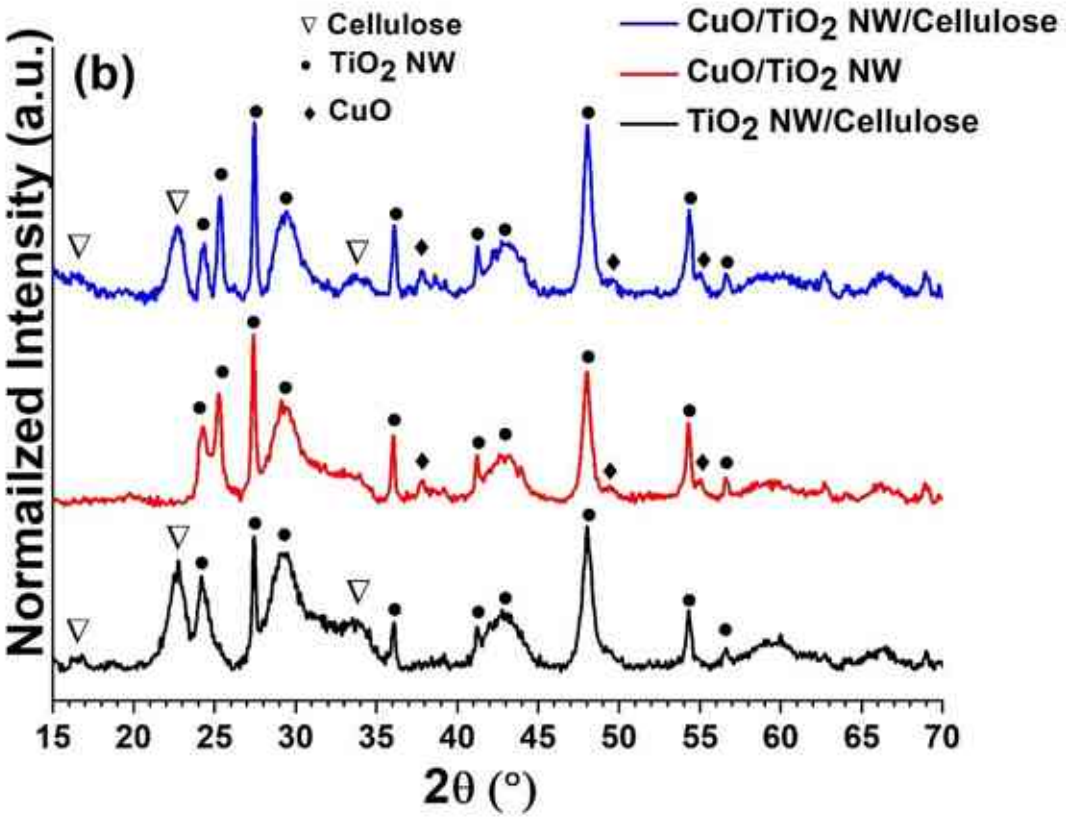

Figure 20. XRD of **(a)** Fe_2O_3/TiO_2 NW/cellulose and **(b)** CuO/TiO_2 NW/cellulose hybrid membranes

Figure 21 shows the XRD investigations of WO_3 NWs-based nanocomposites and membranes, the diffraction peaks at 19.1, 33.4, and 44.5 indexed to (012), (104), and (113), respectively, correspond to Hematite (α-Fe_2O_3) (JCPDS 33-0664). The diffraction peaks at 14.4, 24.9, 28.5, 36.9, 43.1, 50.3, 55.8, 58.7, and 63.7 correspond to reflections at (100), (110), (200), (201), (300), (220), (202), (400), and (401), respectively, belong to the hexagonal structure of WO_3 NW (PDF No. 75-2187). The diffraction peaks at 23.2 and 34.6 correspond to (200) and (400) reflections, respectively, are identified as crystal planes of cellulose (PDF No. 03-0289) (Figure

21 a). All these results agree with [134, 137, 194]. Furthermore, Figure 21 b shows the results of the XRD analysis of the CuO/WO_3 NWs/cellulose hybrid membrane. The diffraction peaks seen at 38.6 48.8, and 53.7 indexed to reflections (200), (202), and (020) corresponding to monoclinic crystal phases of the copper oxide (CuO) (JCPDS card number 45-0937). These findings agree with [195]. Many peak shifts can be observed in WO_3 diffraction after loading additives for the same reasons described earlier.

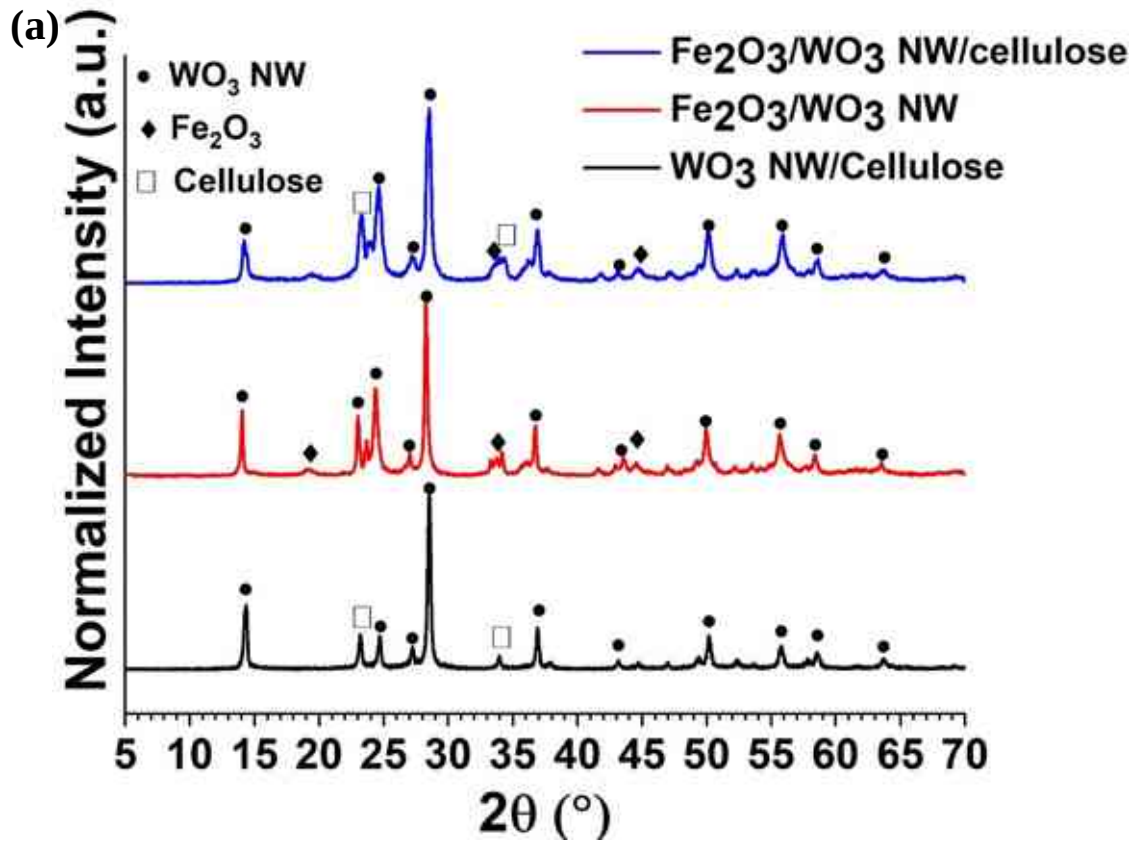

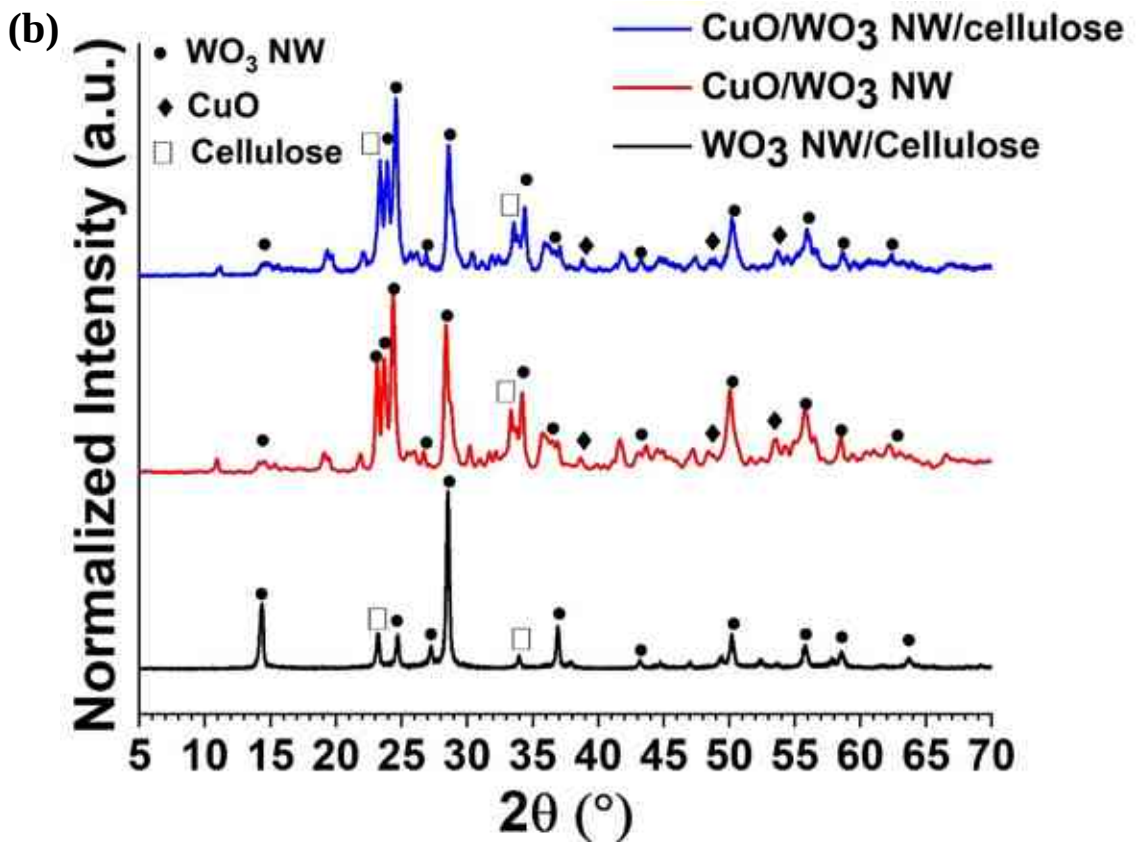

Figure 21. XRD of **(a)** Fe_2O_3/WO_3 NW/cellulose and **(b)** CuO/WO_3 NW/cellulose hybrid membranes

In the next step, we wanted to answer the question of whether chemical bond(s) were formed between the membrane components. In order to demonstrate the chemical interaction between cellulose and the nanowires-based nanocomposite additives, Raman spectroscopy analysis was carried out. The Raman spectra of the CuO/TiO_2 NW and Fe_2O_3/TiO_2 NW nanocomposites (black curves), the pristine cellulose (red curves) and the as-prepared CuO/TiO_2 NW/cellulose and Fe_2O_3/TiO_2 NW/cellulose hybrid membranes (blue curves), respectively. Figure 22 a exhibits Raman spectra with peaks at 143 cm^{-1}, 412 cm^{-1}, and 638 cm^{-1}, representing the E_g (144 cm^{-1}), B_{1g} (399 cm^{-1}), and E_g (639 cm^{-1}) modes of anatase TiO_2 crystals [196] and peaks at 284 cm^{-1} and 636 cm^{-1} correspond to the A_g (296 cm^{-1}) and B_{2g} (636 cm^{-1}) modes of CuO crystals [197]. In Figure 22 a, red curve shows the characteristic cellulose peaks found at 138, 1097, 1365, and 1650 cm^{-1} [198]. In the spectrum of the hybrid membrane shown in Figure 22 a, blue curve shift was seen in the characteristic peaks of the CuO/TiO_2 NW nanocomposite and cellulose. Also, as shown on the hybrid membrane's spectrum, three new peaks show at 1028, 1439, and 1549 cm^{-1} (marked with green arrows in Figure 22a). As there are no

characteristic peaks of the nanocomposite and cellulose in this area, these bands likely resulted from the interaction of the oxygen-containing surface functional groups of cellulose and the CuO/TiO_2 NW nanocomposite. The Raman spectra of the Fe_2O_3/TiO_2 NW/cellulose hybrid membrane exhibits three peaks at 143, 450, and 659 cm^{-1}, which correspond to the E_g (144 cm^{-1}), B_{1g} (399 cm^{-1}), and E_g (639 cm^{-1}) modes of anatase TiO_2 crystals [140], while peaks at 286, 658, and 880 cm^{-1} correspond to the E_g (293, 613, and 814 cm^{-1}) modes of α-Fe_2O_3 crystals [199]. The characteristic peaks of the Fe_2O_3/TiO_2 NW nanocomposite and cellulose were slightly shifted in the spectra of the Fe_2O_3/TiO_2 NW/cellulose hybrid membrane (Figure 22 b blue curve), similar to the CuO/TiO_2 NW/cellulose membrane (Figure 22 a). Moreover, two additional peaks are visible at 993 and 1516 cm^{-1} (marked green in Figure 22 b). These peaks can be attributed to the interaction between cellulose's oxygen-containing surface functional groups and the Fe_2O_3/TiO_2 NW nanocomposite. The cellulose fibers and CuO/TiO_2 NW, Fe_2O_3/TiO_2 NW nanocomposites could form non-covalent interactions, most likely hydrogen bonds, which would cause band shifting and new characteristic peaks [200].

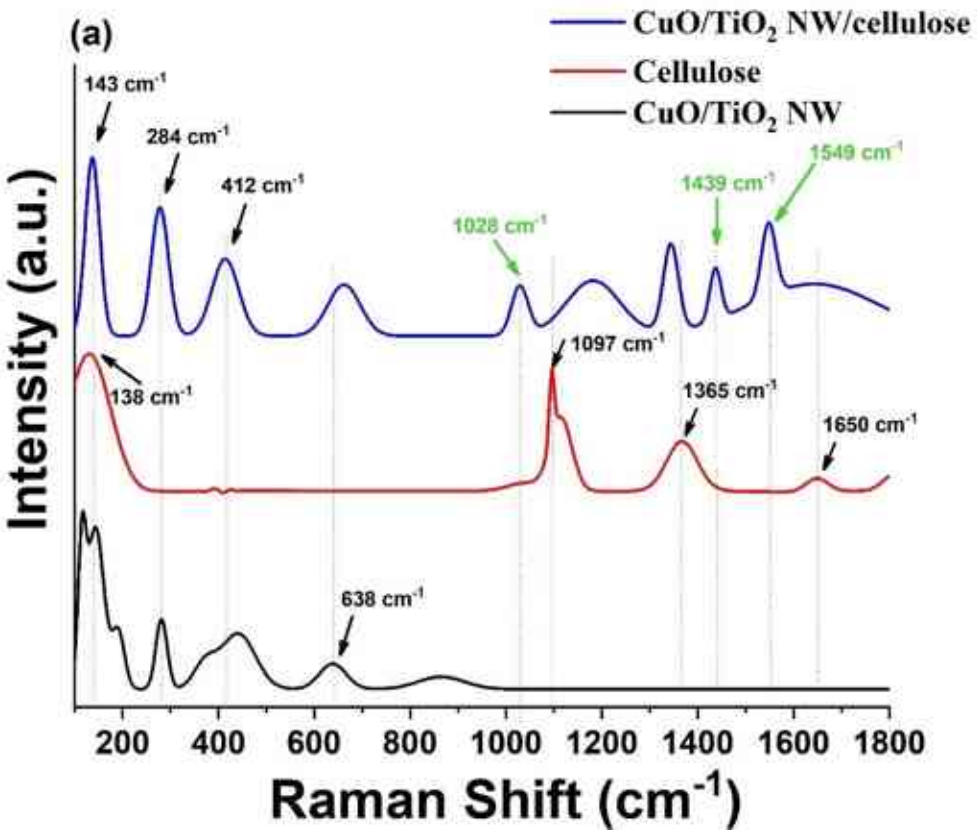

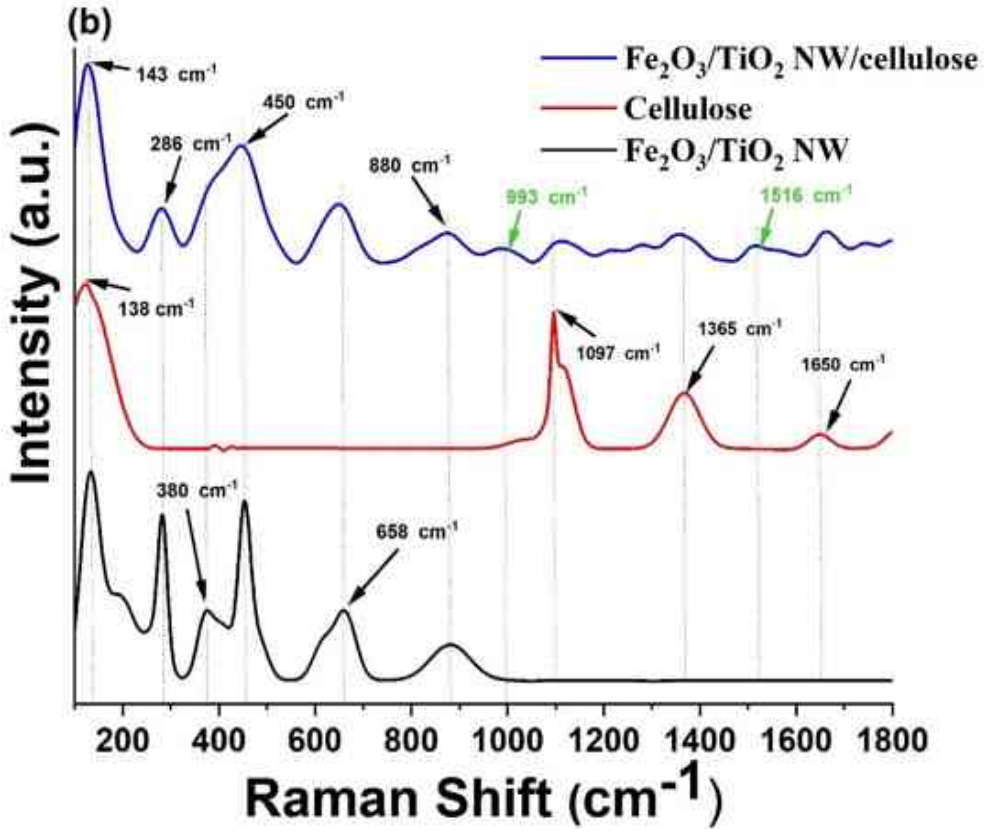

Figure 22. Raman analysis of **(a)** CuO/TiO_2 NW/cellulose and **(b)** Fe_2O_3/TiO_2 NW/cellulose hybrid membranes

In the same context, Raman spectra of CuO/WO_3 NW and Fe_2O_3/WO_3 NW nanocomposites, pristine cellulose and as-prepared CuO/WO_3 NW/cellulose and Fe_2O_3/WO_3 NW/cellulose hybrid membranes are shown in Figure 23 a and b, respectively. Raman analysis was conducted to prove the chemical interaction between membrane components, i.e., the chemical interaction between WO_3 based-inorganic nanoparticles and cellulose.

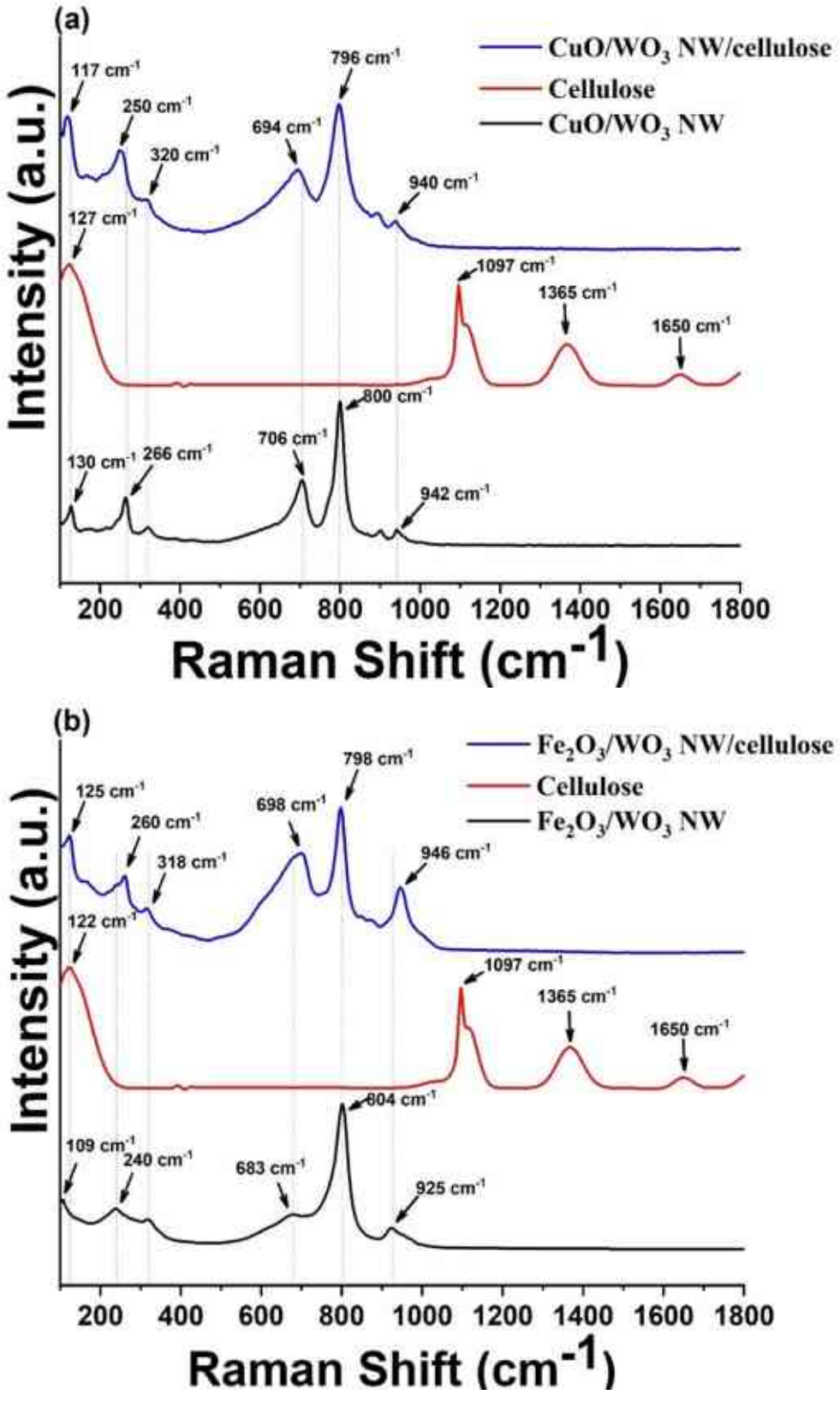

Figure 23. Raman analysis of **(a)** CuO/WO_3 NW/cellulose and **(b)** Fe_2O_3/WO_3 NW/cellulose hybrid membranes

According to the Raman spectra in Figure 23 a, the formation of the vibration of O-O bonds (at 130 cm^{-1}), the bending vibration of the bridging oxygen of W-O-W bonds (318 cm^{-1}), and the stretching vibration bonds (706 cm^{-1}) are all represented by peaks [201]. The peak at 934 cm^{-1} corresponds to the W=O bonds of hexagonal WO_3 nanowires, while the stretching vibration of O-W-O bonds induces the peak at 800 cm^{-1} [202]. The peak at 266 cm^{-1} originates from CuO nanocrystals [203]. As seen in Figure 23 a, red curve, the cellulose peaks may be located at 127, 1097, 1365, and 1650 cm^{-1} [198]. Most of the WO_3 NW and the CuO nanoparticles peaks in the spectrum of the hybrid membrane were shifted, as shown in Figure 23 a, blue curve.

Furthermore, the Raman spectra in Figure 23 b for the Fe_2O_3/WO_3 NW/cellulose hybrid membrane exhibit peaks at 109, 320, and 683 cm^{-1}, which correspond to the formation of vibration of O-O bonds (109 cm^{-1}), the bending vibration of bridging oxygen of W-O-W bonds (320 cm^{-1}), and the stretching vibration bonds (683 cm^{-1}). The peak at 925 cm^{-1} is created by the -W=O bonds of hexagonal WO_3 nanowires, while the stretching vibration of O-W-O bonds induces the peak at 804 cm^{-1}. The peak at E_g 240 cm^{-1} is correspondingly associated with the α-Fe_2O_3 crystals' mode [178]. The Fe_2O_3/WO_3 NW nanocomposite and cellulose peaks were slightly shifted in the spectra of the Fe_2O_3/WO_3 NW/cellulose hybrid membrane (Figure 23 b blue curve), similar to the CuO/WO_3 NW/cellulose membrane (Figure 23 a). The CuO/WO_3 NW, Fe_2O_3/WO_3 NW nanocomposites and cellulose fibers could format non-covalent interactions, most likely hydrogen bonds, which would cause band shifting peaks and explain the phenomena mentioned above [204].

FT-IR analysis was carried out for additional characterization and to definitively confirm a chemical bond formed between the membrane components. In addition to reference cellulose (black curve) and TiO_2 NW/cellulose (red curve), Figure 24 also shows the IR spectra of the hybrid membranes (blue and brown curves) in the range of 400–800 cm^{-1}. The vibrational bands made up primarily of metal-oxygen stretching are present at low frequencies. The TiO_2 NW/cellulose has two bands with an intensity of 439 and 584 cm^{-1}, and cellulose has five bands with intensities at 434, 518, 557, 609, and 663 cm^{-1}, as can be seen from the black curve. In the case of hybrid membranes, the peaks mentioned above were slightly shifted, from 439 cm^{-1} to 440 cm^{-1} and 442 cm^{-1} and from 584 cm^{-1} to 586 cm^{-1}, most likely due to chemical interactions between the CuO, Fe_2O_3, and TiO_2 NW nanoparticles. In addition, a new band at 669 cm^{-1} (marked by green) can be seen in the spectra of both hybrid membranes attributed to the metal-oxygen stretching band as a result of the interaction between TiO_2 NW and CuO and Fe_2O_3

nanoparticles, as there are no recognizable bands of the pristine components in this region [205,206].

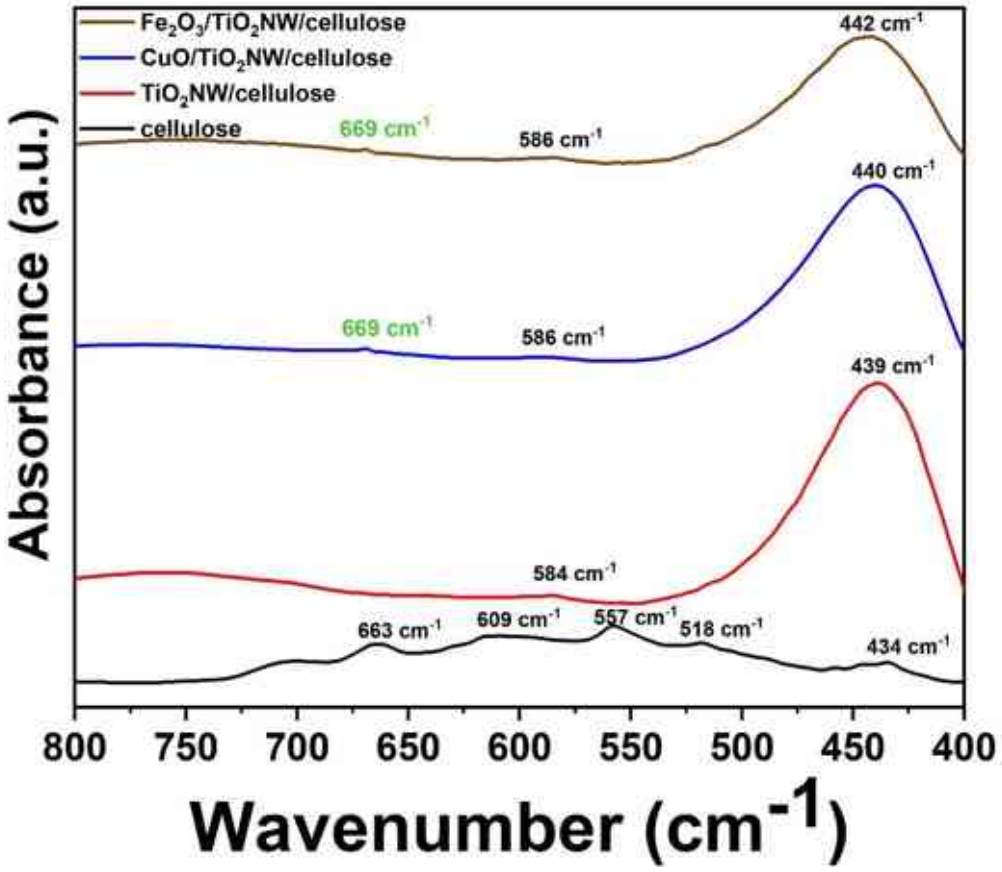

Figure 24. FT-IR analysis of cellulose (black curve), TiO_2 NW/cellulose (red curve), CuO /TiO_2 NW/cellulose (blue curve) and Fe_2O_3/TiO_2 NW/cellulose (brown curve)

Figure 25 shows the FTIR spectra of the WO_3 NW based hybrid membranes (blue and green curves) in addition to the reference cellulose (black curve) and WO_3 NW/cellulose (red curve). This low-frequency range is dominated by vibrational metal-oxygen stretching bands. The black curve shows that cellulose has five bands with considerable intensity at 434, 518, 557, 609 and 663 cm^{-1}, whereas the WO_3 NW/cellulose has four bands with significant intensity at 434, 483, 611, and 807 cm^{-1}. In the case of hybrid membranes, the previously mentioned peaks shifted slightly, from 434 cm^{-1} to 435 and 433 cm^{-1}, from 483 cm^{-1} to 480 and 485 cm^{-1}, from 611 cm^{-1} to 599 and 608 cm^{-1}, and from 807 cm^{-1} to 802 and 809 cm^{-1}, likely due to the chemical interaction between the CuO/WO_3 NW, Fe_2O_3/WO_3 NW nanocomposites and cellulose fibers.

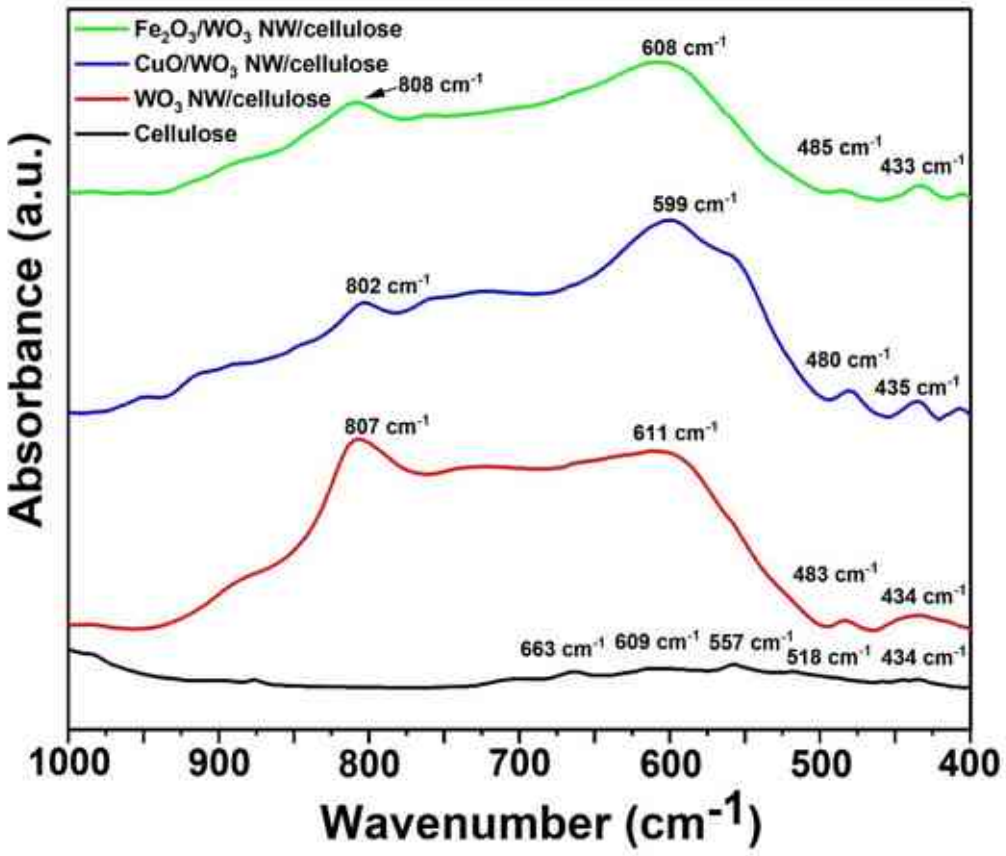

Figure 25. FT-IR analysis of cellulose (black curve), WO_3 NW/cellulose (red curve), CuO/WO_3 NW/cellulose (blue curve) and Fe_2O_3/WO_3 NW/cellulose (green curve)

5.1.4. Textural and surface properties of pristine nanowires, nanowire-based nanocomposites and hybrid membranes

The final characterization step is to determine the surface properties for as-prepared materials such as the specific surface area and surface charge because they are essential factors in the adsorption and photocatalytic process in water treatment. Initially, the N_2 adsorption technique was applied to characterize the as-prepared materials to determine their specific surface area of each sample, as shown in Table 6.

Table 6. Specific surface area of the as-prepared nanowires, nanowires-based composite, nanowires-based hybrid membranes

Sample Name	Specific Surface Area (m^2/g)
TiO_2 NW	168
WO_3 NW	16
Cellulose membrane	6
TiO_2 NW/cellulose	64
WO_3 NW/cellulose	14
Fe_2O_3/TiO_2 NW	146
CuO/TiO_2 NW	139
Fe_2O_3/WO_3 NW	7
CuO/WO_3 NW	6
Fe_2O_3/TiO_2 NW/cellulose	122
CuO/TiO_2 NW/cellulose	117
Fe_2O_3/WO_3 NW/cellulose	8
CuO/WO_3 NW/cellulose	5

As we can see above, the specific surface areas of TiO_2 NW and WO_3 NW were 168 m^2/g and 16 m^2/g, respectively, and the specific surface area was reduced slighltly after loading inorganic nanoparticles: this phenomenon is attributed to the coverage effect when the inorganic nanoparticles tend to agglomerate and cover a portion of the nanowires surface [107]. Also, incorporating nanowires into cellulose resulted in a decrease in their specific surface area due to the mesoporous structure of nanowires being covered by cellulose [207].

To gain more information about the pore system of as-prepared nanowires-based hybrid membranes, the adsorption/desorption isotherm was carried out, as shown in Figure 26.

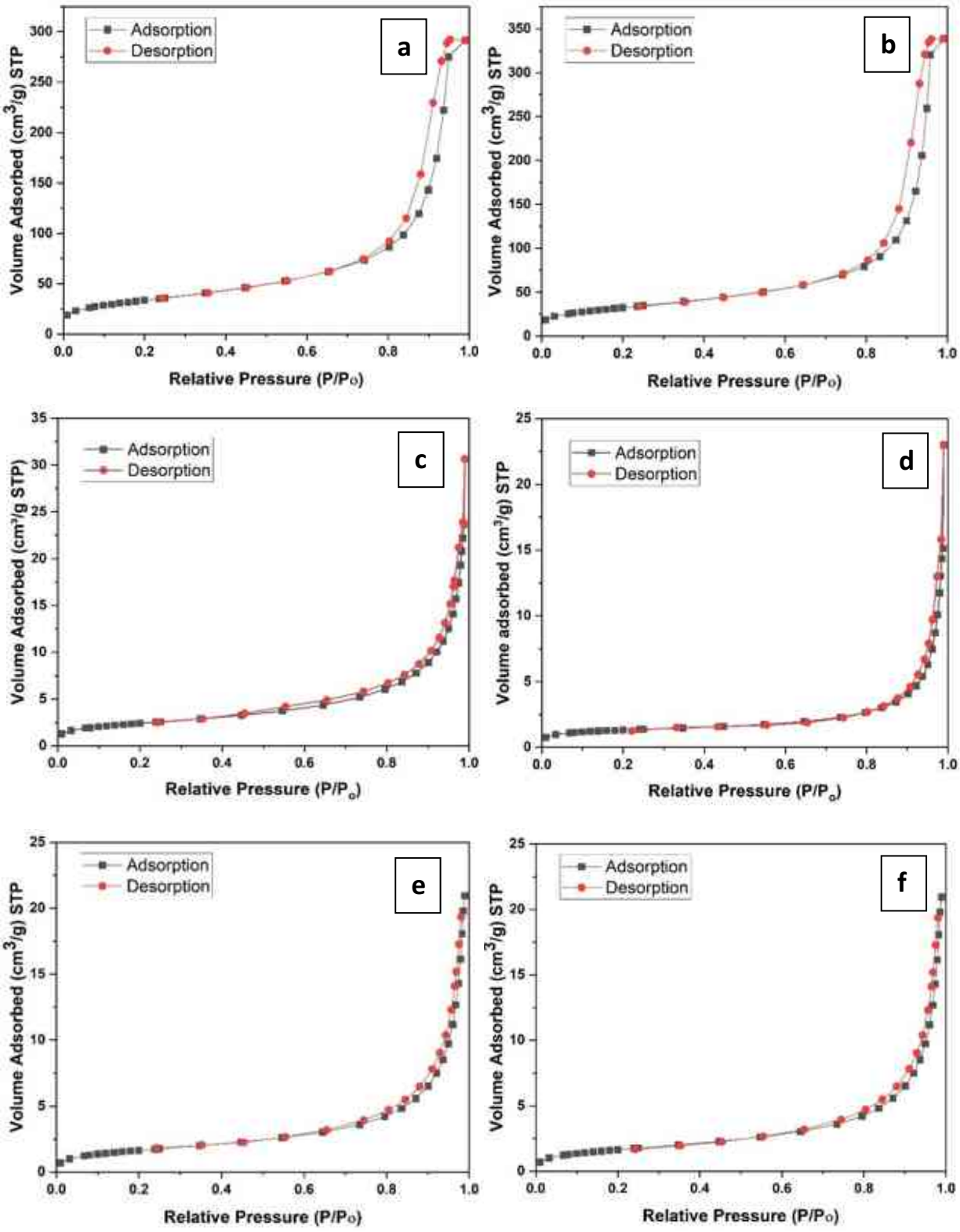
a
Adsorption
Desorption
Volume Adsorbed (cm³/g) STP
Relative Pressure (P/Po)
b
Adsorption
Desorption
Volume Adsorbed (cm³/g) STP
Relative Pressure (P/Po)
c
Adsorption
Desorption
Volume Adsorbed (cm³/g STP)
Relative Pressure (P/Po)
d
Adsorption
Desorption
Volume adsorbed (cm³/g) STP
Relative Pressure (P/Po)
e
Adsorption
Desorption
Volume Adsorbed (cm³/g) STP
Relative Pressure (P/Po)
f
Adsorption
Desorption
Volume Adsorbed (cm³/g) STP
Relative Pressure (P/Po)

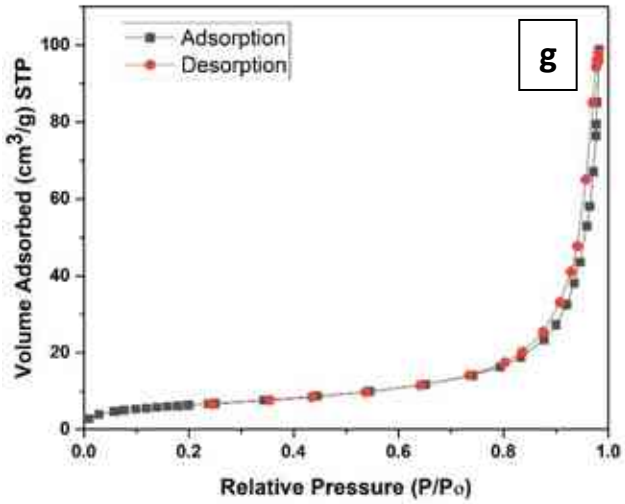

Figure 26. Adsorption/desorption isotherms of **a)** Fe_2O_3/TiO_2 NW/cellulose, **b)** CuO/TiO_2 NW/cellulose, **c)** Fe_2O_3/WO_3 NW/cellulose, **d)** CuO/WO_3 NW/cellulose, **e)** cellulose, **f)** WO_3 NW/cellulose, **g)** TiO_2 NW/cellulose

Figure 26 demonstrates that all samples exhibit type III adsorption/desorption isotherms, as classified by IUPAC, indicating mesoporous materials with a pore size range of 2-50 nm and type H3 hysteresis, which confirms a slit-like layered pore structure [112]. Although the specific surface area of nanowire's-based hybrid membrane was reduced, the performances were enhanced by reducing the band gap or inhibiting the electron-hole recombination rate, which enhanced the photodecolorization ability against MB [106], [110], [196], [208].

Besides specific surface area, surface charge is considered one of the most critical factors in some wastewater treatment processes, especially filtration. Therefore, zeta potential measurement was conducted. The zeta potential (ζ) of the hybrid membranes was assessed at pH 7.0, as shown in Table 7. Before the experiments, the materials were suspended in deionized water to achieve the desired concentration of 0.1 wt.%. Each measurement was repeated three times. By investigating the potential of cellulose, TiO_2 NWs/cellulose, and hybrid membranes (ζ), we can assess whether CuO and Fe_2O_3 nanoparticles attached to the surface of TiO_2 NWs/cellulose can enhance the efficiency of virus retention. Pristine cellulose had a negative zeta potential of (-32.2 mV), while after functionalization the hybrid membranes became more positively charged at (-18.2 and -10.4 mV). The surface treatment of hybrid membranes increases the isoelectric point (IEP), resulting in a higher positive charge on the surface and higher electrostatic contact with bacteriophages. As a result, the filtering effectiveness of MS2

may also increase. Since MS2 has an (ζ) potential of about (-30 mV) [209], it is unexpected to have a high viral retention value from pure cellulose with a zeta potential of (-32.2 mV). Contrarily, it has been demonstrated that Fe_2O_3 and CuO nanoparticles have positive (ζ) potentials at pH 7.0 [210]. As shown in Table 7, it can also be concluded that the surface functionalization of TiO_2 NWs by incorporating CuO and Fe_2O_3 nanoparticles caused the zeta potential values in the case of hybrid membranes to shift to a less negative region. According to these results, the surface electric characteristics of TiO_2 NWs-based membranes are presumably more suitable for the retention of MS2 bacteriophages.

In case of WO_3 NW based hybrid membrane, the (ζ) potential of WO_3 NWs/cellulose, and hybrid membranes has been also analyzed, and it was determined that the CuO and Fe_2O_3 nanoparticles adhered to the surface of WO_3 NWs could also increase the efficacy of virus retention. The zeta potential of the functionalization of hybrid membranes increased their positive charge (-14.5 and -7.6 mV). The surface treatment increases the isoelectric point (IEP), resulting in a higher positive surface charge. The hybrid membranes' surface interacts with bacteriophages through electrostatic forces, as a result, the filtration efficacy of MS2 may also increase. Additionally, the coating of CuO and Fe_2O_3 nanoparticles to the surface of WO_3 NWs altered the zeta potential values for the hybrid membranes to a less negative region, as shown in Table 7. These results indicate that the surface electric properties of WO_3 NWs-based membranes are more favorable to the retention of MS2 bacteriophages.

Table 7. Zeta potential values of the pristine cellulose and the nanowires-based membranes at pH 7.0

Sample	Zeta (ζ) potential (mV)
Cellulose	-32.2 ± 1.1
TiO_2 NWs/cellulose	-27.9 ± 1.0
Fe_2O_3/TiO_2 NWs/cellulose	-18.2 ± 0.5
CuO/TiO_2 NWs/cellulose	-10.4 ± 0.3
WO_3 NWs-cellulose	-21.4 ± 0.8
Fe_2O_3/WO_3 NWs/cellulose	-14.5 ± 0.5
CuO/WO_3 NWs/cellulose	-7.6 ± 0.3

Contact angle measurements were also applied to identify the hydrophilic and/or hydrophobic character of the as-prepared membranes. It was found that, putting the water droplets on the surface of the membranes they were highly absorbed, which can be attributed that the membranes are super hydrophilic nature.

5.2. Applications of membranes

5.2.1. Adsorption and photocatalytic decolorization of methylene blue

Completing the materials science analysis and characterization of the as-prepared nanocomposite powders and membrane materials, we investigated the photodecolorization performance of as-prepared hybrid membranes. The adsorption capacity can be a non-negligible factor in the removal process; thus, we conducted adsorption experiments on P25 and other membranes for 2 h, as shown in Figure 27. The adsorption capacities of TiO_2 NW-based hybrid membranes appeared to be higher than those of WO_3 NW-based hybrid membranes, which may be attributed to a higher specific surface area. Several studies have reported that the adsorption ability of various organic pollutants can be enhanced onto Fe_2O_3 and CuO, making these compounds attractive membrane components for wastewater treatment [100, 211].

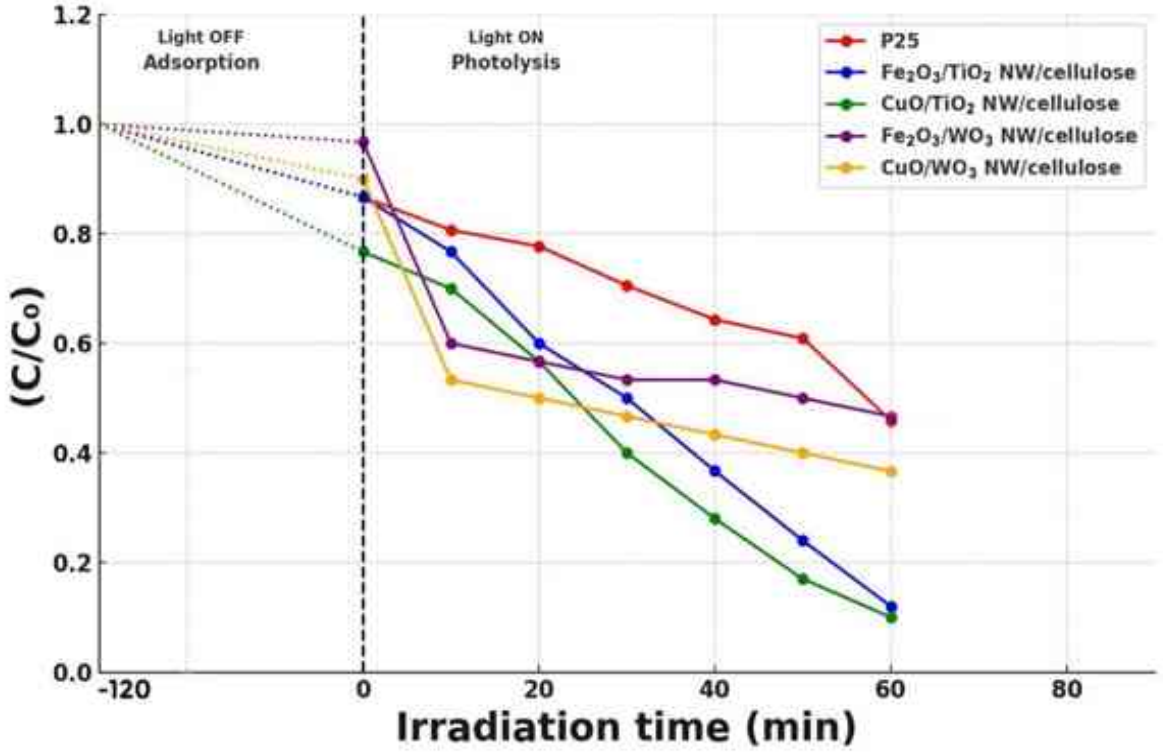

Figure 27. Adsorption and photodecolorization activity of P25 (red line), Fe_2O_3/TiO_2 NW/cellulose (blue line), CuO/TiO_2 NW/cellulose (green line), Fe_2O_3/WO_3 NW/cellulose (purple line), and CuO/WO_3 NW/cellulose (orange line) hybrid membranes in MB tests

The decolorization performance of the as-prepared membranes was evaluated under UV light irradiation against methylene blue dye. Figure 27 shows the MB removal efficiency of the P25, and the as-prepared hybrid membranes under UV irradiation. As it can be seen the TiO_2 NW-based hybrid membranes showed significantly higher MB removal affinity compared to the WO_3 NW-based samples. The decolorization rates of Fe_2O_3/TiO_2 NW/cellulose and CuO/TiO_2 NW/cellulose membranes were approximately 90% in the cases of both samples.

It is essential to note that only P25 and hybrid membranes are shown here because it has been reported that pure cellulose exposed to UV light causes structural deformations. It was one of the main reasons that we utilized a smaller amount of cellulose in the hybrid membranes. The substantial removal of MB by the membranes indicates their ability to degrade organic dye molecules. The outstanding decolorization efficiency may be attributed to the synergistic effects of TiO_2 NWs with nanoparticles (Fe_2O_3, CuO) on their surface and the adsorption of MB on cellulose. In addition, since pure cellulose does not contain any photocatalyst, it is not anticipated that a pure cellulose membrane would possess photocatalytic activity. Also, the high specific surface area of both Fe_2O_3/TiO_2 NW/cellulose and CuO/TiO_2 NW/cellulose is an essential factor in decolorizing MB by providing a high number of active sites on their surface, resulting in the adsorption of large numbers of MB molecules.

Based on our results and other studies (mentioned in literature), we can conclude that CuO/TiO_2 and Fe_2O_3/TiO_2 have outstanding photodecolorization activity against MB, as shown in Figure 27. However, comparing our results with other studies shows that the as-prepared membranes (Fe_2O_3/TiO_2 NW/cellulose and CuO/TiO_2 NW/cellulose) were more efficient than others due to several reasons, such as the decolorization rate was 90% under only 60 min of UV light, and the most crucial reason is that other studies used different nanocomposites. Hence, they need more equipment's to separate them from the solution. On the other hand, here we would like to highlight that our membranes were moderately stable after 60 min application. It was one of the reasons that we used 60 min irradiation, although we applied 2h adsorption tests before the photodecolorization reactions were started. While the photocatalytic activity of the WO_3 NW-based hybrid membranes was also measured by removing methylene blue (MB) after 60 min of exposure to UV light as shown in Figure 27. The results indicate that the maximum decolorization efficiency of the CuO/WO_3 NW/cellulose membrane is approximately 63% compared to 50% of the Fe_2O_3/WO_3 NW/cellulose membrane. In addition, according to the literature, Fe_2O_3 has a lower photocatalytic activity

than CuO [212]; as a result, it can improve the catalytic efficiency of the CuO/WO_3/cellulose membrane. In our investigations, high-pressure tanning lamps (Cosmedico®, Cosmedico, Stuttgart, Germany) were utilized, eliminating visible light emission. Therefore, no cut-off filter was necessary. Some studies used the same materials mentioned to highlight our results and give a better comparison with others, such as Zhao's investigation of the photodegradation of MB using WO_3/Fe_2O_3 under visible light. The results show the degradation rate was 72% at 4h of light exposure [208]. Al Safari et al. evaluated the photocatalytic performance of CuO/WO_3 towards MB; they found the degradation activity rate was 86.5% under visible light within 90 min [213]. Which means that the Fe_2O_3/WO_3 and CuO/WO_3 can be only effective under visible light, while in our study, both can be used under UV light. This section clearly states that tungsten oxide can serve as an effective photocatalyst capable of visible light [214] and UV light [215], while titanium oxide is only effective in UV light.

5.2.2. *E. coli* filtration experiment

Control tests were conducted before starting the filtration testing to explore the possibility of adsorption on the funnel membrane holder without using membranes. Figure 28 shows the *E. coli* removal efficiency values of as-prepared membranes. In TiO_2 cases, membranes containing TiO_2 NW-based inorganic nanocomposite additives demonstrated significantly greater *E. coli* removal (Figure 28, red and green columns) than membrane built using only TiO_2 NW and cellulose without the addition of Fe_2O_3 and CuO nanoparticles (Figure 28, orange column). As can be seen, the Fe_2O_3/TiO_2 NW/cellulose membrane achieved the highest *E. coli* removal efficiency of 61%. (Figure 28 red column). In addition, the performance of the CuO/TiO_2 NW/cellulose membrane was enhanced (Figure 28, green column, 51%) compared to the performance of the pure TiO_2 NW/cellulose membrane (Figure 28, orange column, 39%). Although the removal efficiency of the pure cellulose membrane was also measured, it was not included in Figure 28 because gravity-driven filtration with this membrane was not practicable.

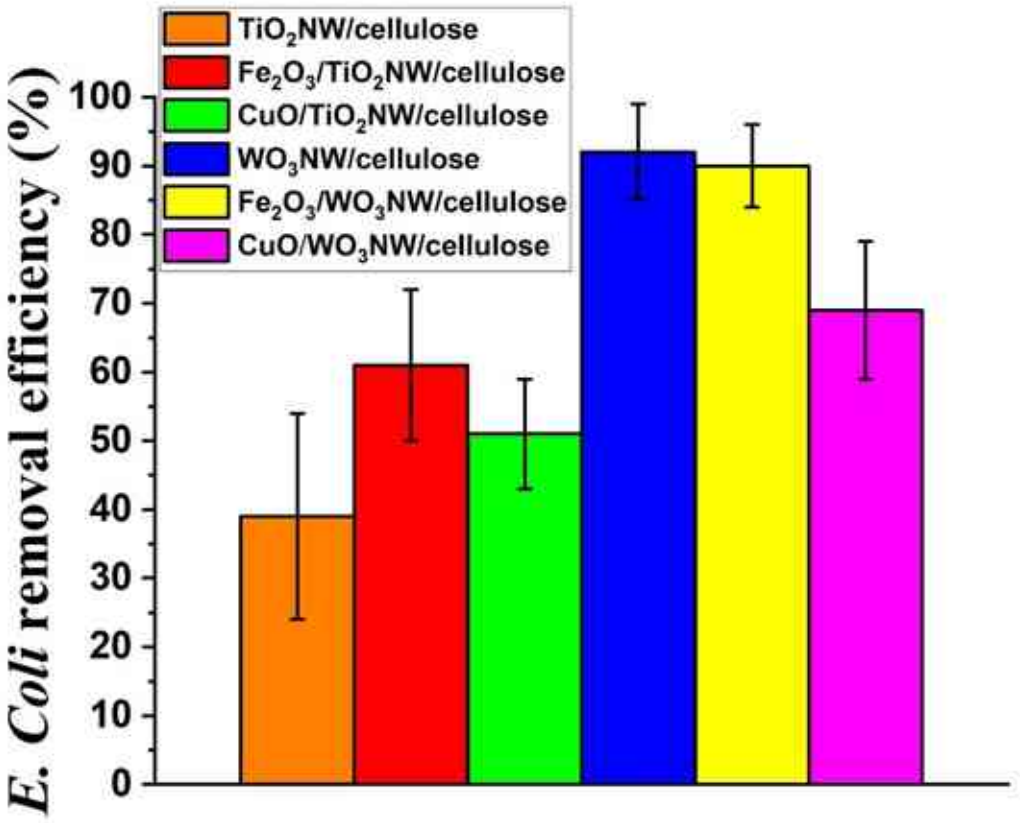

Figure 28. *E. coli* removal efficiency (BFE%) of as-prepared membranes

Based on the findings mentioned above, it was discovered that incorporating Fe_2O_3/TiO_2 NW and CuO/TiO_2 NW nanocomposites into hybrid membrane structures increased the bacteria removal efficiency, as shown in (Figure 28, columns orange, red and green). Consequently, the exceptional filtration performance of hybrid membranes indicates that the removal properties of the membranes are primarily attributable to the nanocomposite Fe_2O_3/TiO_2 NW and CuO/TiO_2 NW additives.

The *E. coli* removal efficacy values of WO_3 NW-based membranes can also be seen in Figure 28. The membrane containing Fe_2O_3/WO_3 NW nanocomposite eliminated significantly more *E. coli* (Figure 28, yellow column) than the membrane containing CuO/WO_3 NW (Figure 28, pink column). The removal efficiency of the WO_3 NW/cellulose membrane (blue column in Figure 28; 92%) was not substantially greater than that of the Fe_2O_3/WO_3 NW/cellulose membrane (89%). While the CuO/WO_3 NW/cellulose membrane had a retention efficiency of 69% for *E. coli*. These results are strongly correlated with the material volume determined using 3D μCT. Based on our prior observations and [191], the *E. coli* filtration and removal

process is primarily attributable to the size exclusion effect and not the electrostatic-based adsorption force. Therefore, membranes with greater material percentage volume, such as WO_3 NW/cellulose membrane (43.8 %) and Fe_2O_3/WO_3 NW/cellulose membrane (47.5 %), are more likely to exhibit greater *E. coli* retention.

5.2.3. MS2 filtration experiment

The results of MS2 filtration experiments are shown in Figures 29 and 30. Both membranes (TiO_2 NW based hybrid membranes and WO_3 NW based hybrid membranes) were found to be capable of retaining MS2 bacteriophages as model contaminants, but their efficiencies were substantially different. As shown in Figure 29 c and Figure 30 green column, the CuO-coated TiO_2 NW membrane exhibited the most promising adsorption characteristics compared with other TiO_2 based hybrid membranes. The LRV of the CuO/TiO_2 NW/cellulose membrane reached up to 2 at pH 7 (Figure 29 c and Figure 30 green column), the LRVs of the Fe_2O_3/TiO_2 NW/cellulose and TiO_2/cellulose membranes demonstrated notably lower virus retention capacity. In the case of Fe_2O_3/TiO_2 NW/cellulose membrane, the virus retention value was 1.2 LRV (Figure 29 b and Figure 30 red column), whereas it was only 0.6 LRV for TiO_2 NW/cellulose membrane (Figure 29 a and Figure 30 orange column).

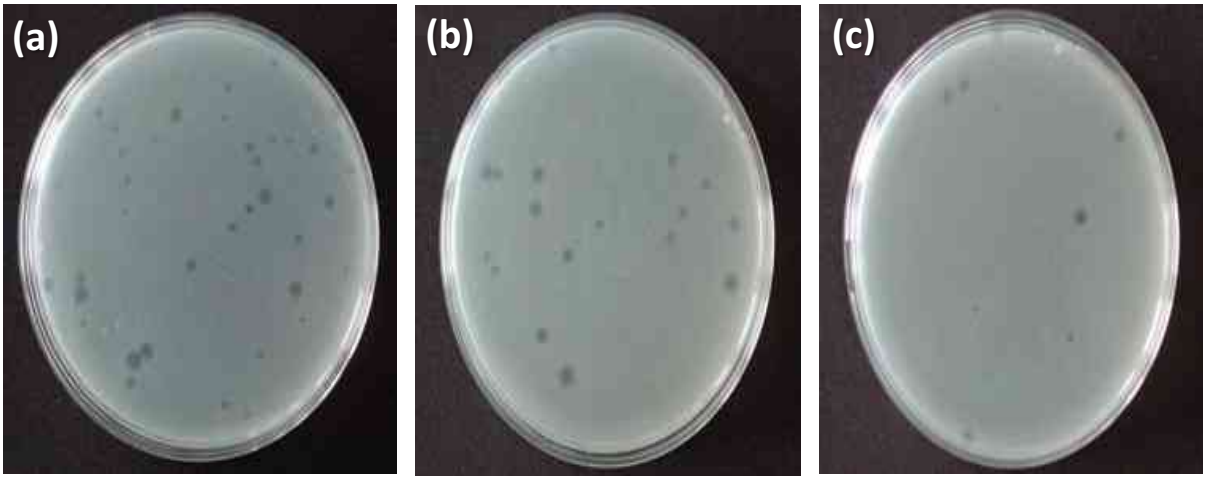

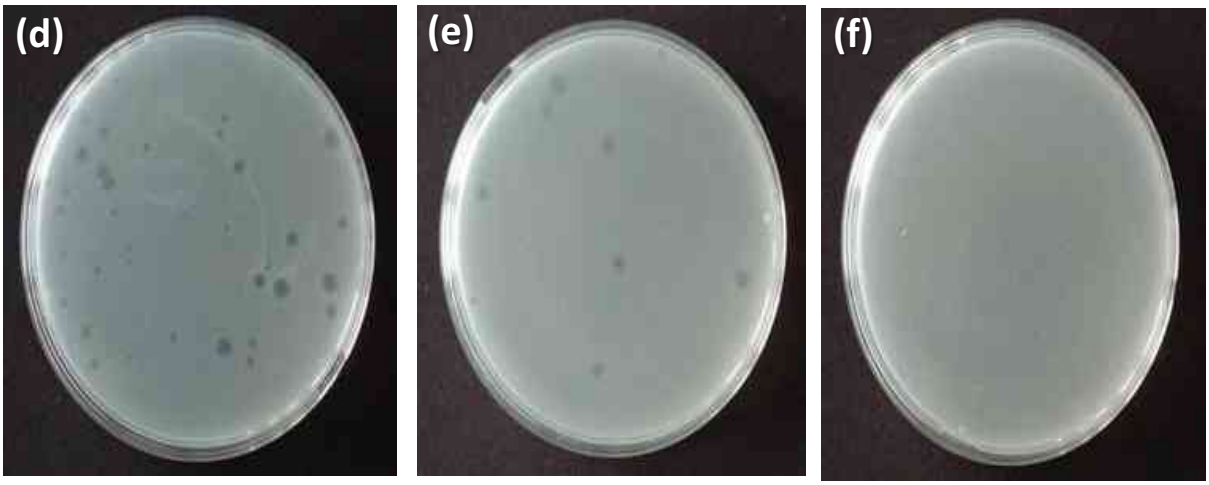

Figure 29. MS2 enumeration plates of TiO_2 NW/cellulose **(a)**; Fe_2O_3/TiO_2 NW/cellulose **(b)** and CuO /TiO_2 NW/cellulose **(c)** membranes after filtration experiments, investigating 2 LRV value. WO_3 NW/cellulose **(d)**; Fe_2O_3/WO_3 NW/cellulose **(e)** and CuO /WO_3 NW/cellulose **(f)** membranes after filtration experiments, investigating 3 LRV value.

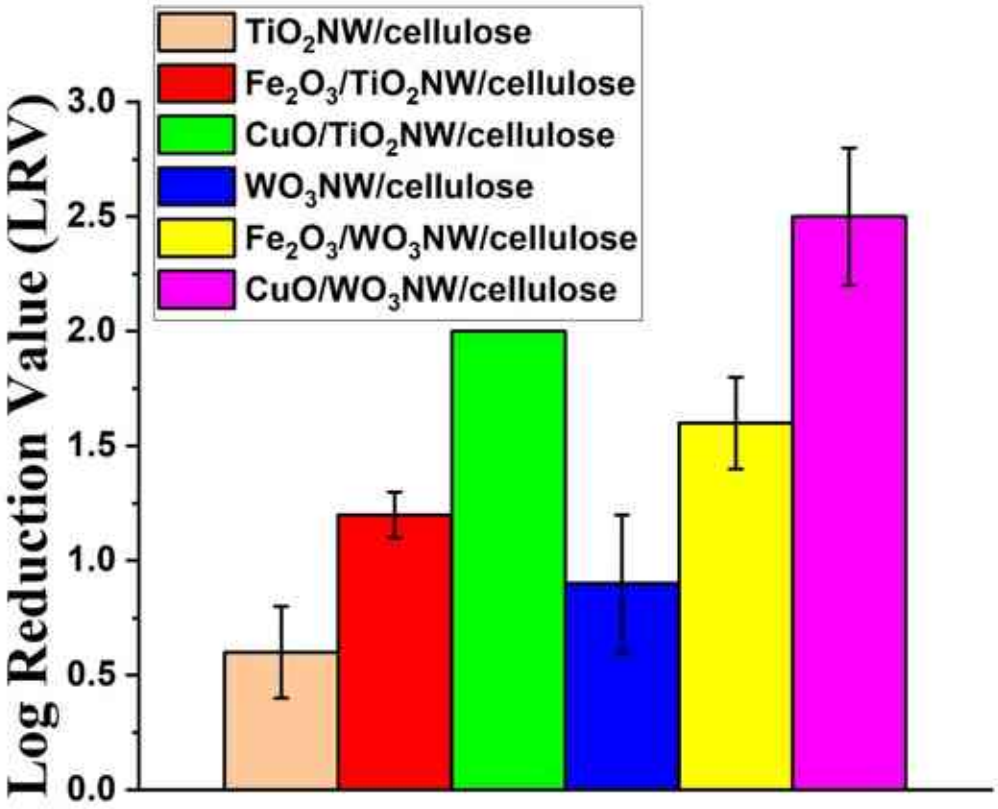

Figure 30. MS2 retention of the nanowires-based hybrid membranes in gravity driven filtration

While the results of MS2 filtration experiments of WO_3 NW based hybrid membrane can also be seen in Figures 29 d-f and 30. All membranes were found to be capable of retaining MS2 bacteriophages as model contaminants, but their efficiencies were substantially different. As shown in the Figures 29 f and 30 pink column, the CuO-coated WO_3 NW membrane exhibited the most promising adsorption properties, the LRV of the CuO/WO_3 NW/cellulose membrane was up to 2.5 at pH 7 (Figure 30 pink column), the LRVs of the Fe_2O_3/WO_3 NW/cellulose and WO_3 NW/cellulose membranes demonstrated significantly less virus retention capacity. The Fe_2O_3/WO_3 NW/cellulose membrane had a virus retention value of 1.6 LRV (Figures 29 e and 30 yellow column), whereas the WO_3 NW/cellulose membrane had a 0.9 LRV (Figures 29 d and 30 blue column).

Based on the results and as previously reported, the specific surface area and the electrostatic force between the bacteriophages and the adsorbents are crucial parameters for virus rejection during virus filtration [216]. The increased virus retention value of the CuO/WO_3 NW/cellulose membrane can be explained by two primary phenomena: the inactivation of virions by CuO nanoparticles and their electrostatic adsorption on the membrane surface [217]. The adsorption properties of TiO_2 NW-based membranes against MS2 were also investigated and described above. Comparing the MS2 adsorption results of WO_3 NW and TiO_2 NW-based hybrid membranes, it was found that the WO_3 NW-based hybrid membranes had higher retention capacity in each case. Based on the obtained results, it can be stated that in addition to the electrostatic interaction between the bacteriophages and the nanoadsorbents, the material quality of the nanowire can contribute significantly to viral filtration.

To measure the total dissolved Cu and Fe content through the filtration process, samples for inductively coupled optical emission spectrometry (ICP-OES) measurements were prepared by filtering pH 7.0 deionized water through a membrane under the previously described experimental conditions. Table 8 reveals that in each instance, the amount of dissolved metal ions was less than the WHO limits (Cu 2 mg/L; Fe-no health-based guideline value is proposed for iron) [218]; consequently, the dissolution of Cu and Fe during filtration does not exceed the international standards. Moreover, based on the obtained values, it is presumed that leaching does not influence the results of *E. coli* and MS2 filtration experiments.

Table 8. Determination of dissolved amount of Cu and Fe content by ICP-OES measurement

Sample	Cu (µg/L)	Fe (µg/L)
Fe_2O_3/TiO_2NWs/cellulose		57 ± 0.0010
CuO/TiO_2NWs/cellulose	46 ± 0.0003	
Fe_2O_3/WO_3 NWs/cellulose		62 ± 0.0010
CuO/WO_3 NWs/cellulose	108 ± 0.0003	

5.2.4. Toxicology experiment

Toxicology testing is considered a critical factor affecting the usability and applicability of as-prepared membranes. After conducting the tests, it was found that none of the membranes exhibited toxic properties under the experimental conditions employed (1 membrane immersed in 500 mL of dilution water and 500 mL of filtered water, respectively). During the testing period, no fish groups exhibited any mortality, concluding that all prepared membranes are not toxic and environmentally friendly and considered a potential high-performance filter for water purification.

6. Summary

This work aims to fabricate stable and self-supported membranes using nanowires-based composite and cellulose fibers as a reinforcement material for water treatment applications. The following conclusions can be obtained from the results of experiments acquired for this PhD work:

- TiO_2 NWs and WO_3 NWs have been successfully synthesized using the hydrothermal method. The morphology and average diameter were investigated by SEM and TEM techniques, and the results revealed the average diameter for TiO_2 NWs and WO_3 NWs was 2-10 and 60-140 nm, respectively. Furthermore, the crystal structure was identified using XRD analysis.

- The synthesis of Fe_2O_3/TiO_2 NWs and Fe_2O_3/WO_3 NWs composite materials was made successful using the hydrothermal preparation method. While CuO/TiO_2 NWs and CuO/WO_3 NWs composite materials were synthesized using the solvothermal technique. Using high-resolution transmission microscopy (HRTEM) to confirm the dispersion of inorganic nanoparticles on the TiO_2 NWs and WO_3 NWs surface and determine their average diameter. The result showed the average diameter of Fe_2O_3 and CuO attached on TiO_2 NWs surface was 20-30 and 2-3 nm, respectively. In contrast, their diameter was 20-30 and 40-50 nm when attached on WO_3 NWs surface. Moreover, Raman measurements confirmed the chemical interaction between TiO_2 NWs, WO_3 NWs and inorganic nanoparticles.

- A new and novel type of cellulose-based hybrid membrane (Fe_2O_3/TiO_2 NWs/cellulose, CuO/TiO_2 NWs/cellulose, Fe_2O_3/WO_3 NWs/cellulose and CuO/WO_3 NWs/cellulose) was developed and characterized. μCT was performed to investigate the 3D morphology and homogeneity for as-prepared membranes; for TiO_2-based hybrid membrane, no significant difference was observed in the membrane structures and a slight difference in percentage by volume of materials. While in the WO_3 NW-based hybrid membrane, a significant difference was found. The percentage by volume of materials value was 43.8 for the WO_3 NW/cellulose, 47.5% in the case of Fe_2O_3/WO_3 NWs/cellulose membrane, and the case of CuO/WO_3 NWs/cellulose membrane, the measured value was only 36.7%, which mean the difference in activity attributed to materials quality and morphology. Raman measurements confirmed the presence of chemical interaction between membrane components. Furthermore, the toxicology measurements reveal that all as-prepared membranes have no toxic properties.

- The photocatalytic decolorization of MB of the different as-prepared membrane (Fe_2O_3/TiO_2 NWs/cellulose, CuO/TiO_2 NWs/cellulose, Fe_2O_3/WO_3 NWs/cellulose and CuO/WO_3 NWs/cellulose) was presented. It was found by comparing the results that CuO/TiO_2 NW/cellulose has higher photocatalytic decolorization of MB obtained at 90 % for 60 min under UV. This finding is attributed to the high specific surface area of TiO_2 NW-based hybrid membranes.

- The antibacterial properties against *Gram-negative E. coli* bacteria of the as-prepared hybrid membranes were studied. The results demonstrated that WO_3 NW/cellulose showed a higher *E. coli* removal filtration value of 92 %. The primary factor responsible for the filtering and elimination of *E. coli* is the size exclusion effect rather than the electrostatic-based adsorption force. Membranes that have a higher percentage volume of material, such as the WO_3 NW/cellulose membrane (43.8%) and the Fe_2O_3/WO_3 NW/cellulose membrane (47.5%), are more likely to have a higher *E. coli* retention.

- The antiviral properties of the different as-prepared membranes (Fe_2O_3/TiO_2 NWs/cellulose, CuO/TiO_2 NWs/cellulose, Fe_2O_3/WO_3 NWs/cellulose and CuO/WO_3 NWs/cellulose) were also investigated. The antiviral properties of the as-prepared hybrid membranes were studied against MS2 bacteriophage. The zeta potential was used to determine the surface charge of the membranes, and the result showed that cellulose has a negative zeta potential, and the hybrid membranes become more positively charged due to functionalization. Since MS2 has an (ζ) potential of about (-30 mV). CuO/WO_3 NW/cellulose showed outstanding MS2 removal ability with an effectiveness of up to 2.5 Log (99.9 %). The results indicate that both the electrostatic interaction between the bacteriophages and the nanoadsorbents, as well as the material quality of the nanowire, play a substantial role in viral filtering.

7. New scientific results

1st thesis: Preparation of hybrid nontoxic membranes by applying cellulose as reinforcement material.

Cellulose is an ideal candidate as an environmentally benign matrix material to fabricate self-supported and stable membranes. Cellulose derivatives are preferably combined with other types of fibrous materials, or the surface of cellulose fibers is decorated with various nanoparticles. In this work, I have shown that it is possible to combine nanocomposites containing two components with cellulose fibers while keeping the cellulose content relatively low (20 wt%), resulting in stable and easy to handle membranes. Four different types of additives such as Fe_2O_3/TiO_2 NW, CuO/TiO_2 NW, Fe_2O_3/WO_3 NW and CuO/WO_3 NW were used for the cellulose-based membranes prepared by screening. Toxicological experiments revealed that all the membranes thus produced do not exhibit toxic properties.

I confirmed that flexible self-supporting cellulose-reinforced hybrid membranes could be synthesized by the combination of 20 wt% of cellulose and different types of nanocomposite additives by using a simple papermaking method. Accurate determination of the cellulose content was essential for the stability and applicability of the membranes to be produced. A non-covalent chemical interaction between the cellulose reinforcement and the nanocomposite additives was proven by Raman and FTIR investigations. Toxicology studies showed that combining cellulose fibers with nanocomposites could open new pathways in the field of environmentally friendly water treatment.

2nd thesis: Application of cellulose-reinforced hybrid membranes for MB decolorization

Decolorization efficiency of the synthesized membranes was evaluated using methylene blue dye as a model pollutant under UV light irradiation. Comparing the results of four types of membranes Fe_2O_3/TiO_2 NWs/cellulose, CuO/TiO_2 NWs/cellulose, Fe_2O_3/WO_3 NWs/cellulose, and CuO/WO_3 NWs/cellulose it was found the TiO_2 NW-based hybrid membranes showed significantly higher MB decolorization affinity compared to the WO_3 NW-based samples. Furthermore, I found that CuO decorated nanowire-based membranes showed higher MB removal efficiency than those containing Fe_2O_3 decorated nanowires in both cases. I verified that CuO/TiO_2 NWs/cellulose membrane showed the highest photocatalytic efficiency (90 %) under 60 min of UV light.

I confirm that the material quality of the membrane components is essential to the efficiency of hybrid membranes in the MB decolorization reaction. It was found that there is a significant difference in performance between WO_3 and TiO_2 based membranes, which is closely related to the number of active binding sites on the surface of the membranes, the adsorption capacity of the membranes and their surface charge. I confirm that applying 60 min UV irradiation the CuO/TiO_2 NWs/cellulose membrane demonstrated the highest MB decolorization efficiency with a percentage of 90%.

3rd thesis: Application of cellulose-reinforced hybrid membranes for bacteria (*E. coli*) filtration

Comparing the TiO_2 NW-based membranes with the WO_3 NW-based membranes in general was concluded that in *E. coli* filtration experiments the WO_3 NW-based membranes showed significantly higher retention ability. Furthermore, it was found that the removal efficiency of WO_3 NW/cellulose membrane (92%) was not significantly higher than that of Fe_2O_3/WO_3 NW/cellulose membrane (89%). In contrast, the CuO/WO_3/cellulose membrane showed lower *E. coli* retention with an efficiency of 69%. These results showed good correlation with the material volume percentages measured by 3D μCT technique. I confirmed that WO_3 NWs/cellulose has a higher material percentage volume, which plays an important role in bacteria retention. Moreover, regarding inductively coupled optical emission spectrometry (ICP-OES) measurements, I confirmed that the amount of metal ions dissolved through filtration is less than the WHO limitation.

I confirm that the material volume of the cellulose-reinforced membranes has played a major role in the filtration experiments. Higher material volume impacts bacteria retention processes and significant E. coli removal (90%) can be reached by applying Fe_2O_3/WO_3 NWs/cellulose membrane.

4th thesis: Application of cellulose-reinforced hybrid membranes for virus (MS2) filtration

The four types of hybrid membranes such as Fe_2O_3/TiO_2 NWs /cellulose, CuO/TiO_2 NWs/cellulose, Fe_2O_3/WO_3 NWs/cellulose, and CuO/WO_3 NWs/cellulose were compared, and I verified that CuO/WO_3 NWs/cellulose showed the highest MS2 retention showed up to 2.5 LRV (log removal value) at pH 7. Furthermore, it was also concluded that CuO decorated samples and membranes provided higher virus retention values in both case than membranes contained Fe_2O_3 nanoparticles. By zeta potential measurements I confirmed that inorganic nanoparticles improve the surface charge of the cellulose-reinforced membranes, which can explain the enhancement in MS2 retention performance.

I confirm that material quality, the type of the applied nanowire and the chosen nanoparticle plus the membrane surface charge can play a significant role and influence the retention processes of MS2 bacteriophages. CuO/WO_3 NWs/cellulose demonstrated the highest antiviral retention up to 2.5 LRV at pH 7.

8. Publications

Articles connecting the dissertation:

1- **Mohammed Ahmed Shehab**, Emma Szori-Doroghazi, Szilvia Szabo, Andrea Valsesia, Tanya Chauhan, Tamas Koos, Gabor Muranszky, Tamas Szabo, Klara Hernadi, Zolta´n Nemeth, *Virus and bacterial removal ability of TiO_2 nanowire-based self-supported hybrid membranes*. Arabian Journal of Chemistry (**2023**) 16, 104388. https://doi.org/10.1016/j.arabjc.2022.104388. **Q1 (IF: 6.212)**

2- **Mohammed Ahmed Shehab**, Nikita Sharma, Andrea Valsesia, Gábor Karacs, Ferenc Kristály, Tamás Koós, Anett Katalin Leskó, Lilla Nánai, Klara Hernadi and Zoltán Németh, *Preparation and Photocatalytic Performance of TiO_2 Nanowire-Based Self-Supported Hybrid Membranes*, Molecules, **(2022)**, 27(9), 2951. https://doi.org/10.3390/molecules27092951 . **Q1 (IF: 4.927)**

3- **Shehab, M.A.**; Sharma, N.; Karacs, G.; Nánai, L.; Kocserha, I.; Hernadi, K.; Németh, Z. *Development and Investigation of Photoactive WO_3 Nanowire-Based Hybrid Membranes*. Catalysts (**2022)**, 12, 1029. https://doi.org/10.3390/catal12091029. **Q2 (IF: 4.501)**

4- **M.A. Shehab**, N. Sharma, G. Karacs, F. Kristaly, B.E. Mrabate, T. Chauhan, T. Koós, A.K. Leskó, Á.B. Palotás, K. Hernádi, Z. Németh. *Effect of the synthesis parameters on the formation of TiO2 nanostructures: controllable synthesis and adsorption properties of nanowires and nanotubes.* Cir. Eco. Environ. Protech. 5 (3) **(2021)**, 16-38.

5- **M.A. Shehab**, G. Karacs, T. Koós, N. Sharma, K. Hernádi, Z. Németh. *Adsorptive removal of methylene blue by TiO_2 nanowire / Fe_2O_3 nanocomposite.* Cir. Eco. Environ. Protech. 5 (2) **(2021)**, 17-28.

6- **Mohammed Ahmed Shehab**, Emma Szőri-Dorogházi, Tímea B. Gerzsenyi, Tanya Chauhan, Andrea Valsesia, Tamás Szabó, Mohammed Alktranee, Qusay F. Alsalhy, Anett Katalin Leskó, Nikita Sharma, Klara Hernadi, Zoltán Németh, *Application of WO_3 nanowire-based hybrid membranes for removal of microorganism in drinking water*, Applied Water Science (Under review).

Other publications:

1- B.E. Mrabate, E. Szőri-Dorogházi, **M.A. Shehab**, T. Chauhan, G. Muránszky, E. Sikora, Á. Filep, N. Sharma, L. Nánai, K. Hernadi, Z. Németh. *Widespread applicability of bacterial cellulose-ZnO-MWCNT hybrid membranes,* Arab. J. Chem. 14 (7) **(2021)**, 103232. https://doi.org/10.1016/j.arabjc.2021.103232. **Q1 (IF: 6.212)**

2- Mohammed Alktranee, **Mohammed Ahmed Shehab**, Zoltan Nemeth, Peter Bencs, Klara Hernadi, Tamas Koos, *Energy and exergy assessment of photovoltaic-thermal system using tungsten trioxide nanofluid: An experimental study*, International Journal of Thermofluids, 16 (**2022**) 100228, https://doi.org/10.1016/j.ijft.2022.100228. **D1 (IF: 9.47)**

3- Al-Maliki, R.M.; Alsalhy, Q.F.; Al-Jubouri, S.; Salih, I.K.; AbdulRazak, A.A.; **Shehab, M.A**.; Németh, Z.; Hernadi, K. *Classification of Nanomaterials and the Effect of Graphene Oxide (GO) and Recently Developed Nanoparticles on the Ultrafiltration Membrane and Their Applications: A Review*. Membranes (**2022)**, 12, 1043. https://doi.org/10.3390/membranes12111043. **Q2 (IF: 4.562)**

4- Mohammed Alktranee, **Mohammed Ahmed Shehab**, Zoltán Németh, Péter Bencs, Klara Hernadi, *Effect of zirconium oxide nanofluid on the behaviour of photovoltaic–thermal system: An experimental study*, Energy Reports 9 **(2023)** 1265–1277. https://doi.org/10.1016/j.egyr.2022.12.065 **Q2 (IF: 4.937)**

5- Tanya Chauhan, Mahitha Udayakumar, **Mohammed Ahmed Shehab**, Ferenc Kristaly, Anett Katalin Lesko, Martin Ek, David Wahlqvist, Pal Toth, Klara Hernadi, Zoltan Nemeth, *Synthesis, characterization, and challenges faced during the preparation of zirconium pillared clays*, Arabian Journal of Chemistry **(2022)** 15, 103706, https://doi.org/10.1016/j.arabjc.2022.103706 . **Q1 (IF: 6.212)**

6- Alktranee, M., **Shehab, M.A**., Németh, Z., Bencs, P. (2023). *Iron Oxide and Tungsten Trioxide Nanofluids to Enhance Automotive Cooling Radiators: Experimental Analysis*. In: Jármai, K., Cservenák, Á. (eds) Vehicle and Automotive Engineering 4. VAE (**2022),** Lecture Notes in Mechanical Engineering. Springer, Cham. https://doi.org/10.1007/978-3-031-15211-5_43. **Q4**

7- Al-Maliki, R.M.; Alsalhy, Q.F.; Al-Jubouri, S.; AbdulRazak, A.A.; **Shehab, M.A**.; Németh, Z.; Hernadi, K.; Majdi, H.S. *Enhanced Antifouling in Flat-Sheet Polyphenylsulfone Membranes Incorporating Graphene Oxide–Tungsten Oxide for Ultrafiltration Applications*. Membranes (**2023)**, 13, 269. https://doi.org/10.3390/membranes13030269 . **Q2 (IF: 4.562)**

8- Dhiyaa A Hussein Al-Timimi, Qusay F Alsalhy, Adnan A AbdulRazak, **Mohammed Ahmed Shehab**, Zoltán Németh, Klara Hernadi, *Optimum Operating Parameters for PES nanocomposite membranes for Mebeverine Hydrochloride Removal*, Journal of Materials Research and Technology, (**2023**), 24, 6779-6790, https://doi.org/10.1016/j.jmrt.2023.04.247 . **D1 (IF: 6.267)**

9- Mohammed Alktranee, **Mohammed Ahmed Shehab**, Zoltán Németh, Péter Bencs, Klara Hernadi, *Experimental study for improving photovoltaic thermal system performance using hybrid titanium oxide-copper oxide nanofluid*, Arabian Journal of Chemistry, **(2023)**, 16(9), 105102, https://doi.org/10.1016/j.arabjc.2023.105102. **Q1 (IF: 6.212)**

10- Mohammed Alktranee, **Mohammed Ahmed Shehab**, Zoltán Németh, Peter Bencs, Klara Hernadi, *Thermodynamic analysis of mono and hybrid nanofluid effect on the photovoltaic-thermal system performance: A comparative study*, Heliyon 9, 12, **(2023)**, e22535. https://doi.org/10.1016/j.heliyon.2023.e22535. **Q1 (IF: 4.0)**

11- Rana I Raja, Khalid T Rashid, MA Toma, Adnan A AbdulRazak, **Mohammed Ahmed Shehab**, Klara Hernadi, *A Novel Polyethersulfone/Chamomile (PES/Chm) Mixed Matrix Membranes for Wastewater Treatment Applications*, Journal of Saudi Chemical Society, 28(2), (**2024**), 101805. https://doi.org/10.1016/j.jscs.2023.101805. **Q1 (IF: 5.6)**

12- Younis Rasheed Taha, Adel Zrelli, Nejib Hajji, Qusay Alsalhy, **Mohammed Ahmed Shehab**, Zoltán Németh, Klara Hernadi, *Optimum content of incorporated nanomaterials: Characterizations and performance of mixed matrix membranes a review*, Desalination and Water Treatment, 317, **(2024)**, 100088. https://doi.org/10.1016/j.dwt.2024.100088. **Q3 (IF: 1.273)**

13- Mohammed Alktranee, Qudama Al-Yasiri, **Mohammed Ahmed Shehab**, Peter Bencs, Zoltán Németh, Klara Hernadi, *Experimental and numerical study of a photovoltaic/thermal system cooled by metal oxide nanofluids*, Alexandria Engineering Journal, 94, **(2024)**, 55-67. https://doi.org/10.1016/j.aej.2024.03.050 . **Q1 (IF: 6.8)**

9. Acknowledgement

This dissertation is a long-term project; a challenge we give ourselves. But above all, it is an excellent story of relationships, meetings, and friendships. This research work could not have been completed without the rich collaboration that I have been able to have with many people and without the precious help and constant support they have given me. I want to show them my gratitude within these few lines. It will be quite hard for me to acknowledge everyone because it is due to the guidance and help of many people that I was able to complete this thesis. I would like to warmly thank **Dr. Zoltán Németh**, Senior Research Fellow, for his confidence in me by accepting the scientific direction of my work. I am thankful to him for allowing me throughout this work to benefit from his great competence, intellectual rigor, dynamism, and willingness to help in all circumstances that I will never forget. Be assured of my devotion and my deep gratitude.

I would like to express my gratitude to all my respected teachers at the **University of Miskolc**, who taught me different subjects during the program's first two years. Also, I am thankful to **Basrah University for Oil and Gas** for supporting me through my study.

I also wish to thank **Prof. Dr. Klára Hernádi** for her continuous guidance and valuable review of my scientific articles. Sincere thanks to all my colleagues who helped me characterize the samples and analyze the results. I am thankful to **Ms. Ágnes Solczi** for her kind help and guidance in the administrative work. I also thank my teachers at the **University of Technology-Baghdad**, who gave me a good scientific foundation that helped me and still does.

Finally, I would like to thank my parents for giving birth to me in the first place and supporting me devoutly throughout my life, my dear wife Sarah, and my beloved’s children Noor, Samer, and Nay, and the rest of my family, for their non-stop support during my studies and preparation of my Ph.D. dissertation.

This research was supported by the European Union and the Hungarian State the National Research, Development, and Innovation Office (NRDI Fund), grant number 2020-2.1.1-ED-2020-00029, Hungary and NRDIO Hungary SNN 143949. The support from Stipendium Hungaricum Scholarship Program is also appreciated.

10. References

[1] Yang, J., Hou, B., Wang, J., Tian, B., Bi, J., Wang, N., Li, X. and Huang, X., **2019**. Nanomaterials for the removal of heavy metals from wastewater. *Nanomaterials*, *9*(3), p.424. http://doi.10.3390/nano9030424

[2] Epelle, E.I., Okoye, P.U., Roddy, S., Gunes, B. and Okolie, J.A., **2022**. Advances in the applications of nanomaterials for wastewater treatment. *Environments*, *9*(11), p.141. https://doi.org/10.3390/environments9110141

[3] Nakum, J. and Bhattacharya, D., **2022**. Various green nanomaterials used for wastewater and soil treatment: a mini-review. *Frontiers in Environmental Science*, *9*, p.724814.http://doi.10.3389/fenvs.2021.724814

[4] Rathi, B.S., Kumar, P.S. and Vo, D.V.N., **2021**. Critical review on hazardous pollutants in water environment: Occurrence, monitoring, fate, removal technologies and risk assessment. *Science of the Total Environment*, *797*, p.149134. https://doi.org/10.1016/j.scitotenv.2021.149134

[5] Lellis, B., Fávaro-Polonio, C.Z., Pamphile, J.A. and Polonio, J.C., **2019**. Effects of textile dyes on health and the environment and bioremediation potential of living organisms. *Biotechnology Research and Innovation*, *3*(2), pp.275-290. https://doi.org/10.1016/j.biori.2019.09.001

[6] Ahmad, S., Almehmadi, M., Janjuhah, H.T., Kontakiotis, G., Abdulaziz, O., Saeed, K., Ahmad, H., Allahyani, M., Aljuaid, A., Alsaiari, A.A. and Muhammad, J., **2023**. The effect of mineral ions present in tap water on photodegradation of organic pollutants: future perspectives. *Water*, *15*(1), p.175. https://doi.org/10.3390/w15010175

[7] Global health estimates **2019**: deaths by cause, age, sex, by country and by region, 2000-2019 [online database]. Geneva: World Health Organization; 2020. (Global health estimates: Leading causes of death (who.int) accessed 14 August 2022)

[8] United Nation Children's Fund (UNICEF) **(2014)** World Water Day 2025: 4,000 children die each day from a lack of safe water., http://www.unicef.org/wash/ index_25637.html

[9] Pohl, A., **2020**. Removal of heavy metal ions from water and wastewaters by sulfur-containing precipitation agents. *Water, Air, & Soil Pollution*, *231*(10), p.503. https://doi.org/10.1007/s11270-020-04863-w

[10]El-Gaayda, J., Titchou, F.E., Oukhrib, R., Yap, P.S., Liu, T., Hamdani, M. and Akbour, R.A., **2021**. Natural flocculants for the treatment of wastewaters containing dyes or heavy metals: A state-of-the-art review. *Journal of Environmental Chemical Engineering*, *9*(5), p.106060. https://doi.org/10.1016/j.jece.2021.106060

[11] Shabangu, K.P., Bakare, B.F. and Bwapwa, J.K., **2022**. The treatment effect of chemical coagulation process in South African brewery wastewater: Comparison of polyamine and aluminum-chlorohydrate coagulants. *Water*, *14*(16), p.2495.https://doi.org/10.3390/w14162495

[12]Charles, J., Bradu, C., Morin-Crini, N., Sancey, B., Winterton, P., Torri, G., Badot, P.M. and Crini, G., **2016**. Pollutant removal from industrial discharge water using individual and combined effects of adsorption and ion-exchange processes: Chemical abatement. *Journal of Saudi Chemical Society*, *20*(2), pp.185-194. https://doi.org/10.1016/j.jscs.2013.03.007
[13]Jamil, S., Loganathan, P., Kandasamy, J., Listowski, A., McDonald, J.A., Khan, S.J. and Vigneswaran, S., **2020**. Removal of organic matter from wastewater reverse osmosis concentrate using granular activated carbon and anion exchange resin adsorbent columns in sequence. *Chemosphere*, *261*, p.127549. https://doi.org/10.1016/j.chemosphere.2020.127549
[14] Crini, G. and Lichtfouse, E., **2019**. Advantages and disadvantages of techniques used for wastewater treatment. *Environmental chemistry letters*, *17*, pp.145-155. https://doi.org/10.1007/s10311-018-0785-9
[15] Anjum, M., Miandad, R., Waqas, M., Gehany, F. and Barakat, M.A., **2019**. Remediation of wastewater using various nano-materials. *Arabian journal of chemistry*, *12*(8), pp.4897-4919. http://dx.doi.org/10.1016/j.arabjc.2016.10.004
[16] Mo, J., Yang, Q., Zhang, N., Zhang, W., Zheng, Y. and Zhang, Z., **2018**. A review on agro-industrial waste (AIW) derived adsorbents for water and wastewater treatment. *Journal of environmental management*, *227*, pp.395-405. https://doi.org/10.1016/j.jenvman.2018.08.069
[17] Yaqoob, A.A., Parveen, T., Umar, K. and Mohamad Ibrahim, M.N., **2020**. Role of nanomaterials in the treatment of wastewater: A review. *Water*, *12*(2), p.495. http://doi.10.3390/w12020495
[18] Shukla, P., **2020**. Microbial nanotechnology for bioremediation of industrial wastewater. *Frontiers in Microbiology*, *11*, p.590631. http://doi.10.3389/fmicb.2020.590631
[19] Ahmed, M., Mavukkandy, M.O., Giwa, A., Elektorowicz, M., Katsou, E., Khelifi, O., Naddeo, V. and Hasan, S.W., **2022**. Recent developments in hazardous pollutants removal from wastewater and water reuse within a circular economy. *NPJ Clean Water*, *5*(1), pp.1-25. https://doi.org/10.1038/s41545-022-00154-5
[20] Obotey Ezugbe, E. and Rathilal, S., **2020**. Membrane technologies in wastewater treatment: a review. *Membranes*, *10*(5), p.89. http://doi.10.3390/membranes10050089
[21] Fundneider, T., Alonso, V.A., Wick, A., Albrecht, D. and Lackner, S., **2021**. Implications of biological activated carbon filters for micropollutant removal in wastewater treatment. *Water research*, *189*, p.116588. https://doi.org/10.1016/j.watres.2020.116588
[22] E. ElSayed, E., Ibrahim, L.A., Ghandour, A., Zelenakova, M., Vranayova, Z. and Abu-Hashim, M., **2021**. Efficiency of natural clay mineral adsorbent filtration systems in wastewater treatment for potential irrigation purposes. *Sustainability*, *13*(10), p.5738. https://doi.org/10.3390/su13105738
[23] Kryvoruchko, A., Yurlova, L. and Kornilovich, B., **2002**. Purification of water containing heavy metals by chelating-enhanced ultrafiltration. *Desalination*, *144*(1-3), pp.243-248. 10.1016/S0011-9164(02)00319-3
[24] Lin, J. and Zhan, Y., **2012**. Adsorption of humic acid from aqueous solution onto unmodified and surfactant-modified chitosan/zeolite composites. *Chemical engineering journal*, *200*, pp.202-213. http://dx.doi.org/10.1016/j.cej.2012.06.039
[25] Wang, X., Guo, Y., Yang, L., Han, M., Zhao, J. and Cheng, X., **2012**. Nanomaterials as sorbents to remove heavy metal ions in wastewater treatment. *J. Environ. Anal. Toxicol*, *2*(7), pp.154-158. http://dx.doi.org/10.4172/2161-0525.1000154
[26] Garcia, R.A., Stevanovic, T., Berthier, J., Njamen, G., Tolnai, B. and Achim, A., **2021**. Cellulose, nanocellulose, and antimicrobial materials for the manufacture of disposable face masks: a review. *BioResources*, *16*(2), p.4321. https://doi.org/10.15376/biores.16.2.Garcia.

[27] Peng, B., Yao, Z., Wang, X., Crombeen, M., Sweeney, D.G. and Tam, K.C., **2020**. Cellulose-based materials in wastewater treatment of petroleum industry. *Green Energy & Environment*, *5*(1), pp.37-49. https://doi.org/10.1016/j.gee.2019.09.003.
[28] Liu, Y., Liu, H. and Shen, Z., **2021**. Nanocellulose based filtration membrane in industrial waste water treatment: A review. *Materials*, *14*(18), p.5398. https://doi.org/10.3390/ma14185398
[29] Abouzeid, R.E., Khiari, R., El-Wakil, N. and Dufresne, A., **2018**. Current state and new trends in the use of cellulose nanomaterials for wastewater treatment. *Biomacromolecules*, *20*(2), pp.573-597. http://doi.10.1021/acs.biomac.8b00839
[30] Arularasu, M.V., Harb, M. and Sundaram, R., **2020**. Synthesis and characterization of cellulose/TiO_2 nanocomposite: Evaluation of in vitro antibacterial and in silico molecular docking studies. *Carbohydrate polymers*, *249*, p.116868. https://doi.org/10.1016/j.carbpol.2020.116868

[31] Chauhan, I. and Mohanty, P., **2015**. In situ decoration of TiO_2 nanoparticles on the surface of cellulose fibers and study of their photocatalytic and antibacterial activities. *Cellulose*, *22*, pp.507-519. https://doi.org/10.1007/s10570-014-0480-3.
[32]Yang, M., Lotfikatouli, S., Chen, Y., Li, T., Ma, H., Mao, X. and Hsiao, B.S., **2022**. Nanostructured all-cellulose membranes for efficient ultrafiltration of wastewater. *Journal of Membrane Science*, *650*, p.120422. https://doi.org/10.1016/j.memsci.2022.120422
[33] Sayyed, A.J., Pinjari, D.V., Sonawane, S.H., Bhanvase, B.A., Sheikh, J. and Sillanpää, M., **2021**. Cellulose-based nanomaterials for water and wastewater treatments: A review. *Journal of Environmental Chemical Engineering*, *9*(6), p.106626. https://doi.org/10.1016/j.jece.2021.106626
[34] Qian, H., Pretzer, L.A., Velazquez, J.C., Zhao, Z. and Wong, M.S., **2013**. Gold nanoparticles for cleaning contaminated water. *Journal of Chemical Technology & Biotechnology*, *88*(5), pp.735-741. https://doi.org/10.1002/jctb.4030
[35] Forstner, C., Orton, T.G., Wang, P., Kopittke, P.M. and Dennis, P.G., **2020**. Wastewater treatment processing of silver nanoparticles strongly influences their effects on soil microbial diversity. *Environmental Science & Technology*, *54*(21), pp.13538-13547. https://doi.org/10.1021/acs.est.0c01312
[36] Ighalo, J.O., Sagboye, P.A., Umenweke, G., Ajala, O.J., Omoarukhe, F.O., Adeyanju, C.A., Ogunniyi, S. and Adeniyi, A.G., **2021**. CuO nanoparticles (CuO NPs) for water treatment: A review of recent advances. *Environmental Nanotechnology, Monitoring & Management*, *15*, p.100443. https://doi.org/10.1016/j.enmm.2021.100443
[37] Rahman, M., Sarmah, T., Dihingia, P., Verma, R., Sharma, S., Srivastava, D.N., Pandey, L.M. and Kakati, M., **2022**. Bulk synthesis of tungsten-oxide nanomaterials by a novel, plasma chemical reactor configuration, studies on their performance for waste-water treatment and hydrogen evolution reactions. *Chemical Engineering Journal*, *428*, p.131111. https://doi.org/10.1016/j.cej.2021.131111
[38] Abel, S., Jule, L.T., Belay, F., Shanmugam, R., Dwarampudi, L.P., Nagaprasad, N. and Krishnaraj, R., **2021**. Application of titanium dioxide nanoparticles synthesized by sol-gel methods in wastewater treatment. *Journal of Nanomaterials*, *2021*, pp.1-6. https://doi.org/10.1155/2021/3039761
[39] Dimapilis, E.A.S., Hsu, C.S., Mendoza, R.M.O. and Lu, M.C., **2018**. Zinc oxide nanoparticles for water disinfection. *Sustainable Environment Research*, *28*(2), pp.47-56. https://doi.org/10.1016/j.serj.2017.10.001
[40] Adel, A.M., **2016**. Incorporation of nano-metal particles with paper matrices. *Interdiscip J Chem*, *1*(2), pp.36-46. https://doi.org/10.15761/ijc.1000107

[41] Armaković, S.J., Savanović, M.M. and Armaković, S., **2022**. Titanium dioxide as the most used photocatalyst for water purification: An overview. *Catalysts*, *13*(1), p.26. https://doi.org/10.3390/catal13010026
[42] Razali, N.A.M., Salleh, W.N.W., Aziz, F., Jye, L.W., Yusof, N. and Ismail, A.F., **2021**. Review on tungsten trioxide as a photocatalysts for degradation of recalcitrant pollutants. *Journal of Cleaner Production*, *309*, p.127438. https://doi.org/10.1016/j.jclepro.2021.127438
[43] Nascimben Santos, E., László, Z., Hodúr, C., Arthanareeswaran, G. and Veréb, G., **2020**. Photocatalytic membrane filtration and its advantages over conventional approaches in the treatment of oily wastewater: A review. *Asia-Pacific Journal of Chemical Engineering*, *15*(5), p.e2533. https://doi.org/10.1002/apj.2533
[44] Zhao, T., Qian, R., Zhou, G., Wang, Y., Lee, W.I. and Pan, J.H., **2021**. Mesoporous WO_3/TiO_2 spheres with tailored surface properties for concurrent solar photocatalysis and membrane filtration. *Chemosphere*, *263*, p.128344. https://doi.org/10.1016/j.chemosphere.2020.128344
[45] The Global Risks Report. **2019**. (14th Edition) World Economic Forum, Geneva. World Economic Forum (weforum.org)
[46] UNEP. Global environmental outlook 4. Environment for development, United Nations Environment Programme; **2007**. Global Environment Outlook 4 | UNEP - UN Environment Programme
[47] Tlili, I. and Alkanhal, T.A., **2019**. Nanotechnology for water purification: electrospun nanofibrous membrane in water and wastewater treatment. *Journal of Water Reuse and Desalination*, *9*(3), pp.232-248. https://doi.org/10.2166/wrd.2019.057
[48] Khraisheh, M., Elhenawy, S., AlMomani, F., Al-Ghouti, M., Hassan, M.K. and Hameed, B.H., **2021**. Recent progress on nanomaterial-based membranes for water treatment. *Membranes*, *11*(12), p.995. https://doi.org/10.3390/membranes11120995
[49] Cevallos-Mendoza, J., Amorim, C.G., Rodríguez-Díaz, J.M. and Montenegro, M.D.C.B., **2022**. Removal of contaminants from water by membrane filtration: a review. *Membranes*, *12*(6), p.570. https://doi.org/10.3390/membranes12060570
[50] Lu, H., Wang, J., Stoller, M., Wang, T., Bao, Y. and Hao, H., **2016**. An overview of nanomaterials for water and wastewater treatment. *Advances in Materials Science and Engineering*, *2016*. http://dx.doi.org/10.1155/2016/4964828
[51] Choi, W.S. and Lee, H.J., **2022**. Nanostructured materials for water purification: Adsorption of heavy metal ions and organic dyes. *Polymers*, *14*(11), p.2183. https://doi.org/10.3390/polym14112183
[52] Mathur, J., Goswami, P., Gupta, A., Srivastava, S., Minkina, T., Shan, S. and D. Rajput, V., **2022**. Nanomaterials for water remediation: an efficient strategy for prevention of metal (loid) hazard. *Water*, *14*(24), p.3998. https://doi.org/10.3390/w14243998
[53] Daghrir, R., Drogui, P. and Robert, D., **2013**. Modified TiO_2 for environmental photocatalytic applications: a review. *Industrial & Engineering Chemistry Research*, *52*(10), pp.3581-3599. https://doi.org/10.1021/ie303468t
[54] Malekshahi Byranvand, M., Nemati Kharat, A., Fatholahi, L. and Malekshahi Beiranvand, Z., **2013**. A review on synthesis of nano-TiO_2 via different methods. *Journal of nanostructures*, *3*(1), pp.1-9. http://doi.10.7508/JNS.2013.01.001

[55] Tetteh, E.K., Rathilal, S., Asante-Sackey, D. and Chollom, M.N., **2021**. Prospects of synthesized magnetic TiO_2-based membranes for wastewater treatment: A review. *Materials*, *14*(13), p.3524. https://doi.org/10.3390/ma14133524
[56] Etacheri, V., Di Valentin, C., Schneider, J., Bahnemann, D. and Pillai, S.C., **2015**. Visible-light activation of TiO_2 photocatalysts: Advances in theory and experiments. *Journal of*

Photochemistry and Photobiology C: Photochemistry Reviews, *25*, pp.1-29. https://doi.org/10.1016/j.jphotochemrev.2015.08.003
[57] Al-Mamun, M.R., Kader, S., Islam, M.S. and Khan, M.Z.H., **2019**. Photocatalytic activity improvement and application of UV-TiO_2 photocatalysis in textile wastewater treatment: A review. *Journal of Environmental Chemical Engineering*, *7*(5), p.103248. https://doi.org/10.1016/j.jece.2019.103248
[58] Riegel, G. and Bolton, J.R., **1995**. Photocatalytic efficiency variability in TiO_2 particles. *The Journal of Physical Chemistry*, *99*(12), pp.4215-4224. https://doi.org/10.1021/j100012a050
[59] Hurum, D.C., Agrios, A.G., Gray, K.A., Rajh, T. and Thurnauer, M.C., **2003**. Explaining the enhanced photocatalytic activity of Degussa P25 mixed-phase TiO_2 using EPR. *The Journal of Physical Chemistry B*, *107*(19), pp.4545-4549. https://doi.org/10.1021/jp0273934
[60] Hu, A., Zhang, X., Luong, D., Oakes, K.D., Servos, M.R., Liang, R., Kurdi, S., Peng, P. and Zhou, Y., **2012**. Adsorption and photocatalytic degradation kinetics of pharmaceuticals by TiO_2 nanowires during water treatment. *Waste and Biomass Valorization*, *3*, pp.443-449. https://doi.org/10.1007/s12649-012-9142-6
[61] Wu, H.B., Hng, H.H. and Lou, X.W.D., **2012**. Direct synthesis of anatase TiO_2 nanowires with enhanced photocatalytic activity. *Advanced Materials*, *19*(24), pp.2567-2571. https://doi.org/10.1002/adma.201200564
[62] Prakash, J., Cho, J. and Mishra, Y.K., **2022**. Photocatalytic TiO_2 nanomaterials as potential antimicrobial and antiviral agents: Scope against blocking the SARS-COV-2 spread. *Micro and Nano Engineering*, *14*, p.100100. https://doi.org/10.1016/j.mne.2021.100100.
[63] Marinho, B.A., de Souza, S.M.G.U., de Souza, A.A.U. and Hotza, D., **2021**. Electrospun TiO_2 nanofibers for water and wastewater treatment: A review. *Journal of Materials Science*, *56*, pp.5428-5448. https://doi.org/10.1007/s10853-020-05610-6
[64] Nataraj, N., Anjusree, G.S., Madhavan, A.A., Priyanka, P., Sankar, D., Nisha, N., Lakshmi, S.V., Jayakumar, R., Balakrishnan, A. and Biswas, R., **2014.** Synthesis and anti-staphylococcal activity of TiO_2 nanoparticles and nanowires in ex vivo porcine skin model. *Journal of biomedical nanotechnology*, *10*(5), pp.864-870. http://doi.org/10.1166/jbn.2014.1756
[65] Camposeco, R., Castillo, S., Navarrete, J. and Gomez, R., **2016**. Synthesis, characterization and photocatalytic activity of TiO_2 nanostructures: Nanotubes, nanofibers, nanowires and nanoparticles. *Catalysis Today*, *266*, pp.90-101.https://doi.org/10.1016/j.cattod.2015.09.018
[66] Cheng, D., Li, Y., Yang, L., Luo, S., Yang, L., Luo, X., Luo, Y., Li, T., Gao, J. and Dionysiou, D.D., **2019**. One–step reductive synthesis of Ti3+ self–doped elongated anatase TiO_2 nanowires combined with reduced graphene oxide for adsorbing and degrading waste engine oil. *Journal of hazardous materials*, *378*, p.120752. https://doi.org/10.1016/j.jhazmat.2019.120752
[67] Nor, A.M., Achoi, M.F., Mamat, M.H., Zabidi, M.M., Abdullah, S. and Mahmood, M.R., **2012**. Synthesis of TiO_2 nanowires via hydrothermal method. *Japanese Journal of Applied Physics*, *51*(6S), p.06FG08. http://doi.org/10.1143/jjap.51.06fg08
[68] Yoshida, R., Suzuki, Y. and Yoshikawa, S., **2005**. Syntheses of TiO_2 (B) nanowires and TiO_2 anatase nanowires by hydrothermal and post-heat treatments. *Journal of solid state Chemistry*, *178*(7), pp.2179-2185. https://doi.org/10.1016/j.jssc.2005.04.025
[69] Du, J., Gu, X., Guo, H., Liu, J., Wu, Q. and Zou, J., **2015**. Self-induced preparation of TiO_2 nanowires by chemical vapor deposition. *Journal of Crystal Growth*, *427*, pp.54-59. http://dx.doi.org/10.1016/j.jcrysgro.2015.07.004
[70] Lee, J.S., Lee, Y.I., Song, H., Jang, D.H. and Choa, Y.H., **2011**. Synthesis and characterization of TiO_2 nanowires with controlled porosity and microstructure using

electrospinning method. *Current applied physics*, *11*(1), pp.S210-S214. https://doi.org/10.1016/j.cap.2010.11.115
[71] Tien, L.H. and Hoa, N.T.Q., **2012**. Solvothermal synthesis of single-crystalline TiO_2 nanowires and their photocatalytic activity. *Electrochemical and Solid-State Letters*, *15*(5), p.K45. http://doi.org/10.1149/2.011206esl
[72] Wang, Y., Wu, M. and Zhang, W.F., **2008**. Preparation and electrochemical characterization of TiO_2 nanowires as an electrode material for lithium-ion batteries. *Electrochimica Acta*, *53*(27), pp.7863-7868. https://doi.org/10.1016/j.electacta.2008.05.068
[73] Le, D.T.T., Vuong, D.D. and Chien, N.D., **2009**, September. Synthesis and LPG-sensing properties of TiO_2 nanowires. In *Journal of Physics: Conference Series* (Vol. 187, No. 1, p. 012086). IOP Publishing. http://doi.org/10.1088/1742-6596/187/1/012086
[74] Turki, A., Ibáñez, P.F., Ghorbel, A., Kochkar, H., Guillard, C. and Berhault, G., **2012**. Synthesis design of TiO_2 nanotubes and nanowires and photocatalytic applications in the degradation of organic pollutants in the presence or not of microorganisms. *MRS Online Proceedings Library (OPL)*, *1442*, pp.mrss12-1442. http://doi.org/10.1557/opl.2012.848
[75] Półrolniczak, P. and Walkowiak, M., **2015**. Titanium dioxide high aspect ratio nanoparticle hydrothermal synthesis optimization. *Open Chemistry*, *13*(1), p.000010151520150006. https://doi.org/10.1515/chem-2015-0006
[76] Hamisu, A., Gaya, U. and Gaya, A., **2020**. Effect of alkali strength on the hydrothermal growth of photoactive TiO_2 nanowires. *Journal of Nanostructures*, *10*(3), pp.639-651. http://doi.org/10.22052/JNS.2020.03.017
[77] Youssef, A.M. and Malhat, F.M., **2014**, March. Selective removal of heavy metals from drinking water using titanium dioxide nanowire. In *Macromolecular Symposia* (Vol. 337, No. 1, pp. 96-101). https://doi.org/10.1002/masy.201450311

[78] Saleh, M.G., Badawy, A.A. and Ghanem, A.F., **2019**. Using of titanate nanowires in removal of lead ions from waste water and its biological activity. *Inorganic Chemistry Communications*, *108*, p.107508. https://doi.org/10.1016/j.inoche.2019.107508
[79] Jain, A. and Vaya, D., **2017**. Photocatalytic activity of TiO_2 nanomaterial. *Journal of the Chilean Chemical Society*, *62*(4), pp.3683-3690. http://dx.doi.org/10.4067/s0717-97072017000403683
[80] Ajmal, A., Majeed, I., Malik, R.N., Idriss, H. and Nadeem, M.A., **2014**. Principles and mechanisms of photocatalytic dye degradation on TiO_2 based photocatalysts: a comparative overview. *Rsc Advances*, *4*(70), pp.37003-37026. https://doi.org/10.1039/C4RA06658H

[81] Ibhadon, A.O. and Fitzpatrick, P., **2013**. Heterogeneous photocatalysis: recent advances and applications. *Catalysts*, *3*(1), pp.189-218.https://doi.org/10.3390/catal3010189
[82] Matsunami, D., Yamanaka, K., Mizoguchi, T. and Kojima, K., **2019**. Comparison of photodegradation of methylene blue using various TiO_2 films and WO_3 powders under ultraviolet and visible-light irradiation. *Journal of Photochemistry and Photobiology A: Chemistry*, *369*, pp.106-114.https://doi.org/10.1016/j.jphotochem.2018.10.020
[83] Phung, H.N.T., Truong, N.D. and Duong, P.A., **2018**. Influence of MoS_2 deposition time on the photocatalytic activity of MoS_2/V, N co-doped TiO_2 heterostructure thin film in the visible light region. *Current Applied Physics*, *18*(6), pp.737-743. https://doi.org/10.1016/j.cap.2018.02.004
[84] Abdel-Wahab, A.M., Al-Shirbini, A.S., Mohamed, O. and Nasr, O., **2017**. Photocatalytic degradation of paracetamol over magnetic flower-like TiO_2/Fe_2O_3 core-shell nanostructures. *Journal of Photochemistry and Photobiology A: Chemistry*, *347*, pp.186-198. https://doi.org/10.1016/j.jphotochem.2017.07.030

[85] Liu, S., Zhu, J., Guo, X., Ge, J. and Wu, H., **2015**. Preparation of α-Fe_2O_3–TiO_2/fly ash cenospheres photocatalyst and its mechanism of photocatalytic degradation. *Colloids and Surfaces A: Physicochemical and Engineering Aspects*, *484*, pp.434-440. https://doi.org/10.1016/j.colsurfa.2015.08.033

[86] Landolsi, Z., Ben Assaker, I., Nunes, D., Fortunato, E., Martins, R., Chtourou, R. and Ammar, S., **2020**. Enhanced electrical and photocatalytic properties of porous TiO_2 thin films decorated with Fe_2O_3 nanoparticles. *Journal of Materials Science: Materials in Electronics*, *31*(23), pp.20753-20773. https://doi.org/10.1007/s10854-020-04588-w

[87] Youssef, A.M., Malhat, F.M. and Abd El-Hakim, A.F.A., **2013**. Preparation and utilization of polystyrene nanocomposites based on TiO_2 nanowires. *Polymer-Plastics Technology and Engineering*, *52*(3), pp.228-235. https://doi.org/10.1080/03602559.2012.735311

[88] Xie, Y., Heo, S.H., Kim, Y.N., Yoo, S.H. and Cho, S.O., **2009**. Synthesis and visible-light-induced catalytic activity of Ag_2S-coupled TiO_2 nanoparticles and nanowires. *Nanotechnology*, *21*(1), p.015703. http://doi.org/10.1088/0957-4484/21/1/015703

[89] Safajou, H., Khojasteh, H., Salavati-Niasari, M. and Mortazavi-Derazkola, S., **2017**. Enhanced photocatalytic degradation of dyes over graphene/Pd/TiO_2 nanocomposites: TiO_2 nanowires versus TiO_2 nanoparticles. *Journal of colloid and interface science*, *498*, pp.423-432. https://doi.org/10.1016/j.jcis.2017.03.078

[90] Hu, A., Zhang, X., Oakes, K.D., Peng, P., Zhou, Y.N. and Servos, M.R., **2011**. Hydrothermal growth of free standing TiO_2 nanowire membranes for photocatalytic degradation of pharmaceuticals. *Journal of Hazardous Materials*, *189*(1-2), pp.278-285. https://doi.org/10.1016/j.jhazmat.2011.02.033

[91] Giuffrida, F., Calcagno, L., Leonardi, A.A., Cantarella, M., Zimbone, M. and Impellizzeri, G., **2023**. Enhancing the photocatalytic properties of doped TiO_2 nanowires grown by seed-assisted thermal oxidation. *Thin Solid Films*, *771*, p.139783. https://doi.org/10.1016/j.tsf.2023.139783

[92] Mofokeng, L.E., Hlekelele, L., Moma, J., Tetana, Z.N. and Chauke, V.P., **2022**. Energy-efficient CuO/TiO_2@ GCN cellulose acetate-based membrane for concurrent filtration and photodegradation of ketoprofen in drinking and groundwater. *Applied Sciences*, *12*(3), p.1649. https://doi.org/10.3390/app12031649

[93] Liang, R., Hatat-Fraile, M., Arlos, M., Servos, M. and Zhou, Y.N., **2014**, August. TiO_2 nanowires membranes for the use in photocatalytic filtration processes. In *14th IEEE International Conference on Nanotechnology* (pp. 975-980). IEEE. http://doi.org/10.1109/NANO.2014.6968144

[94] Rao, G., Brastad, K.S., Zhang, Q., Robinson, R., He, Z. and Li, Y., **2016**. Enhanced disinfection of Escherichia coli and bacteriophage MS2 in water using a copper and silver loaded titanium dioxide nanowire membrane. *Frontiers of Environmental Science & Engineering*, *10*, pp.1-9. https://doi.org/10.1007/s11783-016-0854-x

[95] Nakano, R., Yamaguchi, A., Sunada, K., Nagai, T., Nakano, A., Suzuki, Y., Yano, H., Ishiguro, H. and Miyauchi, M., **2022**. Inactivation of various variant types of SARS-CoV-2 by indoor-light-sensitive TiO_2-based photocatalyst. *Scientific Reports*, *12*(1), p.5804. https://doi.org/10.1038/s41598-022-09402-7

[96] Hajipour, P., Eslami, A., Bahrami, A., Hosseini-Abari, A., Saber, F.Y., Mohammadi, R. and Mehr, M.Y., **2021**. Surface modification of TiO_2 nanoparticles with CuO for visible-light antibacterial applications and photocatalytic degradation of antibiotics. *Ceramics International*, *47*(23), pp.33875-33885. https://doi.org/10.1016/j.ceramint.2021.08.300

[97] Sreeju, N., Rufus, A. and Philip, D., **2017**. Studies on catalytic degradation of organic pollutants and anti-bacterial property using biosynthesized CuO nanostructures. *Journal of Molecular Liquids*, *242*, pp.690-700. https://doi.org/10.1016/j.molliq.2017.07.077.

[98] Hitam, C.N. and Jalil, A.A., **2020**. A review on exploration of Fe_2O_3 photocatalyst towards degradation of dyes and organic contaminants. *Journal of environmental management*, *258*, p.110050. https://doi.org/10.1016/j.jenvman.2019.110050.
[99] Liu, Y., Sun, N., Hu, J., Li, S. and Qin, G., **2018**. Photocatalytic degradation properties of α-Fe_2O_3 nanoparticles for dibutyl phthalate in aqueous solution system. *Royal Society open science*, *5*(4), p.172196. http://dx.doi.org/10.1098/rsos.172196
[100] Zhang, Q., Rao, G., Rogers, J., Zhao, C., Liu, L. and Li, Y., **2015**. Novel anti-fouling Fe_2O_3/TiO_2 nanowire membranes for humic acid removal from water. *Chemical Engineering Journal*, *271*, pp.180-187. https://doi.org/10.1016/j.cej.2015.02.085
[101] Cao, Y.Q., Zi, T.Q., Zhao, X.R., Liu, C., Ren, Q., Fang, J.B., Li, W.M. and Li, A.D., **2020**. Enhanced visible light photocatalytic activity of Fe_2O_3 modified TiO_2 prepared by atomic layer deposition. *Scientific Reports*, *10*(1), p.13437. https://doi.org/10.1038/s41598-020-70352-z
[102] Koe, W.S., Lee, J.W., Chong, W.C., Pang, Y.L. and Sim, L.C., **2020**. An overview of photocatalytic degradation: photocatalysts, mechanisms, and development of photocatalytic membrane. *Environmental Science and Pollution Research*, *27*(3), pp.2522-2565. https://doi.org/10.1007/s11356-019-07193-5
[103] Simamora, A.J., Hsiung, T.L., Chang, F.C., Yang, T.C., Liao, C.Y. and Wang, H.P., **2012**. Photocatalytic splitting of seawater and degradation of methylene blue on CuO/nano TiO_2. *International journal of hydrogen energy*, *37*(18), pp.13855-13858.http://doi:10.1016/j.ijhydene.2012.04.09
[104] Li, R., Jia, Y., Bu, N., Wu, J. and Zhen, Q., **2015**. Photocatalytic degradation of methyl blue using Fe_2O_3/TiO_2 composite ceramics. *Journal of Alloys and Compounds*, *643*, pp.88-93. http://doi:10.1016/j.jallcom.2015.03.266
[105] Ma, J., Tian, Z., Li, L., Lu, Y., Xu, X. and Hou, J., **2022**. Loading nano-CuO on TiO_2 nanomeshes towards efficient photodegradation of methylene blue. *Catalysts*, *12*(4), p.383. https://doi.org/10.3390/catal12040383
[106] Bassim, S., Mageed, A.K., AbdulRazak, A.A. and Al-Sheikh, F., **2023**. Photodegradation of methylene blue with aid of green synthesis of CuO/TiO_2 nanoparticles from extract of citrus aurantium juice. *Bulletin of Chemical Reaction Engineering & Catalysis*, *18*(1), pp.1-16. https://doi.org/10.9767/bcrec.16417
[107] A'srai, A.I.M., Razali, M.H., Amin, K.A.M. and Osman, U.M., **2023**. CuO/TiO_2 nanocomposite photocatalyst for efficient MO degradation. *Digest Journal of Nanomaterials & Biostructures (DJNB)*, *18*(3). https://doi.org/10.15251/DJNB.2023.183.1105
[108] Zhang, J., Hu, Y., Zheng, H. and Zhang, P., **2020**. Hierarchical Z-scheme 1D/2D architecture with TiO_2 nanowires decorated by MnO_2 nanosheets for efficient adsorption and full spectrum photocatalytic degradation of organic pollutants. *Catalysis Science & Technology*, *10*(11), pp.3603-3612. https://doi.org/10.1039/D0CY00419G

[109] Ma, J., Chen, D., Zhang, W., An, Z., Zeng, K., Yuan, M. and Shen, J., **2021**. Enhanced performance and degradation of wastewater in microbial fuel cells using titanium dioxide nanowire photocathodes. *RSC advances*, *11*(4), pp.2242-2252. https://doi.org/10.1039/D0RA08747E

[110] Yao, Y.C., Dai, X.R., Hu, X.Y., Huang, S.Z. and Jin, Z., **2016**. Synthesis of Ag-decorated porous TiO_2 nanowires through a sunlight induced reduction method and its enhanced photocatalytic activity. *Applied Surface Science*, *387*, pp.469-476. http://dx.doi.org/10.1016/j.apsusc.2016.06.130
[111] Hamisu, A. and Auwal, I.A., **2020**. Hydrothermal synthesis of Titania nanowires and their photocatalytic activities for Naphthalene.

[112] Horváth, E., Gabathuler, J., Bourdiec, G., Vidal-Revel, E., Benthem Muñiz, M., Gaal, M., Grandjean, D., Breider, F., Rossi, L., Sienkiewicz, A. and Forró, L., **2022**. Solar water purification with photocatalytic nanocomposite filter based on TiO2 nanowires and carbon nanotubes. *npj Clean Water*, *5*(1), p.10. https://doi.org/10.1038/s41545-022-00157-2.
[113] Li, F., Szeto, W., Huang, H., Li, J. and Leung, D.Y., **2017**. A photocatalytic rotating disc reactor with TiO_2 nanowire arrays deposited for industrial wastewater treatment. *Molecules*, *22*(2), p.337. https://doi.org/10.3390/molecules22020337
[114] Arcadipane, E., Sanz, R., Amiard, G., Boninelli, S., Impellizzeri, G., Privitera, V., Bonkerud, J., Bhoodoo, C., Vines, L., Svensson, B.G. and Romano, L., **2016**. Single-crystal TiO_2 nanowires by seed assisted thermal oxidation of Ti foil: synthesis and photocatalytic properties. *RSC advances*, *6*(60), pp.55490-55498. https://doi.org/10.1039/C6RA09088E

[115] Afreen, G., Upadhyayula, S. and Sunkara, M.K., **2019**. TiO_2 Nanowires as Efficient Heterogeneous Photocatalysts for Waste-Water Treatment. *International Journal of Chemical and Molecular Engineering*, *13*(11), pp.511-515. http://doi.org/10.5281/zenodo.3566399
[116] Zhang, X., Zhang, T., Ng, J. and Sun, D.D., **2009**. High-performance multifunctional TiO_2 nanowire ultrafiltration membrane with a hierarchical layer structure for water treatment. *Advanced Functional Materials*, *19*(23), pp.3731-3736. https://doi.org/10.1002/adfm.200901435

[117] Zhang, X., Pan, J.H., Du, A.J., Fu, W., Sun, D.D. and Leckie, J.O., **2009**. Combination of one-dimensional TiO_2 nanowire photocatalytic oxidation with microfiltration for water treatment. *Water research*, *43*(5), pp.1179-1186. https://doi.org/10.1016/j.watres.2008.12.021
[118] Yu, Z., Zeng, H., Min, X. and Zhu, X., **2020**. High-performance composite photocatalytic membrane based on titanium dioxide nanowire/graphene oxide for water treatment. *Journal of Applied Polymer Science*, *137*(12), p.48488. https://doi.org/10.1002/app.48488

[119] Huang, Y., Zhu, G., Zou, K., Tian, F., Yadav, T.P., Xu, H., Yang, G., Li, H. and Qu, L., **2021**. Highly efficient removal of organic pollutants from wastewater using a recyclable graphene oxide membrane intercalated with g-C_3N_4@ TiO_2-nanowires. *Journal of Molecular Liquids*, *337*, p.116461. https://doi.org/10.1016/j.molliq.2021.116461
[120] Liu, Z., Liu, Z., Cui, T., Dong, L., Zhang, J., Han, L., Li, G. and Liu, C., **2014**. Photocatalyst from one-dimensional TiO_2 nanowires/synthetic zeolite composites. *Materials Express*, *4*(6), pp.465-474. https://doi.org/10.1166/mex.2014.1196
[121] Guo, H., Jiang, N., Wang, H., Lu, N., Shang, K., Li, J. and Wu, Y., **2019**. Degradation of antibiotic chloramphenicol in water by pulsed discharge plasma combined with TiO_2/WO_3 composites: mechanism and degradation pathway. *Journal of hazardous materials*, *371*, pp.666-676. https://doi.org/10.1016/j.jhazmat.2019.03.051
[122] Tahir, M.B., Nabi, G., Rafique, M. and Khalid, N.R., **2017**. Nanostructured-based WO_3 photocatalysts: recent development, activity enhancement, perspectives and applications for wastewater treatment. *International Journal of Environmental Science and Technology*, *14*, pp.2519-2542.https://doi.org/10.1007/s13762-017-1394-z
[123] Azmat, S., Jan, T., Ilyas, S.Z., Hassan, A., Habib, I., Mahmood, Q. and Mahmood, A., **2018**. Solar light triggered photocatalytic performance of WO_3 nanostructures; waste water treatment. *Materials Research Express*, *5*(11), p.115025.http://doi.org/10.1088/2053-1591/aadf0a
[124] Huang, J., Xue, P., Wang, S., Han, S., Lin, L., Chen, X. and Wang, Z., **2022**. Fabrication of zirconium-based metal-organic frameworks@ tungsten trioxide (UiO-66-NH_2@WO_3) heterostructure on carbon cloth for efficient photocatalytic removal of tetracycline antibiotic

under visible light. *Journal of Colloid and Interface Science*, *606*, pp.1509-1523.https://doi.org/10.1016/j.jcis.2021.08.108
[125] Liu, K.I. and Perng, T.P., **2020**. Fabrication of flower-like WO_3/TiO_2 core–shell nanoplates by atomic layer deposition for improved photoelectrochemical water-splitting activity. *ACS Applied Energy Materials*, *3*(5), pp.4238-4244. https://doi.org/10.1021/acsaem.9b02419
[126] Zeb, S., Peng, X., Shi, Y., Su, J., Sun, J., Zhang, M., Sun, G., Nie, Y., Cui, Y. and Jiang, X., **2021**. Bimetal Au-Pd decorated hierarchical WO_3 nanowire bundles for gas sensing application. *Sensors and Actuators B: Chemical*, *334*, p.129584. https://doi.org/10.1016/j.snb.2021.129584
[127] Li, Y., Tang, Z., Zhang, J. and Zhang, Z., **2017**. Fabrication of vertical orthorhombic/hexagonal tungsten oxide phase junction with high photocatalytic performance. *Applied Catalysis B: Environmental*, *207*, pp.207-217. https://doi.org/10.1016/j.apcatb.2017.02.026
[128] Abbaspoor, M., Aliannezhadi, M. and Tehrani, F.S., **2023**. High-performance photocatalytic WO_3 nanoparticles for treatment of acidic wastewater. *Journal of Sol-Gel Science and Technology*, *105*(2), pp.565-576. https://doi.org/10.1007/s10971-022-06002-9
[129] Fularz, A., Almohammed, S. and Rice, J.H., **2020**. Controlling plasmon-induced photocatalytic redox reactions on WO_3 nanowire/AgNPs substrates via defect engineering. *The Journal of Physical Chemistry C*, *124*(46), pp.25351-25360. https://doi.org/10.1021/acs.jpcc.0c07788
[130] Arshad, M., Ehtisham-ul-Haque, S., Bilal, M., Ahmad, N., Ahmad, A., Abbas, M., Nisar, J., Khan, M.I., Nazir, A., Ghaffar, A. and Iqbal, M., **2020**. Synthesis and characterization of Zn doped WO_3 nanoparticles: photocatalytic, antifungal and antibacterial activities evaluation. *Materials Research Express*, *7*(1), p.015407. https://doi.org/10.1088/2053-1591/ab6380
[131] Samuel, O., Othman, M.H.D., Kamaludin, R., Sinsamphanh, O., Abdullah, H., Puteh, M.H. and Kurniawan, T.A., **2022**. WO_3–based photocatalysts: A review on synthesis, performance enhancement and photocatalytic memory for environmental applications. *Ceramics International*, *48*(5), pp.5845-5875. https://doi.org/10.1016/j.ceramint.2021.11.158
[132]Jiang, L., Yuan, X., Zeng, G., Liang, J., Chen, X., Yu, H., Wang, H., Wu, Z., Zhang, J. and Xiong, T., **2018**. In-situ synthesis of direct solid-state dual Z-scheme WO_3/g-C_3N_4/Bi_2O_3 photocatalyst for the degradation of refractory pollutant. *Applied Catalysis B: Environmental*, *227*, pp.376-385. https://doi.org/10.1016/j.apcatb.2018.01.042
[133] Matalkeh, M., Nasrallah, G.K., Shurrab, F.M., Al-Absi, E.S., Mohammed, W., Elzatahry, A. and Saoud, K.M., **2022**. Visible light photocatalytic activity of Ag/WO_3 nanoparticles and its antibacterial activity under ambient light and in the dark. *Results in Engineering*, *13*, p.100313. https://doi.org/10.1016/j.rineng.2021.100313
[134] Sun, X., He, W., Yang, T., Ji, H., Liu, W., Lei, J., Liu, Y. and Cai, Z., **2021**. Ternary TiO_2/WO_3/CQDs nanocomposites for enhanced photocatalytic mineralization of aqueous cephalexin: degradation mechanism and toxicity evaluation. *Chemical Engineering Journal*, *412*, p.128679. https://doi.org/10.1016/j.cej.2021.128679
[135] Zeng, Q., Bai, J., Li, J., Li, L., Xia, L., Zhou, B. and Sun, Y., **2018**. Highly-stable and efficient photocatalytic fuel cell based on an epitaxial TiO_2/WO_3/W nanothorn photoanode and enhanced radical reactions for simultaneous electricity production and wastewater treatment. *Applied energy*, *220*, pp.127-137.https://doi.org/10.1016/j.apenergy.2018.03.042
[136] Tehrani, F.S., Ahmadian, H. and Aliannezhadi, M., **2020**. Hydrothermal synthesis and characterization of WO_3 nanostructures: Effect of reaction time. *Materials Research Express*, *7*(1), p.015911. https://doi.org/10.1088/2053-1591/ab66fc

[137] Choi, H.G., Jung, Y.H. and Kim, D.K., **2005**. Solvothermal synthesis of tungsten oxide nanorod/nanowire/nanosheet. *Journal of the American Ceramic Society*, *88*(6), pp.1684-1686. https://doi.org/10.1111/j.1551-2916.2005.00341.x

[138] Liu, X., Wang, G., Wang, J., Gong, X., Chang, J., Jin, X., Zhang, X., Wang, J., Hao, J. and Liu, B., **2022**. Electrochromic and capacitive properties of WO_3 nanowires prepared by One-Step water bath method. *Coatings*, *12*(5), p.595. https://doi.org/10.3390/coatings12050595

[139] Firkala, T., Keri, O., Gaber, F., Kocs, L., Hórvölgyi, Z., Nagy, D. and Szilágyi, I.M., **2017**. Photocatalytic Properties of Hexagonal WO_3 Nanowires Decorated with Gold Nanoparticles. *REVUE ROUMAINE DE CHIMIE*, *62*(10), pp.767-773.

[140] Xu, C., Ling, Z.W., Qi, Z., Liu, R. and Liu, Y.Q., **2020**. Facile preparation of WO_3 nanowires by bubble-electrospinning and their photocatalytic properties. *Recent Patents on Nanotechnology*, *14*(1), pp.27-34. http://doi:10.2174/1872210513666191107114743.

[141] Kaur, N., Zappa, D., Poli, N. and Comini, E., **2019**. Integration of VLS-Grown WO_3 Nanowires into Sensing Devices for the Detection of H_2S and O_3. *ACS omega*, *4*(15), pp.16336-16343.https://doi.org/10.1021/acsomega.9b01792

[142] Szabó, M., Pusztai, P., Leino, A.R., Kordás, K., Kónya, Z. and Kukovecz, Á., **2013**. Synthesis and characterization of WO_3 nanowires and metal nanoparticle-WO_3 nanowire composites. *Journal of molecular structure*, *1044*, pp.99-103. https://doi.org/10.1016/j.molstruc.2012.11.041

[143] Zheng, F., Zhang, M. and Guo, M., **2013**. Controllable preparation of WO_3 nanorod arrays by hydrothermal method. *Thin Solid Films*, *534*, pp.45-53. https://doi.org/10.1016/j.tsf.2013.01.102

[144] Nagy, D., Firkala, T., Drotár, E., Szegedi, Á., Laszlo, K. and Szilagyi, I.M., **2016**. Photocatalytic WO_3/TiO_2 nanowires: WO_3 polymorphs influencing the atomic layer deposition of TiO_2. *RSC Advances*, *6*(98), pp.95369-95377.https://doi.org/10.1039/C6RA18899K

[145] Song, X.C., Zheng, Y.F., Yang, E. and Wang, Y., **2007**. Large-scale hydrothermal synthesis of WO_3 nanowires in the presence of K_2SO_4. *Materials Letters*, *61*(18), pp.3904-3908.http://doi:10.1016/j.matlet.2006.12.055

[146] Jamali, M. and Tehrani, F.S., **2020**. Effect of synthesis route on the structural and morphological properties of WO_3 nanostructures. *Materials Science in Semiconductor Processing*, *107*, p.104829.http://doi.org/10.1016/j.mssp.2019.104829

[147] Mao, J., Zhang, Q., Li, P., Zhang, L. and Zhang, W., **2018**. Geometric architecture design of ternary composites based on dispersive WO_3 nanowires for enhanced visible-light-driven activity of refractory pollutant degradation. *Chemical Engineering Journal*, *334*, pp.2568-2578. https://doi.org/10.1016/j.cej.2017.10.165

[148] Zhou, M.J., Zhang, N. and Hou, Z.H., **2014**. A facile synthesis of graphene-WO_3 nanowire clusters with high photocatalytic activity for O_2 evolution. *International Journal of Photoenergy*, *2014*. http://dx.doi.org/10.1155/2014/943537

[149] Zhou, H., Xie, J., Yan, F., Guo, W., Gao, P., Qin, H. and Xiao, H., **2022**. Porous Al_2O_3 ceramics with directional gradient pore structure modified by cobweb-bridged WO_3 nanowires for oil/water emulsions separation. *Ceramics International*, *48*(13), pp.18753-18764. https://doi.org/10.1016/j.ceramint.2022.03.150

[150] Dulta, K., Koşarsoy Ağçeli, G., Chauhan, P., Jasrotia, R., Chauhan, P.K. and Ighalo, J.O., **2022**. Multifunctional CuO nanoparticles with enhanced photocatalytic dye degradation and antibacterial activity. *Sustainable Environment Research*, *32*, pp.1-15. https://doi.org/10.1186/s42834-021-00111-w

[151] Dursun, S., Koyuncu, S.N., Kaya, İ.C., Kaya, G.G., Kalem, V. and Akyildiz, H., **2020**. Production of CuO–WO_3 hybrids and their dye removal capacity/performance from wastewater by adsorption/photocatalysis. *Journal of Water Process Engineering*, *36*, p.101390.https://doi.org/10.1016/j.jwpe.2020.101390
[152] Senthil, R.A., Priya, A., Theerthagiri, J., Selvi, A., Nithyadharseni, P. and Madhavan, J., **2018**. Facile synthesis of α-Fe_2O_3/WO_3 composite with an enhanced photocatalytic and photo-electrochemical performance. *Ionics*, *24*, pp.3673-3684. http://doi.org/10.1007/s11581-018-2473-y
[153] Nagy, D., Nagy, D., Szilágyi, I.M. and Fan, X., **2016**. Effect of the morphology and phases of WO_3 nanocrystals on their photocatalytic efficiency. *RSC advances*, *6*(40), pp.33743-33754. https://doi.org/10.1039/C5RA26582G

[154] Han, F., Li, H., Fu, L., Yang, J. and Liu, Z., **2016**. Synthesis of S-doped WO_3 nanowires with enhanced photocatalytic performance towards dye degradation. *Chemical Physics Letters*, *651*, pp.183-187. https://doi.org/10.1016/j.cplett.2016.03.017
[155] Silveira, J.V., Moraes, E.C., Moura, J.V.B., Ghosh, A., Senna, C.A., Archanjo, B.S., Vasconcelos, T.L., Souza Filho, A.G., Freire, P.T.C. and Luz-Lima, C., **2020**. Mo-doped WO_3 nanowires for adsorbing methylene blue dye from wastewater. *Journal of materials science*, *55*, pp.6429-6440. http://doi.org/10.1007/s10853-020-04472-2
[156] Shaheen, N., Waqas, M., Alazmi, A., Alkhudhayri, A.A., Hasan, M., Shahid, M., Warsi, M.F. and Alsafari, I.A., **2022**. Hydrothermal assisted WO_3@C nanowires supported g-C_3N_4 ternary nanocomposites for the removal of colored and colorless organic effluents and bacterial strains. *Materials Chemistry and Physics*, *292*, p.126754. https://doi.org/10.1016/j.matchemphys.2022.126754
[157] Poletto, M., Zeni, M. and Zattera, A.J., **2012**. Effects of wood flour addition and coupling agent content on mechanical properties of recycled polystyrene/wood flour composites. *Journal of Thermoplastic Composite Materials*, *25*(7), pp.821-833. https://doi.org/10.1177/0892705711413627
[158] Ornaghi Jr, H.L., Bolner, A.S., Fiorio, R., Zattera, A.J. and Amico, S.C., **2010**. Mechanical and dynamic mechanical analysis of hybrid composites molded by resin transfer molding. *Journal of applied polymer science*, *118*(2), pp.887-896. https://doi.org/10.1002/app.32388

[159] Romanzini, D., Ornaghi Jr, H.L., Amico, S.C. and Zattera, A.J., **2012**. Influence of fiber hybridization on the dynamic mechanical properties of glass/ramie fiber-reinforced polyester composites. *Journal of Reinforced Plastics and Composites*, *31*(23), pp.1652-1661. https://doi.org/10.1177/0731684412459982
[160] Han, G., Huan, S., Han, J., Zhang, Z. and Wu, Q., **2013**. Effect of acid hydrolysis conditions on the properties of cellulose nanoparticle-reinforced polymethylmethacrylate composites. *Materials*, *7*(1), pp.16-29. https://doi.org/10.3390/ma7010016
[161] Poletto, M., Ornaghi Junior, H.L. and Zattera, A.J., **2014**. Native cellulose: structure, characterization and thermal properties. *Materials*, *7*(9), pp.6105-6119. http://doi.org/10.3390/ma7096105
[162] Klemm, D., Heublein, B., Fink, H.P. and Bohn, A., **2005**. Cellulose: fascinating biopolymer and sustainable raw material. *Angewandte chemie international edition*, *44*(22), pp.3358-3393. https://doi.org/10.1002/anie.200460587
[163] Zhao, S.W., Guo, C.R., Hu, Y.Z., Guo, Y.R. and Pan, Q.J., **2018**. The preparation and antibacterial activity of cellulose/ZnO composite: A review. *Open Chemistry*, *16*(1), pp.9-20. https://doi.org/10.1515/chem-2018-0006

[164] Xu, L., Liu, Y., Hu, Z. and Jimmy, C.Y., **2021**. Converting cellulose waste into a high-efficiency photocatalyst for Cr (VI) reduction via molecular oxygen activation. *Applied Catalysis B: Environmental*, *295*, p.120253. https://doi.org/10.1016/j.apcatb.2021.120253
[165] Sohouli, E., Irannejad, N., Ziarati, A., Ehrlich, H., Rahimi-Nasrabadi, M., Ahmadi, F. and Luque, R., **2022**. Application of polysaccharide-based biopolymers as supports in photocatalytic treatment of water and wastewater: a review. *Environmental Chemistry Letters*, *20*(6), pp.3789-3809. https://doi.org/10.1007/s10311-022-01456-3
[166] Bai, W., Yang, X., Du, X., Qian, Z., Zhang, Y., Liu, L. and Yao, J., **2020**. Robust and recyclable macroscopic g-C_3N_4/cellulose hybrid photocatalysts with enhanced visible light photocatalytic activity. *Applied Surface Science*, *504*, p.144179. https://doi.org/10.1016/j.apsusc.2019.144179
[167] Raizada, P., Soni, V., Kumar, A., Singh, P., Khan, A.A.P., Asiri, A.M., Thakur, V.K. and Nguyen, V.H., **2021**. Surface defect engineering of metal oxides photocatalyst for energy application and water treatment. *Journal of Materiomics*, *7*(2), pp.388-418. https://doi.org/10.1016/j.jmat.2020.10.009
[168]Dong, H., Zeng, G., Tang, L., Fan, C., Zhang, C., He, X. and He, Y., **2015**. An overview on limitations of TiO_2-based particles for photocatalytic degradation of organic pollutants and the corresponding countermeasures. *Water research*, *79*, pp.128-146. https://doi.org/10.1016/j.watres.2015.04.038
[169] Bion, N., Epron, F., Moreno, M., Mariño, F. and Duprez, D., **2008**. Preferential oxidation of carbon monoxide in the presence of hydrogen (PROX) over noble metals and transition metal oxides: advantages and drawbacks. *Topics in Catalysis*, *51*, pp.76-88. https://doi.org/10.1007/s11244-008-9116-x
[170] Rana, A., Sudhaik, A., Raizada, P., Khan, A.A.P., Van Le, Q., Singh, A., Selvasembian, R., Nadda, A. and Singh, P., **2021**. An overview on cellulose-supported semiconductor photocatalysts for water purification. *Nanotechnology for Environmental Engineering*, *6*, pp.1-38. https://doi.org/10.1007/s41204-021-00135-y
[171] Morshed, M.N., Al Azad, S., Deb, H., Shaun, B.B. and Shen, X.L., **2020**. Titania-loaded cellulose-based functional hybrid nanomaterial for photocatalytic degradation of toxic aromatic dye in water. *Journal of Water Process Engineering*, *33*, p.101062. https://doi.org/10.1016/j.jwpe.2019.101062
[172] Qi, B., Chen, T., Liu, Z., Qi, J., Wang, Q., Zhang, W. and Li, X., **2022**. A novel 2D-WO_3/cellulose acetate film: Photocatalytic performance under real solar irradiation in continuous baffled photo-reactor. *Journal of Water Process Engineering*, *47*, p.102739. https://doi.org/10.1016/j.jwpe.2022.102739
[173] Sharma, D., Kumari, M. and Dhayal, V., **2021**. Fabrication and characterization of cellulose/PVA/TiO_2 nanocomposite thin film as a photocatalyst. *Materials Today: Proceedings*, *43*, pp.2970-2974. https://doi.org/10.1016/j.matpr.2021.01.323
[174] Li, H., Zhang, L., Lu, H., Ma, J., Zhou, X., Wang, Z. and Yi, C., **2020**. Macro-/nanoporous Al-doped ZnO/cellulose composites based on tunable cellulose fiber sizes for enhancing photocatalytic properties. *Carbohydrate polymers*, *250*, p.116873. https://doi.org/10.1016/j.carbpol.2020.116873
[175] Tavker, N. and Sharma, M., **2020**. Designing of waste fruit peels extracted cellulose supported molybdenum sulfide nanostructures for photocatalytic degradation of RhB dye and industrial effluent. *Journal of environmental management*, *255*, p.109906. https://doi.org/10.1016/j.jenvman.2019.109906
[176] Tavker, N., Gaur, U.K. and Sharma, M., **2020**. Agro-waste extracted cellulose supported silver phosphate nanostructures as a green photocatalyst for improved photodegradation of RhB dye and industrial fertilizer effluents. *Nanoscale Advances*, *2*(7), pp.2870-2884. https://doi.org/10.1039/D0NA00181C

[177] Zeng, J., Liu, S., Cai, J. and Zhang, L., **2010**. TiO_2 immobilized in cellulose matrix for photocatalytic degradation of phenol under weak UV light irradiation. *The Journal of Physical Chemistry C*, *114*(17), pp.7806-7811. https://doi.org/10.1021/jp1005617
[178] Mahmoud, M.E. and Abdelwahab, M.S., **2020**. Rapid and efficient removal of lead from water by α-FeOOH/Cellulose/TiO_2 nanocomposite. *Materials Science and Engineering: B*, *262*, p.114689. https://doi.org/10.1016/j.mseb.2020.114689
[179] Pecson, B.M., Martin, L.V. and Kohn, T., **2009**. Quantitative PCR for determining the infectivity of bacteriophage MS2 upon inactivation by heat, UV-B radiation, and singlet oxygen: advantages and limitations of an enzymatic treatment to reduce false-positive results. *Applied and environmental microbiology*, *75*(17), pp.5544-5554. https://doi.org/10.1128/AEM.00425-09

[180] Wang, Y. and Zhang, J., **2020**. Ultrafine TiO_2 (B) nanowires for ultrahigh-rate lithium-ion batteries. *Ionics*, *26*, pp.1159-1164. https://doi.org/10.1007/s11581-019-03291-z
[181] Zhou, Y., Peng, Y., Yin, Y., Zhou, F., Liu, C., Ling, J., Lei, L., Zhou, W. and Tang, D., **2016**. Modulating memristive performance of hexagonal WO_3 nanowire by water-oxidized hydrogen ion implantation. *Scientific Reports*, *6*(1), p.32712. https://doi.org/10.1038/srep32712
[182] Yuan, H.J., Chen, Y.Q., Yu, F., Peng, Y.H., He, X.W., Zhao, D. and Tang, D.S., **2011**. Hydrothermal synthesis and chromic properties of hexagonal WO_3 nanowires. *Chinese Physics B*, *20*(3), p.036103. http://doi.org/10.1088/1674-1056/20/3/036103
[183] Li, Y., Yu, H., Yang, Y., Zheng, F., Ni, H., Zhang, M. and Guo, M., **2016**. Synthesis of potassium hexatitanate whiskers with high thermal stability from Ti-bearing electric arc furnace molten slag. *Ceramics International*, *42*(9), pp.11294-11302. https://doi.org/10.1016/j.ceramint.2016.04.047

[184] Mao, R., Meng, N., Tu, W. and Peijs, T., **2017**. Toughening mechanisms in cellulose nanopaper: the contribution of amorphous regions. *Cellulose*, *24*, pp.4627-4639. https://doi.org/10.1007/s10570-017-1453-0
[185] Zainuri, M., **2017**, May. Hematite from natural iron stones as microwave absorbing material on X-band frequency ranges. In *IOP conference series: materials science and engineering* (Vol. 196, No. 1, p. 012008). IOP Publishing. http://doi.org/10.1088/1757-899X/196/1/012008
[186] Luu, C.L., Nguyen, Q.T., Ho, S.T. and Nguyen, T., **2013**. Characterization of the thin layer photocatalysts TiO_2 and V_2O_5-and Fe_2O_3-doped TiO_2 prepared by the sol–gel method. *Advances in Natural Sciences: Nanoscience and Nanotechnology*, *4*(3), p.035003. http://doi.org/10.1088/2043-6262/4/3/035003

[187] Safari, M., Talebi, R., Rostami, M.H., Nikazar, M. and Dadvar, M., **2014**. Synthesis of iron-doped TiO_2 for degradation of reactive Orange16. *Journal of Environmental Health Science and Engineering*, *12*, pp.1-8.http://doi.org/10.1186/2052-336X-12-19
[188] Zhao, T.X., Feng, Y.J., Huang, J.H., He, J.F., Liu, Q.H., Pan, Z.Y. and Wu, Z.Y., **2015**. Local structure and optical absorption characteristic investigation on Fe doped TiO_2 nanoparticles. *Chinese Physics C*, *39*(2), p.028001. http://doi.org/10.1088/1674-1137/39/2/028001

[189] Trenczek-Zajac, A., Synowiec, M., Zakrzewska, K., Zazakowny, K., Kowalski, K., Dziedzic, A. and Radecka, M., **2022**. Scavenger-supported photocatalytic evidence of an extended type I electronic structure of the TiO_2@ Fe_2O_3 interface. *ACS Applied Materials & Interfaces*, *14*(33), pp.38255-38269. https://doi.org/10.1021/acsami.2c06404

[190] Karim, K.M.R., Jebi, M.A.P., Ong, H.R., Abdullah, H., Tarek, M., Cheng, C.K. and Khan, M.M.R., **2018**. CuO-TiO_2 as a visible light responsive photocatalyst for the photoelectroreduction of CO2 to methanol. In *Natl. Conf. Postgrad. Res* (pp. 103-111).
[191] Maheswari, P., Sugapriya, S., Krishnaveni, N. and Senthil, T.S., **2022**. Investigation of Pure and CuO-and ZnO-Loaded TiO_2 Nanocomposites Prepared by Modified Hydrothermal Cum Green Synthesis (Hybanthus enneaspermus Extract) Method for Photocatalytic and Antioxidant Applications. *Brazilian Journal of Physics*, *52*(4), p.142.https://doi.org/10.1007/s13538-022-01112-9
[192] Siti K. K., Nur F. M. YUNOS, B. J., Suhaimi I. and Muhammad A. I., **2018**. Effect of CuO doped TiO2 on Morphology, Crystal Structure and Photocatalytic Activity, *International Journal of Current Science, Engineering & Technology, (AMCT 2017), Malaysia*, http://doi.org/10.30967/ijcrset.1.S1.2018.239-244
[193] Sokoidanto, H., Taufik, A. and Saleh, R., **2020**. Structural and optical study of Cu-doped TiO_2 nanoparticles synthesized by co-precipitation method. In *Journal of Physics: Conference Series* (Vol. 1442, No. 1, p. 012008). IOP Publishing. http://doi.org/10.1088/1742-6596/1442/1/012008
[194] Lei, R., Ni, H., Chen, R., Zhang, B., Zhan, W. and Li, Y., **2017**. Hydrothermal synthesis of WO_3/Fe_2O_3 nanosheet arrays on iron foil for photocatalytic degradation of methylene blue. *Journal of Materials Science: Materials in Electronics*, *28*, pp.10481-10487. http://doi.org/10.1007/s10854-017-6821-x
[195] Altanany, S.M., Gondal, M.A. and Baig, U., **2018**, June. Synthesis and characterization of CuO/WO_3 nanocomposite using hybrid method: Simple precipitation and pulsed laser ablation in liquids technique. In *AIP Conference Proceedings* (Vol. 1976, No. 1). AIP Publishing. https://doi.org/10.1063/1.5042381
[196] Pawlewicz, W.T., Exarhos, G.J. and Conaway, W.E., **1983**. Structural characterization of TiO_2 optical coatings by Raman spectroscopy. *Applied Optics*, *22*(12), pp.1837-1840. https://doi.org/10.1364/ao.22.001837
[197] Yu, T., Zhao, X., Shen, Z.X., Wu, Y.H. and Su, W.H., **2004**. Investigation of individual CuO nanorods by polarized micro-Raman scattering. *Journal of crystal growth*, *268*(3-4), pp.590-595. https://doi.org/10.1016/j.jcrysgro.2004.04.097
[198] Schenzel, K. and Fischer, S., **2001**. NIR FT Raman spectroscopy–a rapid analytical tool for detecting the transformation of cellulose polymorphs. *Cellulose*, *8*, pp.49-57. https://doi.org/10.1023/A:1016616920539
[199] Mansour, H., Omri, K., Bargougui, R., Ammar, S., **2020**. Novel a-Fe_2O_3/TiO_2 nanocomposites with enhanced photocatalytic activity. *Appl. Phys. A.* 126, 151, https://doi.org/10.1007/s00339-020-3320-3
[200] El Mrabate, B., Udayakumar, M., Csiszár, E., Kristály, F., Leskó, M., Somlyai Sipos, L., Schabikowski, M. and Németh, Z., **2020**. Development of bacterial cellulose–ZnO–MWCNT hybrid membranes: a study of structural and mechanical properties. *Royal Society open science*, *7*(6), p.200592. https://doi.org/10.1098/rsos.200592
[201] Garcia-Sanchez, R.F., Ahmido, T., Casimir, D., Baliga, S. and Misra, P., **2013**. Thermal effects associated with the Raman spectroscopy of WO_3 gas-sensor materials. *The Journal of Physical Chemistry A*, *117*(50), pp.13825-13831. https://doi.org/10.1021/jp408303p
[202] Song, W., Zhang, R., Bai, X., Jia, Q. and Ji, H., **2020**. Exposed crystal facets of WO_3 nanosheets by phase control on NO_2-sensing performance. *Journal of Materials Science: Materials in Electronics*, *31*, pp.610-620. https://doi.org/10.1007/s10854-019-02565-6
[203] Yu, T., Zhao, X., Shen, Z.X., Wu, Y.H. and Su, W.H., **2004**. Investigation of individual CuO nanorods by polarized micro-Raman scattering. *Journal of crystal growth*, *268*(3-4), pp.590-595. https://doi.org/10.1016/j.jcrysgro.2004.04.097

[204] El Mrabate, B., Szőri-Dorogházi, E., Shehab, M.A., Chauhan, T., Muránszky, G., Sikora, E., Filep, Á., Sharma, N., Nánai, L., Hernadi, K. and Németh, Z., **2021**. Widespread applicability of bacterial cellulose-ZnO-MWCNT hybrid membranes. *Arabian Journal of Chemistry*, *14*(7), p.103232. https://doi.org/10.1016/j.arabjc.2021.103232
[205] Keabadile, O.P., Aremu, A.O., Elugoke, S.E. and Fayemi, O.E., **2020**. Green and traditional synthesis of copper oxide nanoparticles—comparative study. *Nanomaterials*, *10*(12), p.2502. https://doi.org/10.3390/nano10122502
[206] Lassoued, A., Dkhil, B., Gadri, A. and Ammar, S., **2017**. Control of the shape and size of iron oxide (α-Fe_2O_3) nanoparticles synthesized through the chemical precipitation method. *Results in physics*, *7*, pp.3007-3015. https://doi.org/10.1016/j.rinp.2017.07.066
[207] Chai, Y.D., Pang, Y.L., Lim, S., Chong, W.C., Lai, C.W. and Abdullah, A.Z., **2021**. Role of oil palm empty fruit bunch-derived cellulose in improving the sonocatalytic activity of silver-doped titanium dioxide. *Polymers*, *13*(20), p.3530. https://doi.org/10.3390/polym13203530
[208] Zhao, J., **2022**. Excellent photocatalytic degradation and antibiosis of WO_3/Fe_2O_3 heterojunction. *Materials Research Express*, *9*(5), p.055010. https://doi.org/10.1088/2053-1591/ac5274
[209] Syngouna, V.I. and Chrysikopoulos, C.V., **2010**. Interaction between viruses and clays in static and dynamic batch systems. *Environmental science & technology*, *44*(12), pp.4539-4544. https://doi.org/10.1021/es100107a
[210] Kosmulski, M., **2009**. *Surface charging and points of zero charge*. CRC press. https://doi.org/10.1201/9781420051896
[211] Cong, Y., Li, Z., Zhang, Y., Wang, Q. and Xu, Q., **2012**. Synthesis of α-Fe_2O_3/TiO_2 nanotube arrays for photoelectro-Fenton degradation of phenol. *Chemical Engineering Journal*, *191*, pp.356-363. https://doi.org/10.1016/j.cej.2012.03.031
[212] Asenath-Smith, E., Ambrogi, E.K., Barnes, E. and Brame, J.A., **2020**. CuO enhances the photocatalytic activity of Fe_2O_3 through synergistic reactive oxygen species interactions. *Colloids and Surfaces A: Physicochemical and Engineering Aspects*, *603*, p.125179. https://doi.org/10.1016/j.colsurfa.2020.125179
[213] Alsafari, I.A., Chaudhary, K., Warsi, M.F., Warsi, A.Z., Waqas, M., Hasan, M., Jamil, A. and Shahid, M., **2023**. A facile strategy to fabricate ternary WO_3/CuO/rGO nano-composite for the enhanced photocatalytic degradation of multiple organic pollutants and antimicrobial activity. *Journal of Alloys and Compounds*, *938*, p.168537. https://doi.org/10.1016/j.jallcom.2022.168537
[214] Bai, S., Zhang, K., Sun, J., Luo, R., Li, D. and Chen, A., **2014**. Surface decoration of WO_3 architectures with Fe_2O_3 nanoparticles for visible-light-driven photocatalysis. *CrystEngComm*, *16*(16), pp.3289-3295. https://doi.org/10.1039/C3CE42410C
[215] Lima, M.S., Cruz-Filho, J.F., Noleto, L.F., Silva, L.J., Costa, T.M. and Luz Jr, G.E., **2020**. Synthesis, characterization and catalytic activity of Fe_3O_4@ WO_3/SBA-15 on photodegradation of the acid dichlorophenoxyacetic (2, 4-D) under UV irradiation. *Journal of Environmental Chemical Engineering*, *8*(5), p.104145. https://doi.org/10.1016/j.jece.2020.104145
[216] Németh, Z., Szekeres, G.P., Schabikowski, M., Schrantz, K., Traber, J., Pronk, W., Hernádi, K. and Graule, T., **2019**. Enhanced virus filtration in hybrid membranes with MWCNT nanocomposite. *Royal Society open science*, *6*(1), p.181294. https://doi.org/10.1098/rsos.181294
[217] Sellaoui, L., Badawi, M., Monari, A., Tatarchuk, T., Jemli, S., Dotto, G.L., Bonilla-Petriciolet, A. and Chen, Z., **2021**. Make it clean, make it safe: A review on virus elimination

via adsorption. *Chemical Engineering Journal*, *412*, p.128682. https://doi.org/10.1016/j.cej.2021.128682
[218] World Health Organiztaion, Guidelines for drinking-water quality. 4th ed. Geneva, **2017**, pp. 242-244. https://www.who.int/publications/i/item/9789241549950